WARD-D-0050, REV. 3
WARD-D Category II

Clinch River Breeder Reactor Plant

CRBRP CORE ASSEMBLIES HOT CHANNEL FACTORS PRELIMINARY ANALYSIS

SEPTEMBER 1979

Prepared for the United States Department of Energy under contracts EY-76-C-15-2395 and EY-76-C-15-0003.

Westinghouse Electric Corporation
ADVANCED REACTORS DIVISION
BOX 158
MADISON, PENNSYLVANIA 15663

CHANGE CONTROL RECORD Westinghouse Advanced Reactors Division	TITLE CRBRP Core Assemblies Hot Channel Factors Preliminary Analysis	DOCUMENT NO. WARD-D-0050

REV NO./DATE	CHANGE RELEASE DOCUMENT	PAGES AFFECTED	REMARKS
Rev. 2 - 11/78	N/A	Entire Document	Document completely rewritten
Rev. 3 - 9/79	N/A	iv, viii, 1, 15, 19, 27, 31, 49, 58, 59, 67, 71, 84, 88, 97, 99, 104, 108, 114, 120, 142, 143, 144, 145, Attachment p. 17	Delete mention of "AFMS". Clarify applicability to heterogeneous core. Correct typographical errors.

1630 003

WARD-D-0050, Rev. 3
WARD-D Category II

CRBRP CORE ASSEMBLIES HOT CHANNEL FACTORS PRELIMINARY ANALYSIS

September 1979

PREPARED: A. J. Friedland, Core T&H Analysis — 9-11-79 Date

APPROVED: R. A. Markley, Manager Core T&H Analysis — 9/11/79 Date

INFORMATION CONCERNING USE OF THIS DOCUMENT

PRELIMINARY DOCUMENT

This document contains information of a preliminary nature prepared in the course of work for the U. S. Department of Energy. This information is subject to correction or modification upon the collection and evaluation of additional data.

NOTICE

WESTINGHOUSE ELECTRIC CORPORATION

ADVANCED REACTORS DIVISION

BOX 158

MADISON, PENNSYLVANIA 15663

CONTRIBUTORS:

A. Biancheria
A. A. Bishop (Univ. of Pgh.)
M. D. Carelli
F. C. Engel
W. L. Howarth
J. A. Lake
R. R. Lowrie
J. Marshall (WRL)
D. Y. Nee
H. P. Planchon
T. S. Roth
E. C. Schwegler
D. R. Spencer
B. E. Sundquist
G. H. Ursin

TABLE OF CONTENTS

1630 007

TABLE OF CONTENTS (Con't)

1630 008

TABLE OF CONTENTS (Con't)

1630 009

TABLES

1630 010

TABLES (Continued)

TABLES (Continued)

1630 012

FIGURES

FIGURES (Continued)

1630 014

1.0 INTRODUCTION AND SUMMARY

The impact of uncertainties associated with theoretical and experimental analyses, instrumentation accuracy, manufacturing tolerances, physical properties and physical phenomena correlations must be considered in predicting the reactor thermal-hydraulic performance to ensure the safe and reliable operation of the CRBRP core and to guarantee that proper margins are provided to meet both lifetime and safety design limits and requirements.

The effects of the various uncertainties are accounted for in the "hot channel factors" or "hot spot factors" analyses. The basis of such analyses is to characterize a hot channel as the one affected by the simultaneous occurrence of all uncertainties and thereby predict the temperature of the hot channel or hot spot, which will be compared with the required limits. The use of hot channel factors has evolved over a long period of time, initially in light water reactors and more recently in liquid metal cooled fast breeder reactors.

This report documents the methodology, supporting bases including data base and computed values for the hot channel factors used in the heterogeneous core thermal-hydraulic analyses. The analytical procedures are discussed in Section 2.0. The hot channel factors for the fuel and blanket assemblies for the heterogeneous core are discussed in Sections 3.0 and 4.0, respectively, and are summarized in Section 6.0. The hot channel factors for the primary control assemblies are preliminary values which were developed for the homogeneous core and are being updated. They are discussed in Section 5.0 and are also summarized in Section 6.0. The results presented here are preliminary in nature. Changes in plant design and operating conditions. growth of the supporting data base and ongoing development of analytical methods will result in continued updating as the design proceeds. Final results will be presented in the FSAR.

The hot channel factors used in calculations of the coolant temperature, cladding temperature, and gas plenum pressure for the CRBRP fuel, blanket, and primary control assemblies are presented in Tables 6.1A through 6.10. Results of uncertainty analyses associated with fuel power-to-melt calculations are addressed in the appropriate sections of this report.

For convenience, the uncertainties associated with the fuel and blanket assemblies are grouped according to engineering (table numbers with the "A" suffix) and nuclear considerations (table numbers with the "B" suffix). Note that 3σ statistical values are applied to the plant thermal-hydraulic design conditions when performing safety analyses. The 2σ level is applied to plant expected operating conditions when calculating parameters such as cladding temperature and pressure, which are input to replaceable core assembly lifetime analyses. The hot channel factors in this report are applicable at full power steady state conditions. The 3σ uncertainties associated with the thermal-hydraulic values are conservatively used as the initial conditions for emergency and faulted transient and safety analyses.

The hot channel factors reported in Tables 6.1A through 6.10 are considered to be conservative. This will be further established as additional data become available from tests which are planned or in progress. These include: additional irradiation experiments on fuel, blanket, and primary control rods; engineering mockup critical experiments in the ZPPR; pressure drop tests of fuel, blanket, and control assemblies and orifice configurations; heat transfer tests on a 61 fuel rod bundle in sodium; cross flow measurements in a 5:1 scale blanket rod bundle sector in air; and heat transfer tests in sodium on a prototypic blanket rod bundle. These data will be included in the FSAR analyses. A more detailed tabulation of the forthcoming T&H tests is given in Table 6.11.

1630 016

2.0 ANALYTICAL PROCEDURE

The impact of theoretical and experimental analytic uncertainties, instrumentation accuracy, manufacturing tolerances, physical properties and correlations uncertainties must be considered in predicting the reactor thermal-hydraulic performance to ensure the safe and reliable operation of the CRBRP core and to guarantee that proper margins are provided so as not to exceed the design limits and requirements.

The effects of the various uncertainties are accounted for in the "hot channel factors" or "hot spot factors" analysis. The basis of such an analysis is to characterize a hot channel as the one affected by the simultaneous occurrence of all uncertainties and thereby predict the temperature of the hot channel or hot spot, which will be compared with the required limits.

Consistent with PWR, FFTF and Westinghouse proposal studies, the semi-statistical hot spot analysis is used for the CRBRP. Use of the semi-statistical method requires the separation of the variables which cause the hot spot temperatures into two principal categories; one of statistical origin and the other non-statistical. The two categories are defined below.

A non-statistical (or direct) uncertainty is defined as a variation in a design variable which is known or conservatively assumed to occur, but is not included in the nominal analysis. Computationally, the non-statistical factors represent multipliers applied to the nominal magnitudes of the variables to provide the worst values which will occur. A variable which has a random frequency distribution of occurrence is treated statistically. For example, experimental data (such as materials properties) are treated statistically since there is random error in their evaluation.

Direct and statistical factors employed in deriving CRBRP fuel rod hot channel/spot temperatures, for example, are shown in Tables 6.1A and 6.1B.

The direct factors in these tables are related to effects that are assumed to occur with certainty. That is, power level measurement and control system deadband, inlet flow maldistribution direct bias, subchannel flow distribution

1630 017

simulation bias, cladding temperature increase beneath the wire wrap, pellet-cladding eccentricity, physics analysis calculational methods and control rod effects are direct consequences of the design and result in known temperature non-uniformities at some time during core life. The statistical factors, on the other hand, are based on random occurrences (i.e., timewise, spatial-wise or data/tolerance distribution) such that the probability of departure from the nominal value is given by a probability distribution. Typical of such random effects are manufacturing variability of fissile fuel content, dimensional tolerances, instrumentation uncertainties, and experimental uncertainties in measured values. In the CRBRP statistical factors, manufacturing variability and dimensional tolerances affect fissile fuel maldistribution, rod diameter and pitch, and cladding thickness; instrumentation uncertainties affect power level measurement; and uncertainties in experimental data affect nuclear power distribution, film coefficient, cladding conductivity and power-to-melt.

The hot channel factors may be grouped into categories which indicate the basis for each factor:

Statistical - The data base is sufficient to provide a statistical basis for the hot channel factor.

Empirical or Bounding - The data base is small and/or only a bounding value can be calculated.

Engineering Judgement - Little or no data are available.

Analytical - Represents analytical adjustments to the nominal analysis rather than uncertainties.

This report provides the basis for each factor and subfactor.

1630 018

2.1 Treatment of Statistical Factors

Before describing the method of combining direct and statistical factors, some discussion of the treatment of statistical factors is warranted.

If a temperature, T, can be expressed as a linear function of independent random variables, x_i,

$$T = a_0 + a_1 x_1 + a_2 x_2 + \ldots + a_n x_n \tag{2.1}$$

then the variance of T is equal to the sum of the variances of the $a_i x_i$'s,

$$\sigma_T^2 = \sum_{i=1}^{n} a_i^2 \sigma_i^2 \tag{2.2}$$

If the independent variables have normal distributions then T will have a normal distribution. If the independent variables do not have normal distributions, T will still tend to approach a normal distribution as the number of independent variables becomes large.

If T is an arbitrary function of the independent variables,

$$T = T(x_1, x_2, \ldots x_n) \tag{2.3}$$

then T takes the value $\bar{T}$ when each variable is at its mean value, $\bar{x}_i$. Since the concern is with what happens to the temperature when a variable departs from the mean by some arbitrary amount Δx_i, the temperature can be approximated by a Taylor series expansion about $T = \bar{T}$ in which only linear terms are retained:

$$T - \bar{T} \cong \sum_{i=1}^{n} \frac{\overline{\partial T}}{\partial x_i} \Delta x_i \tag{2.4}$$

where $\frac{\overline{\partial T}}{\partial x_i}$ is $\frac{\partial T}{\partial x_i}$ evaluated at $x_j = \bar{x}_j$ for j = 1, 2, ... n.

Dropping the higher order terms results in negligible error provided departures from the mean are relatively small, as is the case with most hot channel factor applications.

Substituting Equation (2.4) in (2.2) results in

$$\sigma_T^2 \cong \sum_{i=1}^{n} \left(\frac{\overline{\partial T}}{\partial x_i}\right)^2 \sigma_i^2 \tag{2.5}$$

1630 019

If T has a normal distribution, then the probability that $\bar{T} + 2\sigma_T$ will not be exceeded is 97.73% and the probability that $\bar{T} + 3\sigma_T$ will not be exceeded is 99.87%.

One type of uncertainty commonly encountered is that of a variable, such as a dimension, with specified bounds. In such a case, it is reasonable to assume that the mean value has a uniform probability of lying anywhere within the bounds. For such a rectangular distribution, the bounds correspond to $\pm\sqrt{3}\sigma$. The actual distributions of dimensions of fabricated components will be used where available for the FSAR uncertainty analyses. As previously noted, as the number of independent variables becomes large, the distribution of their sum approaches a normal distribution. If some of the independent variables have rectangular distributions and some have normal distributions, then the 2σ or 3σ coverage calculated using Equation (2.5) will be greater (more conservative) than if the distributions were all normal with the same standard deviations.

2.2 Tolerance Interval

The use of Equation (2.5) implies that the variances of the independent variables are known. This is often not the case, and it is necessary to infer the variance of the population from a sample set of data. If the number of observations is large, the variance of the sample,

$$S_i^2 = \frac{\sum_{j=1}^{n_i} (x_{ij} - \bar{x}_i)^2}{n_i - 1} \qquad (2.6)$$

approaches the variance of the population. If the number of observations is small, it is still possible to give tolerance limits on the possible values of T. A detailed discussion is given in the Attachment to this report, and is summarized in the remainder of this section.

If the distribution of T is normal, and a set of n observations on T is available, statistical theory provides two classical methods for determining the coverage in hypothetical repeat samples. The first type of tolerance interval is called the β-expectation type and determines the average coverage. The second type is called the β-content type and determines the probability that the coverage is at least a given amount. The first type will be used

for the hot channel factor analyses. This is felt to be more appropriate, as the coverage, β, is more directly related to the coverage for the known variance case. The upper tolerance limit is given by

$$\bar{T} + t_{\beta}\,(n-1)\,\sqrt{1 + 1/n}\;S \tag{2.7}$$

where $t_{\beta}\,(n-1)$ is found from a table of the t-distribution. This is a value which an n-1 degree of freedom t-variate will exceed with probability $1-\beta$.

For the case where T is a linear function of x_i's (Equation 2.1), with a random sample of size n_i on each x_i, Satterthwaite's approximation is used to determine the degrees of freedom to be associated with a linear combination of variance estimates. The upper tolerance limit is given by

$$\bar{T} + t_{\beta}\,(\nu_e)\,S_e \tag{2.8}$$

where

$$S_e = \left[\sum_{i=1}^{n} (a_i^2\,S_i^2)\,(n_i+1)/n_i\right]^{1/2} \tag{2.9}$$

$$\nu_e = (S_e^2)^2 / \left[\sum_{i=1}^{n} (a_i^2\,S_i^2\,(n_i+1)/n_i)^2/\nu_i\right] \tag{2.10}$$

$$\bar{x}_i = \left(\sum_{j=1}^{n_i} x_{ij}\right)/n_i \tag{2.11}$$

$$S_i^2 = \left(\sum_{j=1}^{n_i} (x_{ij} - \bar{x}_i)^2\right)/(n_i - 1) \tag{2.12}$$

Using available t-tables, as a close approximation of the 2σ and the 3σ limits which are used for known σ's, $\beta = 0.975$ is taken to correspond to "2σ" and $\beta = 0.999$ is taken to correspond to "3σ".

The interval computed by Equation (2.8) will have coverage β on the average. Another interpretation is that Equation (2.8) yields a $100\beta\%$ confidence limit for the next observation on T.

1630 021

2.3 Overall Uncertainty

Calculation of fuel rod temperatures for the hot channel is shown in Figure 2.1. The nominal temperature difference ΔT_{nom} is multiplied by the product of the direct hot channel factors to give the temperature rise including non-statistical factors ΔT_{dir}. Using this value, the nominal temperature T_{nom} is increased to T_{dir} (or $T_{0\sigma}$). T_{dir} represents the mean value about which the statistical uncertainties are applied. The nominal channel can be any channel in the assembly, with the nominal channel coolant ΔT calculated using subchannel analysis codes. In practice, the channel with the highest coolant temperature is singled out for application of hot channel factors, thus calculation of hot channel temperatures.

The hot channel factors used in the CRBRP analyses are shown in Tables 6.1A through 6.1O. Independent variables appear on separate horizontal lines. Hot channel factors appearing on the same line are not independent, and their overall effect must be calculated directly before combining statistically with the other factors. For example, in Table 6.1A, the statistical effect of pellet-cladding eccentricity affects both film and cladding ΔT's. Therefore, the overall uncertainty in film and cladding ΔT's is calculated directly before being combined statistically with the remaining statistical temperature uncertainties. This will be illustrated by the sample calculation in the next section.

It may be noted that a more conservative procedure was followed in the PSAR analyses. In those analyses, the statistical uncertainties for a given component (coolant, film or cladding) were combined statistically and the resulting temperature uncertainties for each component were added directly to provide the overall temperature uncertainty. This "vertical-horizontal" procedure was conservatively adopted for convenience in calculation and to provide additional margin in the early stages of design. However, the present procedure is more exact, and is being used for future analyses.

Several approximations have been mentioned in the analytical procedure: a) the variables are assumed to have normal distributions when calculating the probability of exceeding the 2σ or 3σ value; and b) the temperature is assumed to be a linear function of the variables.

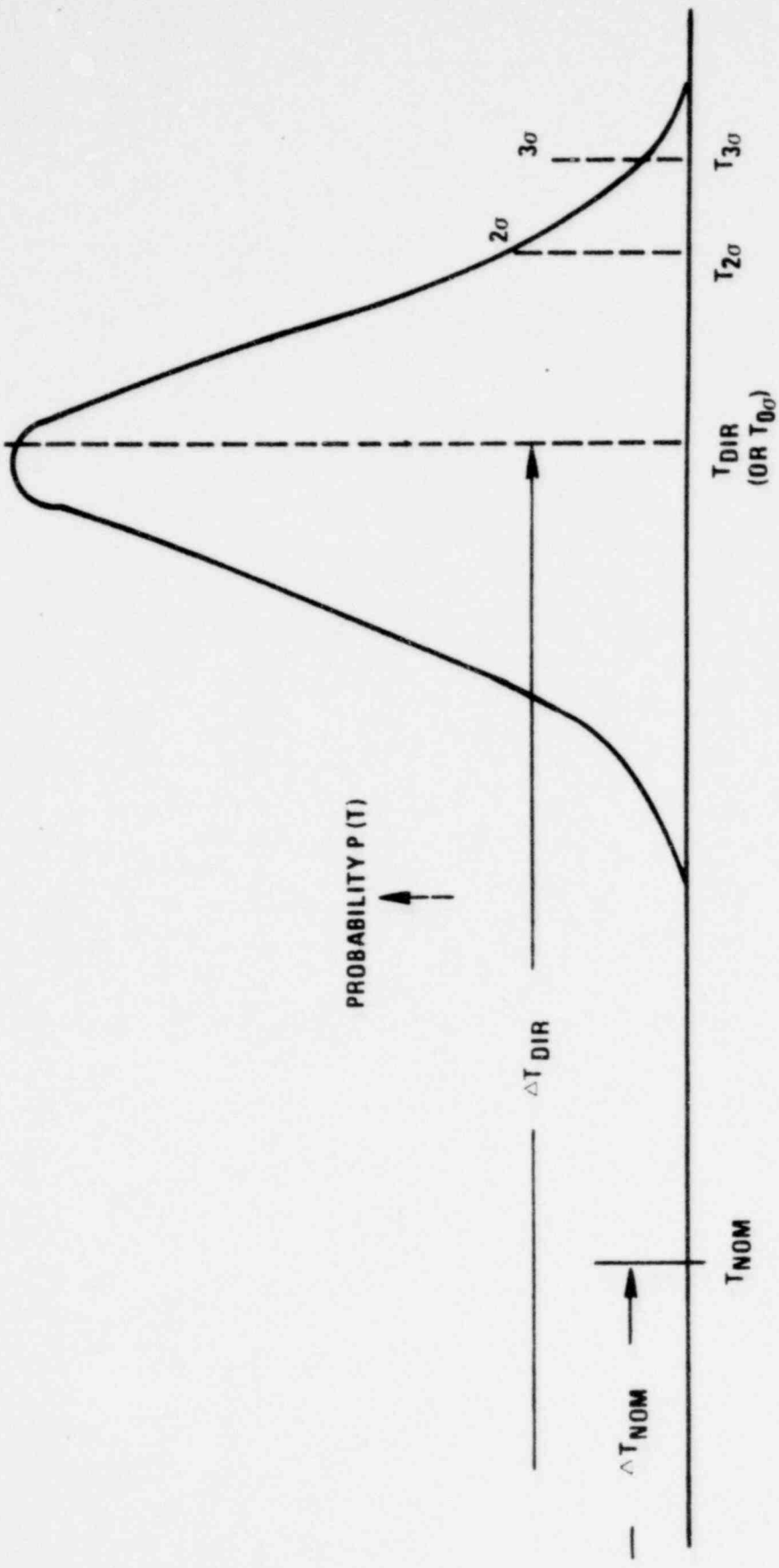

Figure 2-1. Graphical Illustration of Semistatistical Method.

1630 023

9926-1

Regarding Item (a), the non-normal probability distributions most commonly encountered are rectangular distributions. As previously noted, this leads to conservative results, i.e., the probability of exceeding the 2σ or 3σ values is lower if some of the variables have rectangular probability distributions than if they all have normal distributions.

Regarding Item (b), the most significant non-linearities are encountered in fuel power-to-melt analyses. In Section 3.2, it is shown that even for the most significant non-linearity, the relation between power-to-melt and pellet diameter, the linearization selected is a close approximation of the actual relation over the range of interest. Furthermore, as noted in the previous paragraph, conservatism is provided by the rectangular probability distribution associated with the pellet diameter.

For the FSAR analyses, it is planned to include the effects of non-normal probability distributions and non-linearities directly in the analyses.

2.4 Sample Calculation

To illustrate the analytical procedure, assume that the 2σ cladding midwall (M.W.) temperature for plant expected operating conditions is to be calculated at the top of the core for a typical beginning-of-life first core fuel assembly not adjacent to a control rod, with a 1.0 ZPPR-7 flux tilt factor and with the cladding circumferential temperature variation factor of 2.1 on the film ΔT and 0.9 on the cladding (M.W.) ΔT. Assume that the nominal ΔT's for the hot channel calculated using CØTEC and NICER are:

Coolant ΔT:	420°F
Film ΔT:	12°F
Cladding (M.W.) ΔT:	13°F

Applying the direct factors in Tables 6.1A and 6.1B, the 0σ ΔT's are:

Coolant ΔT:	459.1
Film ΔT:	32.4
Cladding (M.W.) ΔT:	15.0

1630 024

Applying the statistical hot channel factors from Tables 6.1A and 6.1B to these 0σ ΔT's, the temperature uncertainties shown in Table 2.1 are calculated. These uncertainties are added horizontally, and the resulting independent temperature uncertainties in the right-hand column are combined statistically to give the overall 3σ uncertainty of 87.3°F. Since the 2σ uncertainty is required, 2/3 of this value is taken (58.2°F). Adding the ΔT's to the first core nominal plant expected inlet temperature of 704°F, results in the following maximum cladding midwall temperatures in this fuel assembly:

Nominal:	1149°F
0σ:	1210.5°F
2σ:	1268.7°F

The above analysis is based on using the variance of a sample as an estimate of the variance of the total population. Applying the tolerance interval method previously discussed to those uncertainties which are based directly on the variance of small samples, and referring to the discussions in Section 3.1 on the bases for the hot channel factors, the inlet flow maldistribution factors of 1.059 on coolant ΔT and [illegible] on film ΔT and the coolant properties factor of 1.017 on coolant ΔT may be broken down into subfactors (where n is the number of data points):

	HCF (3σ)		n
	Coolant ΔT	Film ΔT	
Flow Maldistribution	1.050	1.014	-
	1.020	1.005	33
	1.024	1.006	7
Coolant Properties	1.009	--	-
	1.015	--	5

Repeating the analysis in Table 2.1 and applying Equations (2.8) through (2.12),

$$\nu_e = 13103$$

$$3S_e = 87.6$$

The effective three standard deviations, $3S_e$, is nearly identical with that calculated in Table 2.1, the effective degrees of freedom, ν_e, is extremely large, and therefore the results are essentially the same as previously analyzed.

TABLE 2.1

SAMPLE CALCULATION OF FUEL ASSEMBLY ROD CLADDING MIDWALL TEMPERATURE

	COMPONENT TEMPERATURES, °F				
	INLET T	COOLANT ΔT	FILM ΔT	CLADDING (M.W.)ΔT	TOTAL
NOMINAL:	704	420	12	13	1149
0σ:	704	459.1	32.4	15.0	1210.5
	3σ TEMPERATURE UNCERTAINTIES, °F				
Reactor ΔT and Inlet Temperature Variation		62.2			62.2
Inlet Flow Maldistribution		27.1	0.5		27.6
Loop Temperature Imbalance	7.4				7.4
Wire Wrap Orientation		4.6			4.6
Subchannel Fl Area		8.7			8.7
Film Heat Transfer Coefficient			3.9		3.9
Pellet-Cladding Eccentricity			5.6	2.6	8.2
Cladding Thickness and Conductivity				0	0
Coolant Properties		7.8			7.8
Flow Distribution Calculational Uncertainty (Calibration)		26.6	0.2		26.8
Experimental (Nuclear)		32.1	2.3	1.1	35.5
Criticality		4.6	0.3	0.2	5.1
Fissile Fuel Maldistribution		23.9	1.7	0.8	26.4
				Overall $3\sigma = [\Sigma(3\sigma_i)^2]^{1/2}$ =	87.3

3.0 FUEL ASSEMBLIES HOT SPOT FACTORS

3.1 Fuel Rod Cladding and Coolant Temperatures Hot Spot Factors for Fuel Assemblies

The hot spot factors for evaluation of CRBRP fuel assemblies rod cladding and channel coolant temperatures are presented in Tables 6.1A and 6.1B.

3.1.1 Power Level Measurement and Control System Dead Band

This bounding factor is 1.03, which is a reactor system design requirement. It is applied as a direct factor to thermal hydraulic design value (THDV) conditions. It does not appear directly for plant expected operating value (PEOV) conditions which are used for core assembly lifetime calculations. For PEOV conditions, its subfactors are included statistically in the Inlet Temperature Uncertainty and in the Reactor ΔT Variation.

A total bounding margin of 15% steady state overpower is provided between the reactor rated power conditions and the first reactor trip. This steady state overpower margin defines the reactor short time design conditions and is used, in conjunction with 3σ hot channel factors, to determine if fuel centerline melting is attained. The power level measurement and control system dead band factor is not applied simultaneously with the 15% overpower.

3.1.2 Cladding Circumferential Temperature Variation

In a close packed rod bundle array, the coolant velocity and temperature distribution in the subchannel formed by three adjacent rods is not uniform, but varies circumferentially around the rod. Consequently, the cladding temperature has a circumferential distribution, depending on the P/D radio, the rod power rating, the coolant and cladding thermal conductivities and the bulk coolant velocity. The maximum cladding temperature occurs at the minimum gap between the rods, which is consequently the hot spot. The presence of the wire wrap further skews the peripheral temperature distribution, enhancing the hot spot magnitude. Analyses for CRBRP fuel assemblies using the FATHOM-360 computer program[1] showed that the analytical hot spot factor is in the range of 1.6 to 1.9 across the film (depending upon assembly operating conditions), approximately 0.8 from cladding OD to midwall and approximately 0.9 from cladding OD to ID.

The analyses conservatively assumed uniform heat flux at the cladding inner surface and the coolant temperatures were determined by solving the turbulent momentum and energy equations.

A detailed analysis is performed for the lifetime-limiting assembly in each flow zone. In addition, a 20% uncertainty which is a bounding value based on limiting case analyses is applied to the deviations from the nominal case to conservatively account for uncertainties resulting from finite difference modeling, flow distribution uncertainties and flow mixing uncertainties.

Hot spot temperatures have been experimentally measured at HEDL[2] and ORNL[3] on wire-wrapped, electrically heated pins of nominal CRBRP dimensions. The HEDL 7-pin tests indicate the ratio of hot spot/nominal film temperature drop is approximately 21°F/18°F. The ORNL 19-pin tests indicate the ratio is approximately 27°F/17°F. Since these data result in film subfactors of about 1.2 and 1.6, the previously mentioned application of 1.6 to 1.9 for the nominal film subfactor is conservative.

The effect of the cladding circumferential temperature variation and of the wire wrap is accounted for if calculating the local cladding temperature. For maximum fuel temperature calculations, however, an average cladding inner diameter temperature is the most appropriate boundary condition; thus, the cladding circumferential variation factor in this case, is equal to 1 by definition.

3.1.3 Reactor ΔT and Inlet Temperature Variation

Two sets of plant conditions are used in the thermal-hydraulic design, i.e., plant thermal-hydraulic design values (THDV) conditions and plant expected operating values (PEOV) conditions. The THDV conditions (730°F inlet/995°F outlet temperature; total reactor flow 41.446 x 10^6 lb/hr) are the Clinch River rated plant conditions and therefore no plant system uncertainties apply to these values. They are used in: a) analyzing permanent components which have the same 30 years lifetime as the plant's; b) transient and safety analyses, since they are more conservative than the plant expected conditions. This latter set represents the plant conditions at which the CRBRP is expected to operate accounting for the operating conditions of the heat transfer systems such as pump characteristics, primary loop pressure drop uncertainties, fouling

and plugging of heat exchangers, etc. Expected operating values for the primary heat transport system principal parameters (inlet, outlet temperature and ΔT) are thus evaluated, together with the associated uncertainties. The results of this study, which comprised a Monte Carlo type analysis, are reported in Table 3.1. The study included: 1) the consideration of the progressive fouling of the heat exchangers during the plant 30 years lifetime, which affects the predicted values of the plant operating conditions, and 2) a comprehensive accounting of all uncertainties affecting plant operation. Empirical or bounding values were used for the effect of fouling and for the uncertainties affecting plant operation. Plant expected operating conditions are adopted in core thermofluids analyses of replaceable components, such as the core assemblies, chiefly in determining the fuel rod parameters (cladding temperature, fission gas pressure) which are the basis for evaluating the structural behavior and for assessing whether lifetime/burnup objectives are actually met.

Plant expected operating conditions adopted in the first and second core thermal-hydraulic analyses are reported in Table 3.2. Following is a brief discussion of the rationale in determining the values reported in Table 3.2 from the ones in Table 3.1. PEOV conditions will be updated for the FSAR.

First, the mean values of Table 3.1 are chosen as the nominal values of Table 3.2, thus including the bias factor directly into the nominal values. Since the most critical times for core assemblies is at the end-of-life, when the cladding strain and damage function are maximum, first core values have been selected as corresponding to two-year fouling and second core values as corresponding to four-year fouling conditions. Due to the fact that four-year fouling conditions were not evaluated, it was conservatively assumed that the same difference in plant parameters between year two and year zero repeats between year four and year two. Again, the selected approach is conservative for two reasons: 1) plant conditions have been considered constant over the two years span and equal to the worst end-of-span conditions, thus neglecting the more favorable conditions which exist throughout the core lifetime; and 2) the effect of fouling is not linear with time, but it is rather pronounced at the beginning and then tapers off during the plant lifetime, as can be seen by comparing plant parameters in

Table 3.1 for 0, 2, and 30 years. Thus, the assumption that the same deterioration of plant conditions which occurs in the first two years (first core) also occurs during the third and fourth year (second core) is very conservative.

If primary cold leg temperature (T_{Ri}) and primary ΔT (ΔT_R) were statistically independent, then the primary hot leg temperature (T_{Ro}) variance would be related to the other variances by

$$\sigma_{T_{Ro}}^2 = \sigma_{T_{Ri}}^2 + \sigma_{\Delta T_R}^2 \qquad (3.1)$$

Since $\sigma_{T_{Ro}}^2$ is smaller than the value given by Equation (3.1), it is evident that there is a negative correlation between T_{Ri} and ΔT_R, i.e., higher-than-average values of T_{Ri} tend to be associated with lower-than-average values of ΔT_R. The more general form of Equation (3.1) which covers this case is

$$\sigma_{T_{Ro}}^2 = \sigma_{T_{Ri}}^2 + \sigma_{\Delta T_R}^2 + 2\sigma_{T_{Ri},\,\Delta T_R} \qquad (3.2)$$

where $\sigma_{T_{Ri},\,\Delta T_R}$ is the covariance between T_{Ri} and ΔT_R. From the two-year fouling data in Table 3.1,

$$\sigma_{T_{Ro}}^2 = 169$$

$$\sigma_{T_{Ri}}^2 = 121$$

$$\sigma_{\Delta T_p}^2 = 144$$

from which

$$2\sigma_{T_{Ri},\,\Delta T_R} = -96$$

The coolant temperature rise in a given fuel assembly channel (ΔT_c) is proportional to ΔT_R:

$$\Delta T_c = C\,\Delta T_R \qquad (3.3)$$

From the definitions of variance and covariance,

$$\sigma_{\Delta T_c}^2 = C^2\,\sigma_{\Delta T_R}^2$$

1630 030

$$\sigma_{T_{Ri},\,\Delta T_c} = C\,\sigma_{T_{Ri},\,\Delta T_R}$$

Therefore, the variance in T_c is given by

$$\sigma_{T_c}^2 = \sigma_{T_{Ri}}^2 + \sigma_{\Delta T_c}^2 + 2\sigma_{T_{Ri},\,\Delta T_c} \tag{3.4}$$

$$= \sigma_{T_{Ri}}^2 + C^2\sigma_{\Delta T_R}^2 + 2C\,\sigma_{T_{Ri},\,\Delta T_c} \tag{3.5}$$

From the two-year fouling data in Table 3.1,

$$\sigma_{T_c}^2 = 144\,C^2 - 96\,C + 121 \tag{3.6}$$

Also,

$$\overline{\Delta T_R} = 250$$

so that Equation (3.6) may be written as

$$\sigma_{T_c}^2 = 0.002304\,\Delta T_c^2 - 0.384\,\Delta T_c + 121 \tag{3.7}$$

The σ's in Table 3.1 show little variation with fouling and therefore Equation (3.7) will be used for the second core as well as the first core.

Typical HCF values on ΔT_c are tabulated below:

ΔT_c	$\sigma_{\Delta T_c}$	HCF (3σ)
250	13	1.156
300	14.6	1.146
400	18.3	1.137
500	22.5	1.135

1630 031

TABLE 3.1

PLANT EXPECTED OPERATING CONDITIONS AND UNCERTAINTIES

Parameter	Clean & Unplugged Heat Exchangers (New Plant)				Estimated (2 Year Fouling)				Fouled & Plugged Heat Exchangers (30 Year Fouling)			
	Nominal	Mean	σ	$T_{97.7}$	Nominal	Mean	σ	$T_{97.7}$	Nominal	Mean	σ	$T_{97.7}$
Primary Hot Leg Temperature, T_{Ro} (°F)	943	946	13	968	950	954	13	976	960	964	13	987
Primary Cold Leg Temperature, T_{Ri} (°F)	698	697	13	722	705	704	11	725	714	714	12	736
Primary ΔT, ΔT_R (°F)	245	249	12	273	245	250	12	274	246	250	12	275
Power (MWt)	975	975		1004	975	975		1004	975	975		1004

NOTE: Design and control uncertainties are included

The $T_{97.7}$ values are those that are not exceeded with 97.7% probability. If the distribution were normal these would equal the mean plus 2σ.

TABLE 3.2

PLANT EXPECTED CONDITIONS CONSIDERED IN
HETEROGENEOUS CORE THERMOFLUIDS ANALYSES

	First Core	Second Core
Nominal Inlet Temperature (°F)	704	711
Nominal Reactor ΔT (°F)	250	250

3.1.4 Loop Temperature Imbalance

The maximum cold leg loop-to-loop temperature imbalance is 34°F, which a plant control system design requirement.

Loop imbalance mixing tests were performed in the Inlet Plenum Feature Model at HEDL[4].

A test run consisted of injecting an electrolyte in a downcomer and measuring the steady state concentration in the inlet modules. Individual loop injection permitted the assessment of how that loop affected mixing in the 61 inlet modules. From these data, inlet module fluid temperatures due to loop temperatures imbalances were calculated. The results are shown in Figures 3.1 through 3.3.

A Monte Carlo type of analysis was performed in which the temperature imbalances in two of the loops were chosen at random (all values equally probable) and the third one adjusted so that their sum was zero, subject to the restraint of a maximum difference of 34°F between loops. The resulting inlet module 2σ temperature uncertainties are shown in Figure 3.4. The maximum 2σ value for all inlet modules is 4.6°F. The uncertainty in that value because of the experimental error in the measured loop mixing constants is $\pm$0.3°F giving an overall maximum 2σ bounding uncertainty of 4.9°F on inlet temperature. Even though the analysis shows that this applies to only the worst module (7 core assemblies), it has conservatively been applied to all assemblies.

1630 034

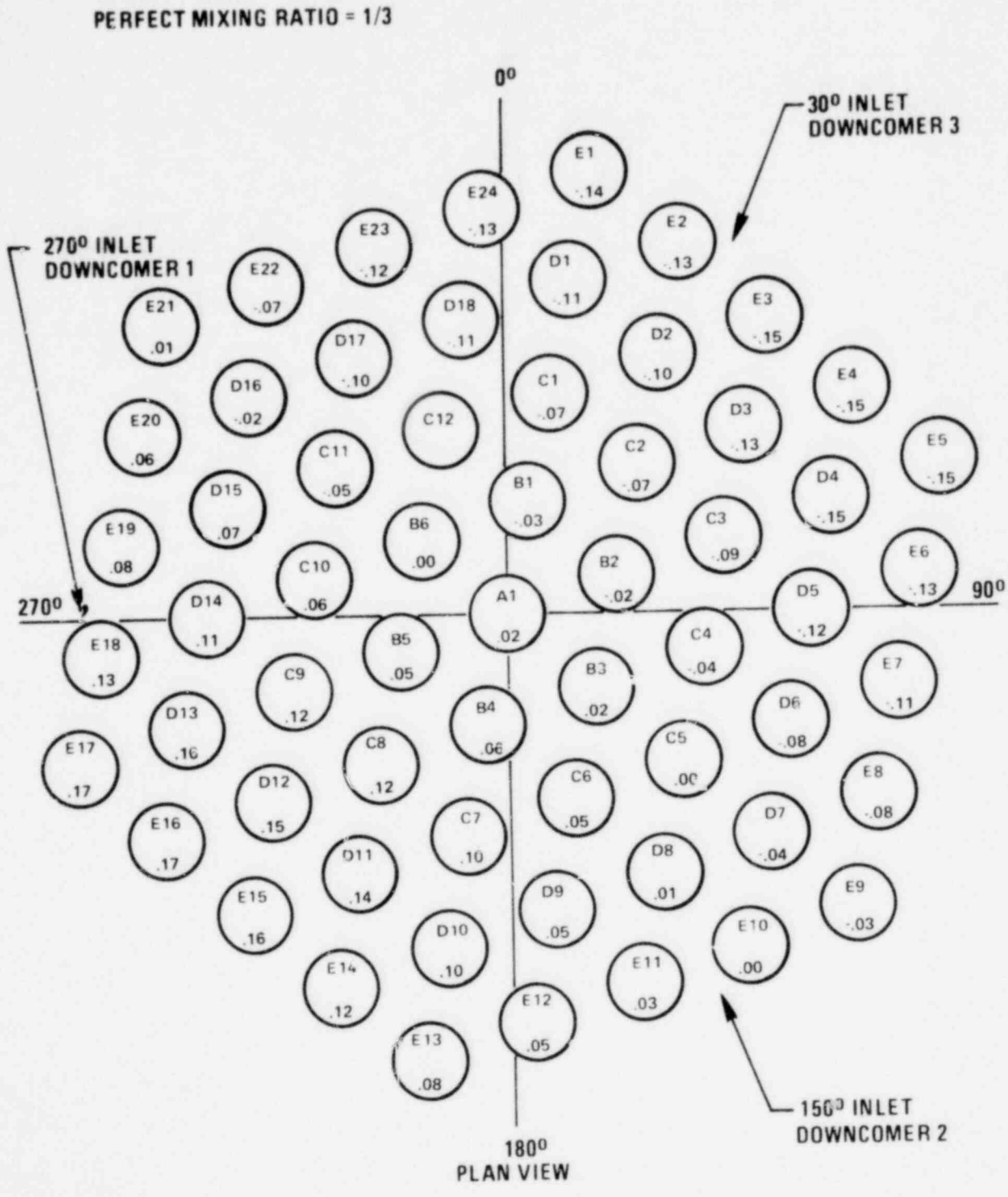

Figure 3-1. Deviation in Inlet Module Steady State Mixing Ratio from Perfect Mixing for 3 Loop 100% Flow and Injection in Loop #1.

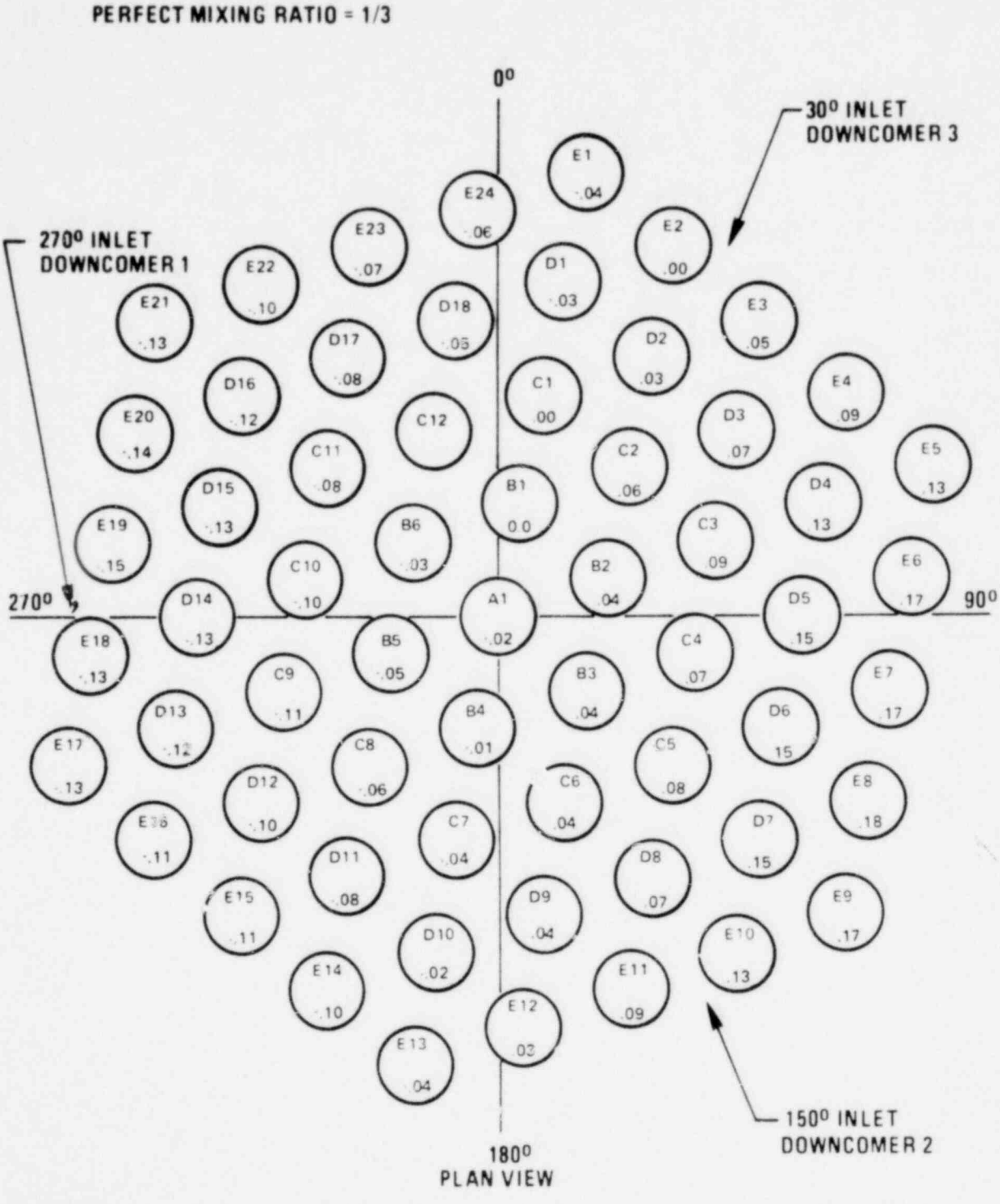

Figure 3-2. Deviation in Inlet Module Steady State Mixing Ratio from Perfect Mixing for 3 Loop 100% Flow and Injection in Loop = 2.

9926-3

1630 036

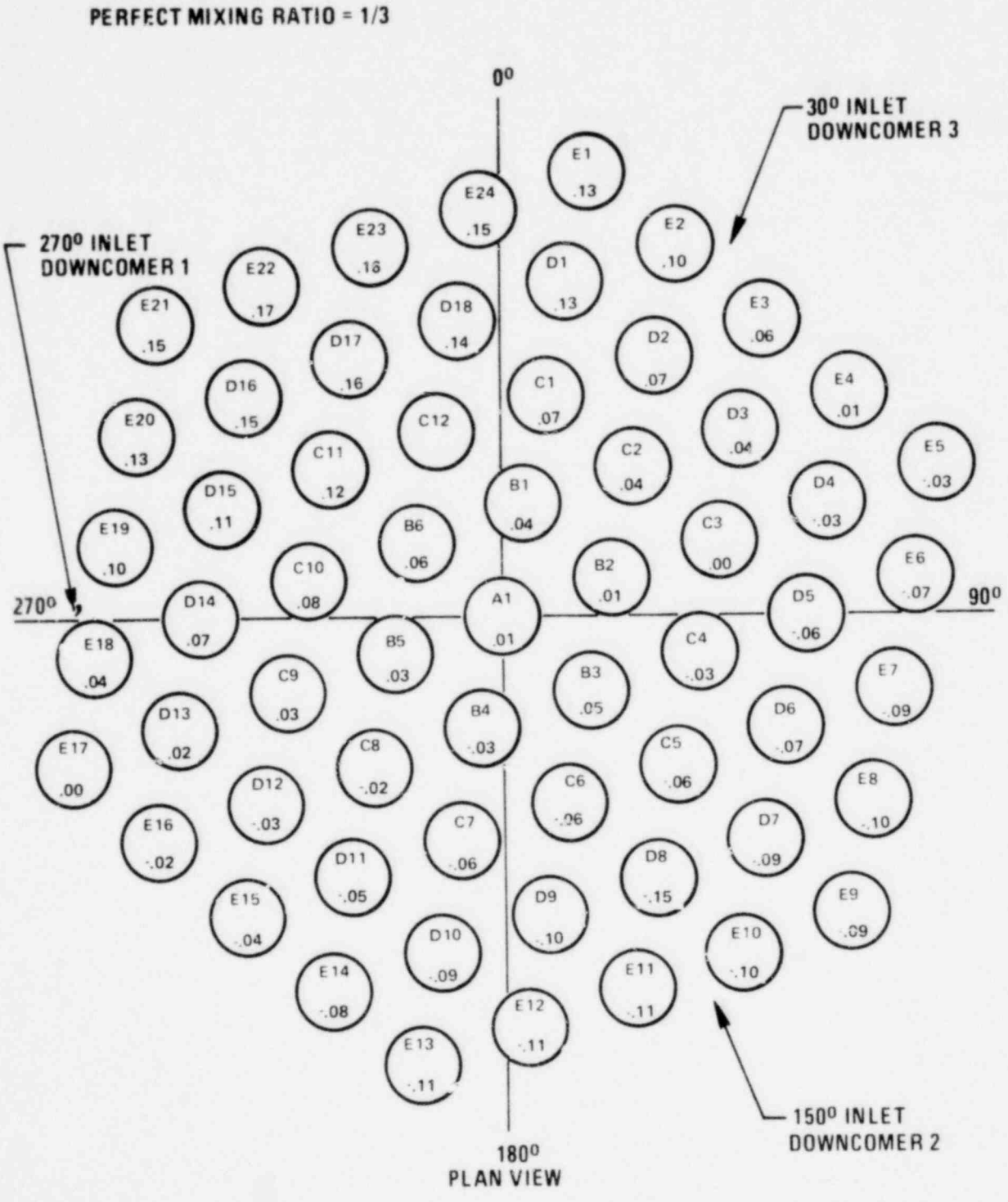

Figure 3-3. Deviation in Inlet Module Steady State Mixing Ratio from Perfect Mixing for 3 Loop 100% Flow and Injection in Loop #3.

9926-4

1630 037

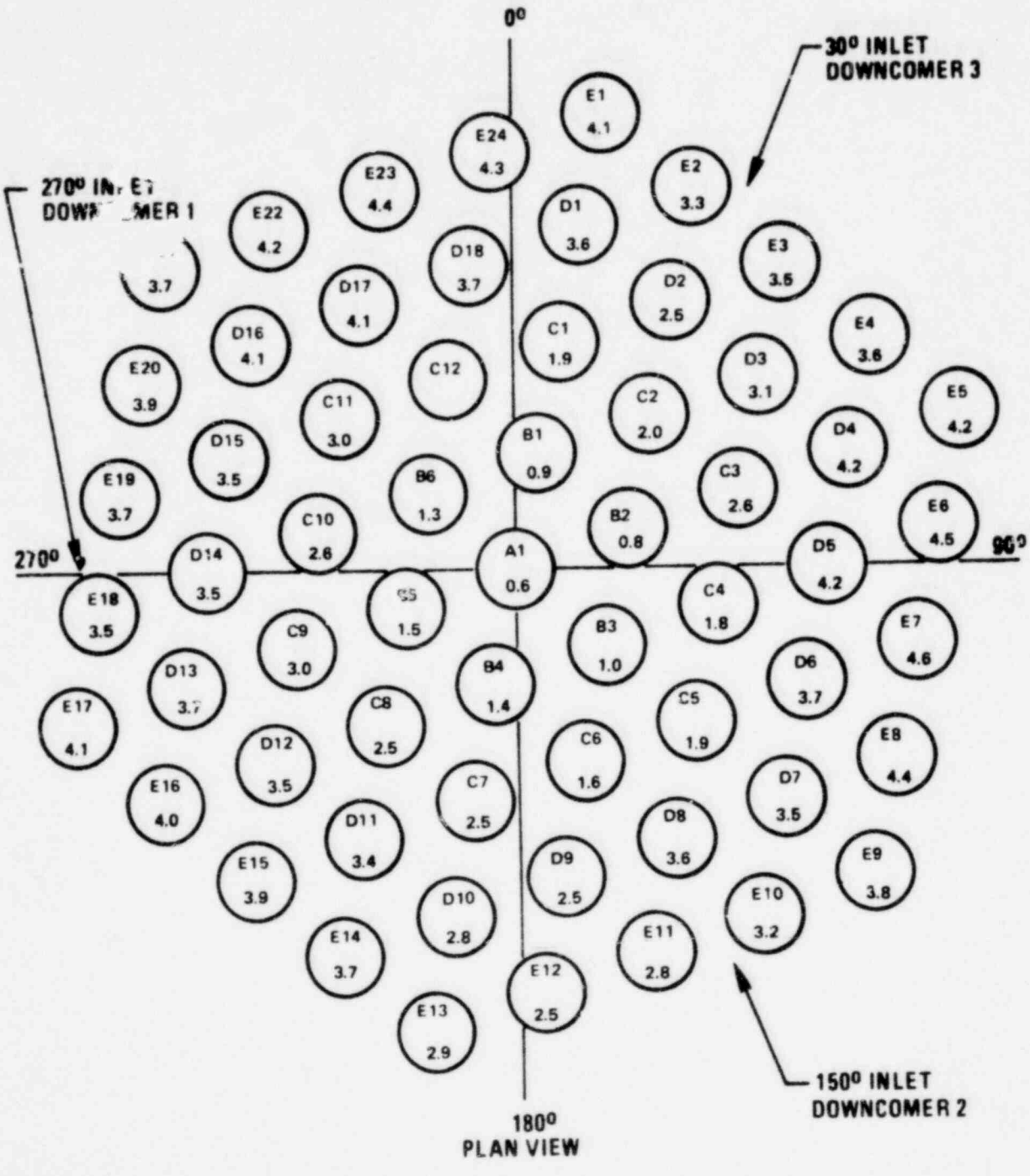

Figure 3-4. 2σ Inlet Module Temperature Uncertainty Based on a Loop Temperature Imbalance of up to 34°F, for 3-Loop Operation.

3.1.5 Inlet Flow Maldistribution

This factor accounts for uncertainties in the calculated assembly flow due to flow maldistribution in the lower and upper plena, internals structure tolerances (both these effects cause variation in the nominal static pressure profile), assembly orificing uncertainties, and loop flow imbalances.

The individual subfactors are shown in Table 3.5 and can be categorized under four headings:

1) Component Hydraulic Characteristics
2) Manufacturing Tolerances
3) Configuration
4) Systematic Error Interaction

Component Hydraulic Characterization

Variations due to component hydraulic characterization result from pressure drop and flow rate measurement errors during component flow testing and the accuracy with which the test article geometry is measured.

Systematic errors for the fuel assembly inlet and outlet nozzle flow tests[5] are estimated as

Flow rate, 200-1200 gpm,	±1% of reading
Differential pressure, 10-250 psi,	±1% of reading
Flow area	± 0.5%
Fluid density	Negligible

These uncertainties are judged to represent 2σ values based on previous experience with the experimental instrumentation. Therefore for $\Delta P \simeq KW^2$, the overall 3σ uncertainty in flow due to systematic errors is:

$$\frac{3}{2}\left[(.01)^2 + (.005)^2 + (.005)^2\right]^{\frac{1}{2}} = \underline{0.018}$$

The orifice configurations tested[5] probably will not be used for the final design because of potential cavitation problems. However, the random errors in the test data are judged to be typical of what will be obtained for the final configurations. Figure 3.5 shows a typical set of test data. Allowing for 1σ = 3% on pressure drop based on these previous data, the 3σ uncertainty in flow due to random errors is 0.045.

1630 039

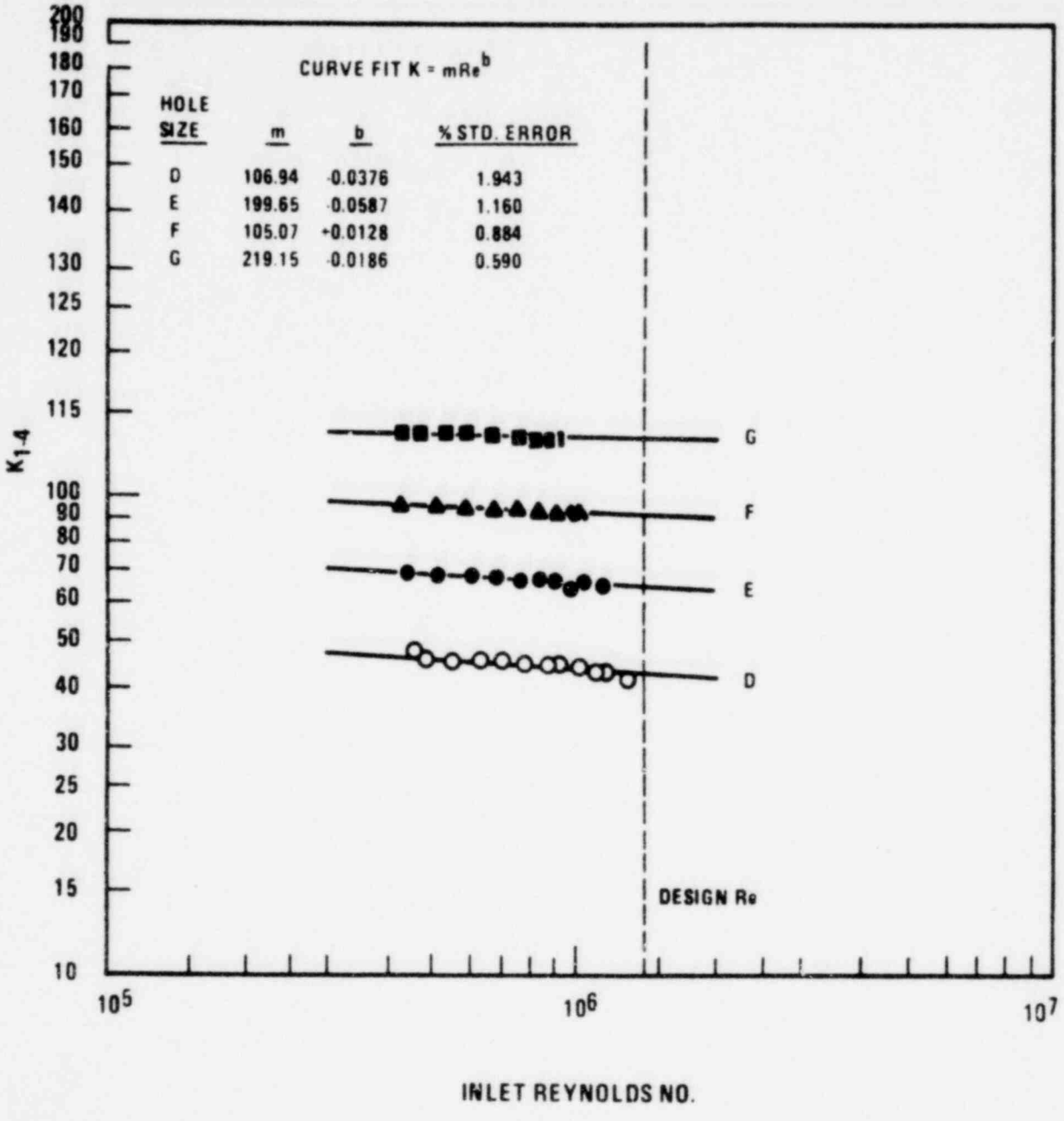

Figure 3-5. Fuel Assembly Inlet Nozzle Flow Resistance Versus Reynolds Number: Orifice Group No. 5.

4926-6

1630 040

Manufacturing Tolerances

A detailed analysis was performed of the major independent geometric parameters contributing to the fuel assembly hydraulic characteristics (inlet hole diameter, inlet nozzle diameter, orifice rounding, shield hole diameter). Each parameter was assumed to have a rectangular probability distribution within the tolerance limits specified on the design drawings. The rod bundle region was excluded as it is considered separately in the subchannel flow area analysis. The remaining uncertainties were combined statistically and the resulting bounding 3σ flow uncertainty due to manufacturing tolerances is 0.013.

Configuration

Inlet Plenum Feature Model (IPFM) test[4] data were obtained on flow maldistribution from the reactor inlet plenum to the Lower Inlet Module (LIM) for the homogeneous core configuration. The results of a typical run are shown in Figure 3.6, and the results of four runs are given in Table 3.3. A statistical analysis of the four-run average flow for each LIM showed a 3σ variation of 0.0138 based on 33 data points.

The effect of loop-to-loop flow variations was determined empirically by interpolating between the IPFM data for 3 loop and for 2 loop operation. IPFM 2 loop test[4] data showed a 3σ variation of 0.0268 in LIM flow, compared to 0.0138 for 3 loop operation. The maximum bounding loop-to-loop flow variation is $\pm$3.37% of nominal, resulting in a maximum difference between loops of 6.74% of nominal. Since 2 loop operation is equivalent to the case of 3 loop operation with 100% flow reduction in one loop, the case of 6.74% flow variation may be estimated by interpolating between the 3 loop and 2 loop results:

3σ variation in LIM flow including loop-to-loop variation =
$(6.74/100)(0.0260-0.0138)+0.0138 = 0.0146$

This conservatively assumes that the loop-to-loop variation is at its maximum value.

Allowing for possible differences between homogeneous and heterogeneous core configurations, a value of 0.020 will be used. This is a

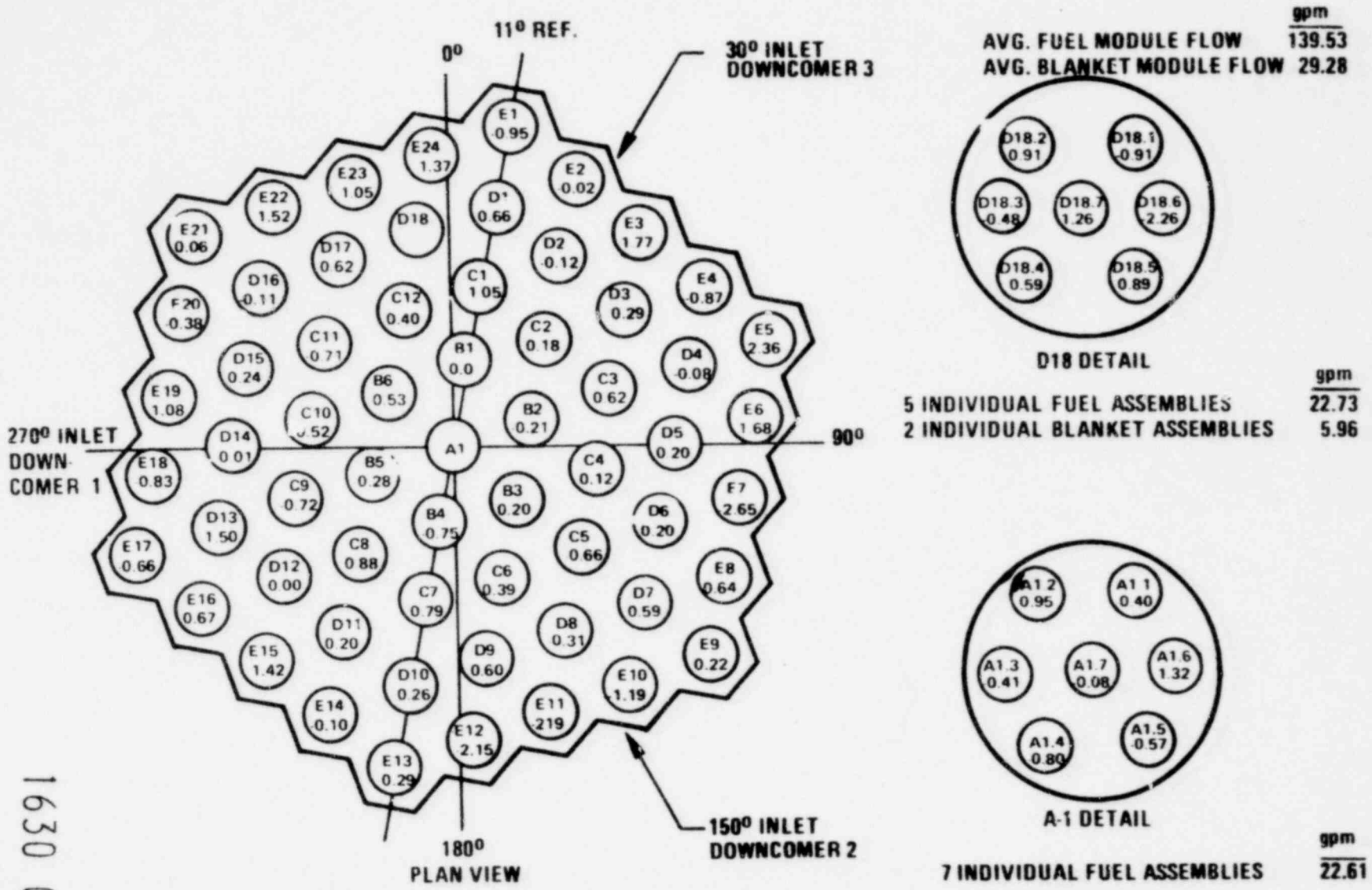

Figure 3-6. Core Flow Distribution Map, Run A5.2, 103.8%, 3-Loop Flow, 140°F.

TABLE 3.3

RESULTS OF FOUR IPFM FLOW
DISTRIBUTION TESTS AT ~100% FLOW, 3 LOOPS

	FLOW DEVIATION FROM AVERAGE, %			
LIM	RUN 1	RUN 2	RUN 3	RUN 4
B1	.00	-.20	-.21	-.19
B6	.53	.07	.15	.14
B5	-.28	-.05	.03	-.07
B4	-.75	-.46	-.59	-.53
B3	.20	.26	.25	.20
B2	-.21	-.15	.09	-.12
C1	-1.05	-1.56	-.99	-.96
C12	.40	.36	.31	.12
C11	-.71	-.81	-.74	-.78
C10	.52	.34	.33	.26
C9	-.72	-.80	-.66	-.68
C8	.88	.55	.46	.61
C7	.79	.33	.60	.44
C6	.39	.20	.20	.36
C5	-.66	-.37	-.34	-.37
C4	.12	.40	.28	.34
C3	-.62	-.09	.16	.01
C2	.18	.10	.07	.04
D1	.66	.39	.42	.43
D16	-.11	.14	.02	.14
D15	.24	.17	.07	.17
D14	-.01	.02	-.20	.11
D13	-1.50	-.97	-1.03	-1.26
D11	.20	.16	.05	-.09
D9	.60	.59	.20	.50
D8	-.31	-.14	-.17	-.25
D7	.59	.83	.85	.75
D6	.05	.35	.03	.50
D5	.20	-.06	-.05	.01
D4	-.08	.11	-.07	-.16
D3	.29	.01	-.01	-.00
D2	-.12	.27	.24	.29
D10	.26	.02	.23	.04

1630 043

TABLE 3.4

RESULTS OF FOUR IPFM ASSEMBLY-TO-ASSEMBLY FLOW DISTRIBUTION TEST RESULTS AT ~100% FLOW, 3 LOOPS

Assembly	Location Within LIM	Flow Deviation From Average, % Run 1	2	3	4
1	Peripheral	- .40	- .49	- .45	.36
2		.95	.94	1.07	.91
3		- .41	- .07	- .09	- .24
4		- .80	-1.18	-1.14	-1.21
5		- .57	- .60	- .61	- .73
6		1.32	1.20	1.13	1.00
7	Central	-. 08	.12	.09	- .08

conservative estimate empirically based upon the observed differences between fuel assembly and radial blanket assembly (Section 4.1.2) LIM flow variations in the IPFM test.

Assembly-to-assembly variation was determined by measuring the flow variation for the seven assemblies within a LIM. The data for four runs are given in Table 3.4.

The average peripheral assembly flow rate was nearly identical to the central assembly flow rate. The four-run average flow for each assembly showed a 3σ variation of 0.0242 based on 7 data points. This value includes random variations among similarly located assemblies as well as any "side effects".

Systematic Error Interaction

This factor accounts for systematic errors in the calibration of one core component affecting the flow to another core component. For example, if systematic errors cause the blanket assemblies to be overcooled they will result in the fuel assemblies being undercooled, and vice versa. From Table 4.2, blanket assemblies can have 1.8% flow increase (3σ) due to systematic errors. An analysis of the reactor flow distribution with this change in the flow impedance of all blanket assemblies resulted in a decrease in fuel assembly flow by a factor of 1.002. Thus the 3σ uncertainty in fuel assembly flow due to systematic error interaction is calculated to be 0.002.

Overall

The Inlet Flow Maldistribution 3σ subfactors are listed in Table 3.5. The overall factor calculated as the root-mean-square of the subfactors ($F = 1 + (\Sigma(F_i-1)^2)^{1/2}$) is also shown. The effect of the small number of data points for several subfactors on the overall tolerance interval is negligible as shown in Section 2.4.

An additional direct bias of 1.02 is applied based on engineering judgement to blanket any additional uncertainties which may be uncovered in the heterogeneous core design. Additional data from the fuel assembly flow and vibration test and from the inlet nozzle flow test (see Table 6.11) will be utilized to update these uncertainties for the FSAR.

TABLE 3.5

FUEL ASSEMBLY INLET FLOW MALDISTRIBUTION SUBFACTORS (3σ)

Hydraulic Characteristics		
Systematic	1.018	
Random	1.045	
Manufacturing Tolerances	1.013	
Configuration		
Among LIM's	1.02	(33)*
Among Assemblies	1.024	(7)*
Systematic Error Interaction	1.002	
Overall (3σ)	1.059	

*Number of data points shown in parentheses

1630 046

3.1.6 Flow Distribution Calculational Uncertainty

The coolant flow and temperature distribution within the various subchannels of a wire wrapped assembly is calculated by subchannel analysis codes, e.g., CØTEC, CØBRA and THI-3D.

Empirical factors in the CØTEC code to model the effects of turbulent mixing, pumping (displacement of coolant by wire wrap), sweeping (forced flow following the wire wrap) in the interior channels and swirl in the edge channels are selected by calibration of the code against available experimental data. An extensive comparison of the CØTEC code with experimental data from ORNL (19 rod bundle FFM tests)[6], ANL (91 rod bundle mixing tests)[7,8], HEDL (217 rod bundle mixing tests)[9], ARD (11:1 scale section of a 217 pin wire wrapped rod bundle air flow test)[10], and JOYO (experimental study on coolant mixing effect in JOYO 19 rod blanket assembly)[11] was performed.

The 11:1 scale tests[10] were selected as providing the most detailed data for the calibration of the CØTEC factors for pumping, sweeping and swirl. These factors were then used in CØTEC analyses of the HEDL data[9] where the turbulent mixing factor, which has a secondary effect, was adjusted to provide the best fit. Approximately 3000 data points from the HEDL tests were compared with the CØTEC predictions using the final calibration. Typical results are shown in Figures 3.7, 3.8 and 3.9. Figure 3.7 shows experimental data (average of four runs) 12 inches downstream of the injection plane along the row of channels with the highest concentrations. The data for all of the channels at the 12-inch level were used as input for a CØTEC analysis, and the results at 24 inches and 36 inches are compared to the experimental data in Figures 3.8 and 3.9.

CØTEC predictions are also compared with the ORNL data[6] in Figures 3.10 through 3.13 for a heated 19-rod bundle in sodium. The present CØTEC calibration conservatively overpredicts the peak temperatures in the ORNL tests.

Regarding the statistical calibration uncertainty, the calibration analysis treats the differences between the CØTEC calculated temperatures and the measured or experimentally determined temperatures as a random

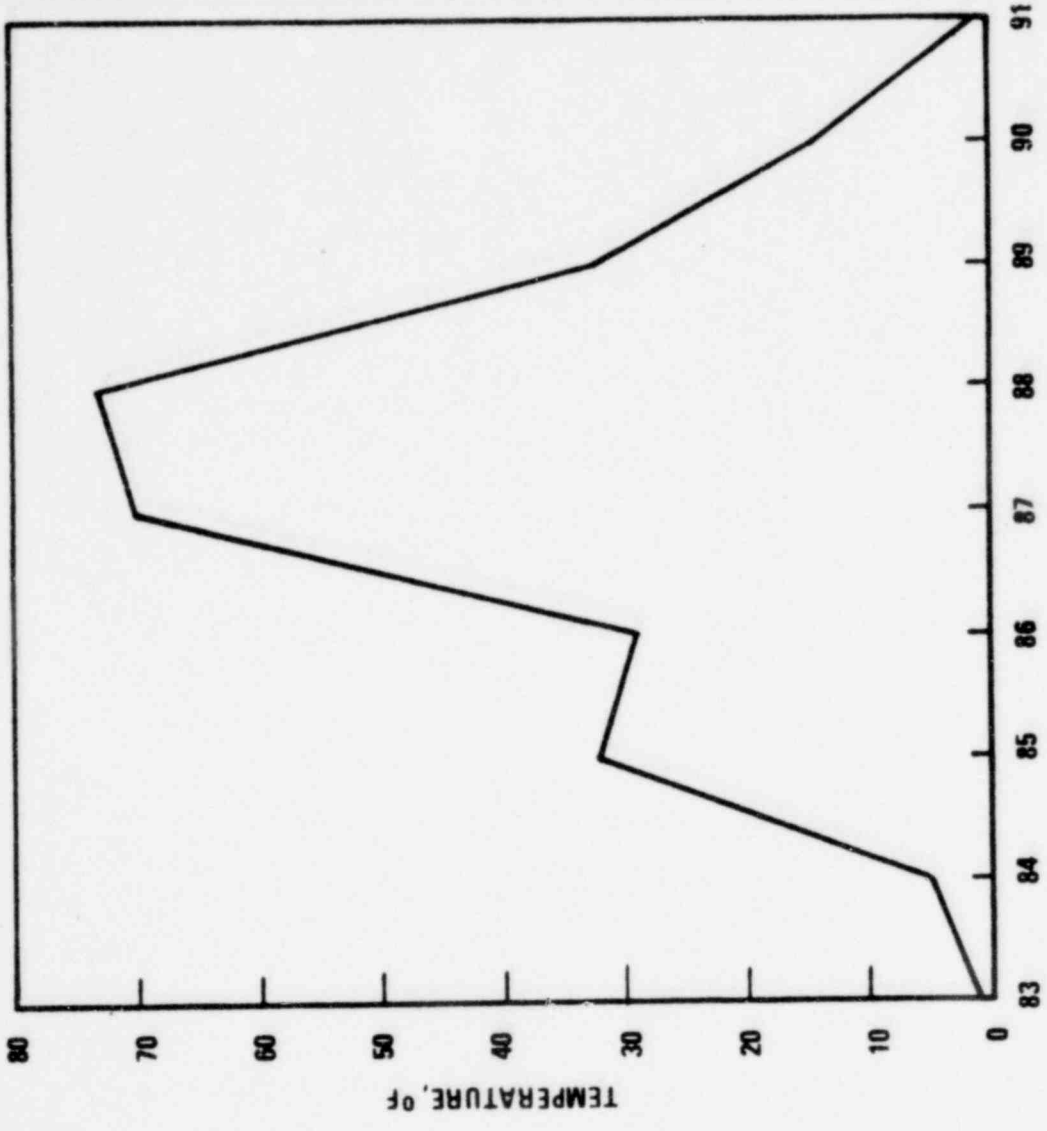

Figure 3-7. 12-Inch HEDL Experimental Data

9926-8

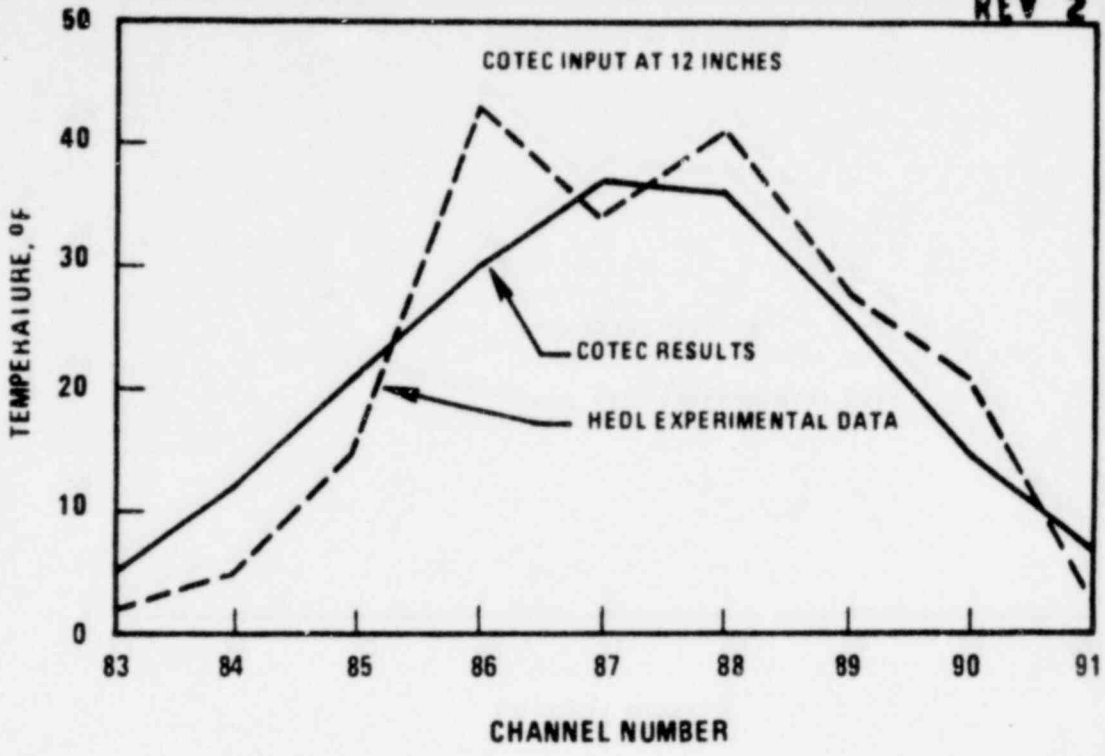

Figure 3-8. Comparison Between COTEC Results and HEDL Data at 24 Inches

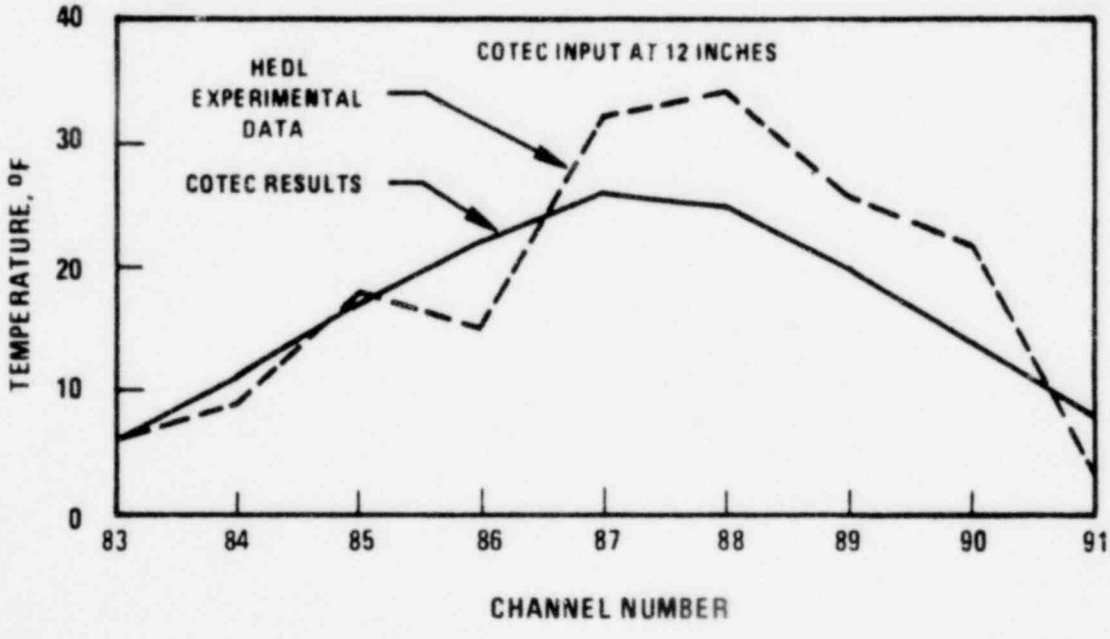

Figure 3-9. Comparison Between COTEC Results and HEDL Data at 36 Inches

9926-9.10

1630 049

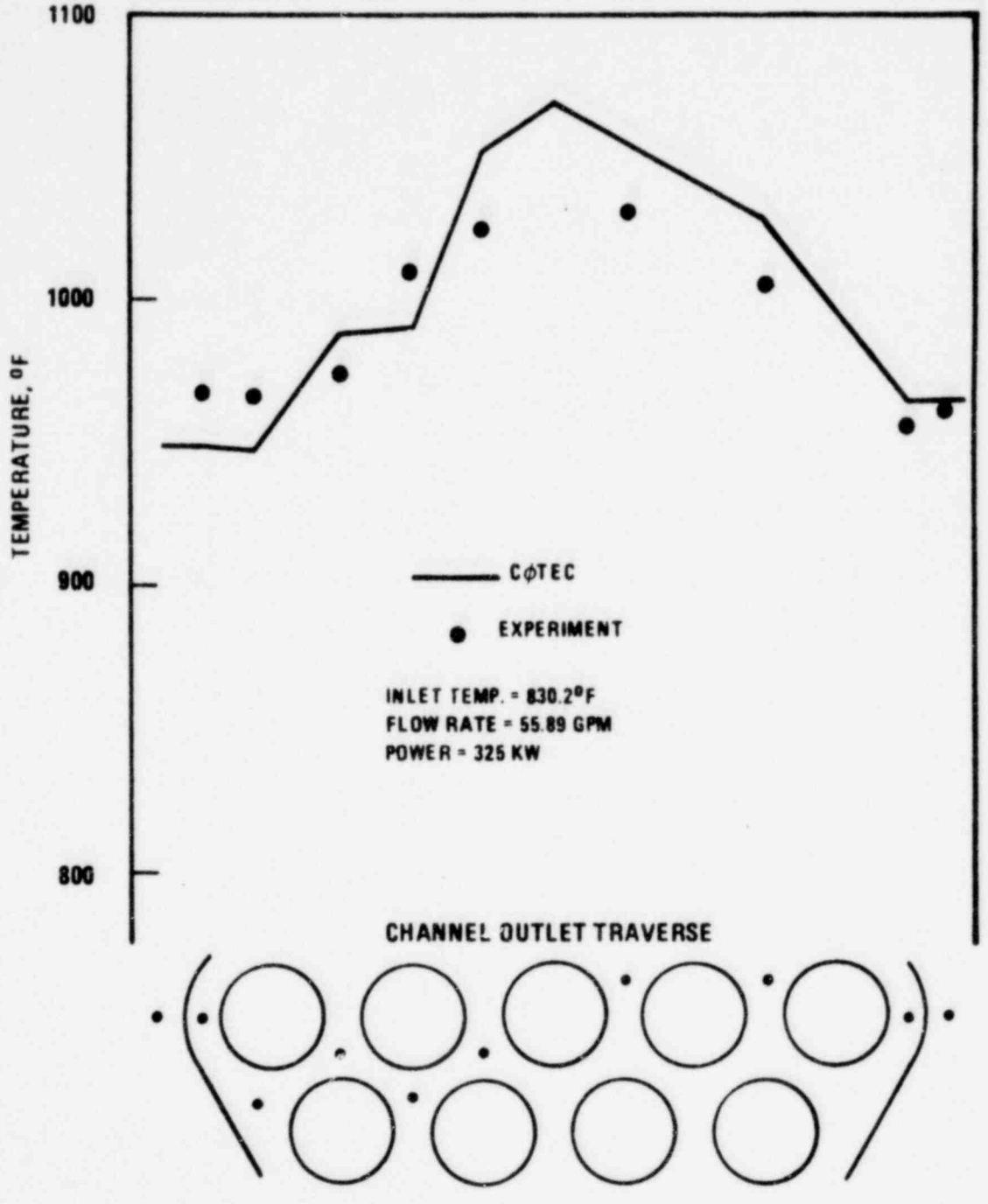

Figure 3-10. ORNL Test Series # 2, Test = 02, Run # 105

9926-11

1630 050

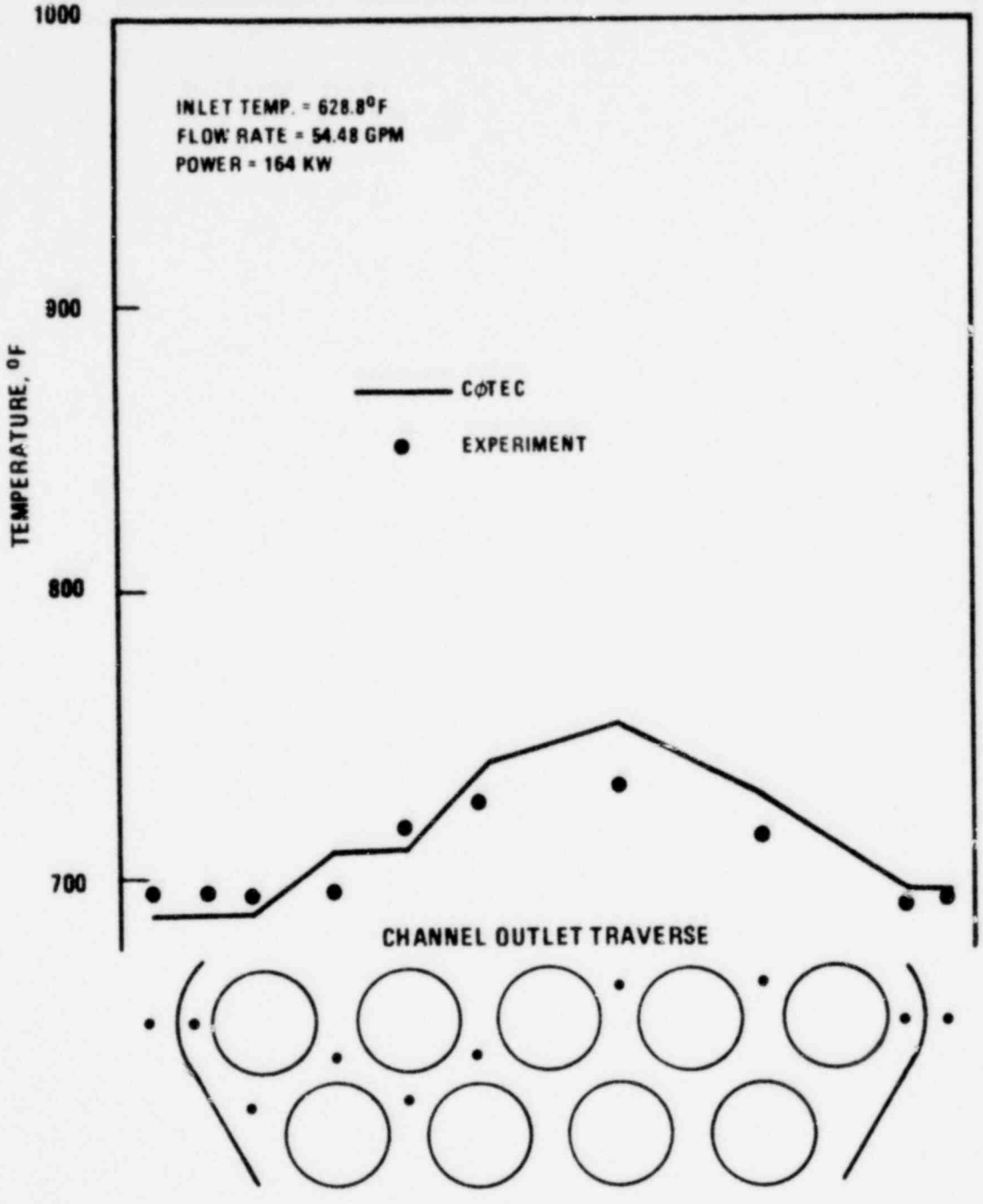

Figure 3-11. ORNL Test Series #2 Test #02 Run #109

9926-12

1630 051

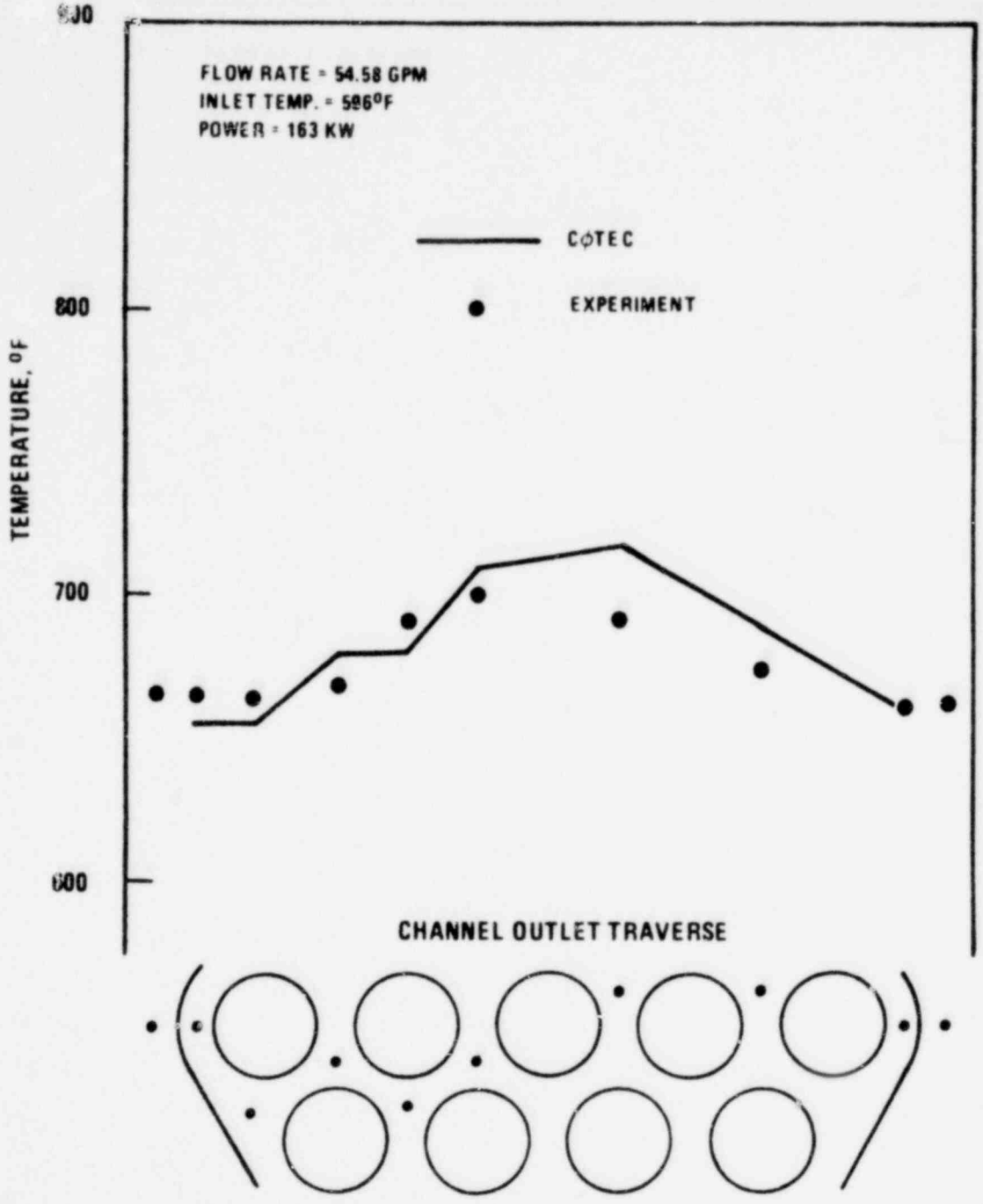

Figure 3-12. ORNL. Test Series #2. Test #3, Run #201

9926-13

1630 052

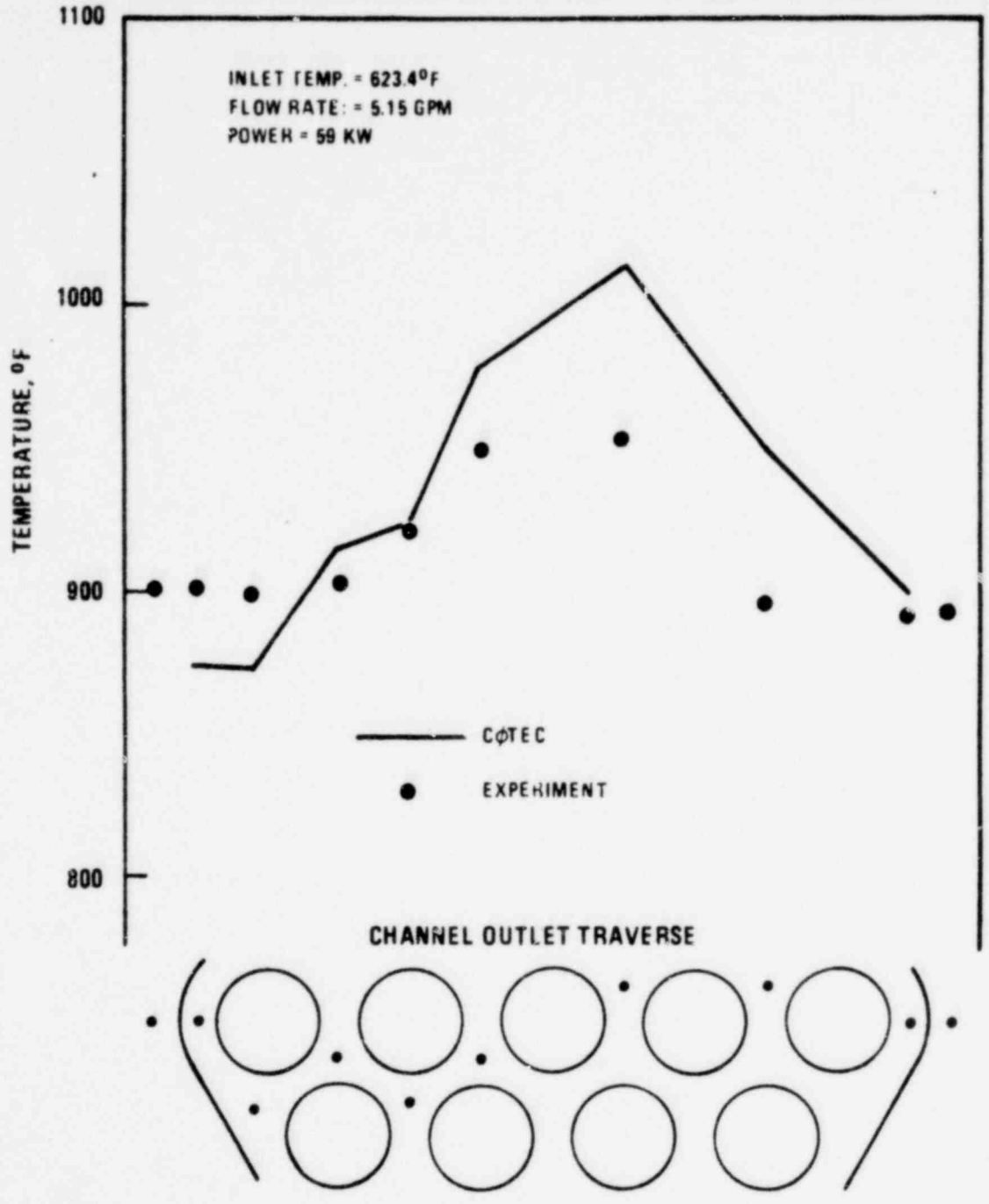

Figure 3-13 ORNL Test Series = 2, Test = 04, Run = 205

9926-14

1630 053

variable, i.e., analogous to the displacement of a particle from its initial position while undergoing a one-dimensional random walk. The absence of perfect agreement between CØTEC and experimental data is expected and it must be attributed to the inability of the CØTEC mixing model to completely represent the axial and transverse flows in a wire wrapped bundle. Thus, it can be deduced that the local transverse coolant temperature distribution directly affects the differential increment of temperature calculational uncertainty, while a flat temperature profile would not contribute to a temperature calculation uncertainty. Since the average coolant temperature gradient in the assembly, $(T_{max}-T_{min})$ is a coarse measure of the coolant temperature profile, the following equation[12] represents the uncertainty associated with the use of CØTEC:

$$\delta T_{1\sigma}(x) = \left[C_{1\sigma_o} \int^{x} (T_{max}(\xi) - T_{min}(\xi))^2 \, d\xi\right]^{1/2} \qquad (3.8)$$

where $\delta T_{1\sigma}(x)$ = temperature variation (uncertainty at x)

$T_{max}(\xi)$ = maximum coolant temperature at elevation $x = \xi$

$T_{min}(\xi)$ = minimum coolant temperature at elevation $x = \xi$

x = elevation

C = experimentally determined coefficient = 0.4376×10^{-4} in^{-1}.

The coefficient C was determined using an earlier CØTEC calibration which did not compare as well with the data as the present calibration, and is therefore conservative.

The integrand depends upon the transverse gradient of coolant temperature within a one-sixth sector of the wire wrapped 217 pin bundle and will vary from assembly to assembly with flow rate and power shape. Thus, to obtain an uncertainty interval for the coolant temperature and concomitant hot channel factor representative of all subassemblies of a specified type (e.g., fuel or blanket), it was necessary to envelope the uncertainties by estimating the assembly flow requirement and selecting the most critical assemblies (i.e., those with greatest power skew and with largest total power) for analysis. CØTEC calculations were performed for these selected assemblies to compute the estimated uncertainty intervals for each critical assembly.

Numerical integration with Euler's method using a 2-inch step size was used to calculate the temperature uncertainties. The temperature uncertainty increases with elevation and the uncertainty at the top of the core was used to calculate the hot channel factor. This is the approximate location of the cladding peak temperature elevation. The largest temperature uncertainty and hot channel factor for the fuel assemblies occurs in the peak skew fuel assembly. The analytically derived statistical hot channel factor is 1.054 (3σ). Adoption of the maximum calculated value of the hot channel factor as an envelope for all fuel assemblies is obviously conservative.

In addition to the aforementioned factors in CØTEC, it is also necessary to specify the flow split among the several types of channels (interior, side and corner) because in wire wrapped rod bundles, the flow split is not found to agree with that predicted on the basis of the hydraulic diameter of the channels. The results of a number of experiments on the ratio of side to average channel velocity are shown in Table 3.6. The information in Table 3.6 was obtained from the referenced reports and from discussions with the experimenters. The analysis of these results was limited to the turbulent flow regime, so the laminar flow data of Chen and Todreas[13] (Re = 640) were omitted. The dye tracer data of Pedersen, et. al.[8,14] were rejected as being inconsistent with the remaining data including Pederson's thermal tracer data. The reduced side wire data of Graves and Catton[15], although confirming the remaining data, were not included in the analysis as not prototypic of CRBRP geometry. For the remaining seven investigations, the mean ratio of side to average channel velocity, $\overline{U}_S/\overline{U}$, was 1.015 $\pm$ 0.042 (2σ). These results are consistent with $\overline{U}_S/\overline{U}$ = 1.00 which was selected for the nominal CØTEC analyses and with the maximum expected uncertainties reported in Table 3.6. The uncertainty factor on $\overline{U}_S$ will be conservatively taken as 1.02 $\pm$ 0.05 (2σ). Interior channel flow uncertainty is found from the relation (total side channel flow) x (side channel flow uncertainty) = - (total interior channel flow) x (interior channel flow uncertainty). Thus, for a 217 rod bundle, the corresponding uncertainty factor on interior coolant temperature rise, conservatively neglecting inter-channel mixing is 1.005 $\pm$ 0.013 (2σ) or 1.005 $\pm$ 0.020 (3σ), i.e., direct: 1.005; statistical (3σ): 1.020, due to flow split uncertainty.

The overall statistical uncertainty combining the CØTEC calibration uncertainty and flow split uncertainty is 1.058 (3σ).

In addition to the statistical uncertainty, a direct factor of 1.03 is also applied. This includes the direct flow split factor of 1.005 as well as additional margin, which based on previous experience with sodium heat transfer experiments in rod bundles is judged to be sufficient to cover the testing biases and uncertainties which might be uncovered during the heat transfer testing at ORNL of a 61 rod bundle in liquid sodium (See Table 6.11) since the experimental data for the 217 pin fuel assembly were derived from mixing tests which measured salt solution diffusion or from velocity measurement tests in simulation fluids (water, air). The code calibration and uncertainty data from the 61 rod bundle test in sodium will be used in the FSAR evaluation.

TABLE 3.6

RATIO OF SIDE SUBCHANNEL AXIAL AVERAGE VELOCITY TO BUNDLE AXIAL AVERAGE VELOCITY

RODS-IN-BUNDLE	EXPERIMENTER	$(\bar{U}_s/\bar{U})_{nominal}$	REYNOLDS NUMBER	METHOD	MAXIMUM EXPECTED ERROR
7	Ginsberg-Lorenz (Reference 16)	1.00†	13,000-17,000	Isokinetic	
19	Graves & Catton (Reference 15)	1.00	10,000-90,000	Salt Tracer	±5%
19	Graves & Catton* (Reference 15)	1.00	10,000-90,000	Salt Tracer	±5%
61	Chen-Todreas	1.1[illegible]	640	Laser Beam	±4%
61	Chen-Todreas (Reference 13)	1.04	4500	Laser Beam	±4%
91	Pedersen, et al.	1.17	5,000-20,000	Dye Tracer	±4%
91	Pedersen, et al. (References 8, 14)	1.03	5,000-20,000	Thermal Tracer	±4%
91	Lorenz, et al. (Reference 17)	0.99	9,000-25,000	Isokinetic	
217	Graves & Catton (Reference 15)	1.00	10,000-90,000	Salt Tracer	±5%
217	Graves & Catton* (Reference 15)	1.00	10,000-90,000	Salt Tracer	±5%
217**	Bartholet, et al. (Reference 18)	1.04**	73,000	Pitot Tube	±5%

*Side channel area decreased by reducing wire wrap diameter;

**Section of 217 rod bundle. $\bar{U}_s/\bar{U}$ converted to full bundle;

†All 12 subchannels sampled.

3.1.7 Wire Wrap Orientation

Due to the swirl flow induced by the wire wrap in the peripheral channels, the flow and temperature distribution in the assembly depends slightly on the relative orientation of the wire wrap and the power skew. An analysis conducted with the CØTEC code, investigating the power skew range in CRBRP fuel assemblies and the six possible orientations of the wire wrap, indicated a maximum bounding deviation in the hot channel ΔT of the order of 1%.

3.1.8 Subchannel Flow Area

An analysis was made of the effects of rod bundle dimensional tolerances and fuel rod bowing on the hot channel coolant temperature. The rod diameter, wire wrap diameter and duct inside width were each assumed to have rectangular probability distributions within the tolerance limits specified on the design drawings. The actual distributions of dimensions of fabricated fuel assembly components are expected to be available for the FSAR final hot channel factor analyses. All of the rods and all of the wires within a fuel assembly were assumed to have the same diameters. This assumption is reasonable in that each lot of rod cladding and of wire is sufficient to supply more than one fuel assembly, and leads to more conservative results than allowing the diameters to vary. The average rod spacing, S, for each subchannel was assumed to have a rectangular probability distribution in the range $0 \leq S \leq 2S_{nom}$, and the rod spacings for the various subchannels were assumed to be independent.

COBRA I analyses were performed for the cases of a) a single nested subchannel ($S = 0$), b) six nested subchannels surrounding the hot rod, and c) the hot subchannel and the three adjacent subchannels all nested. From the results of these analyses, the influence of reduced flow in one subchannel on the temperature distribution among all subchannels was determined.

The overall 3σ uncertainty in hot channel coolant temperature rise due to uncertainties in rod, wire and duct dimensions and rod spacings, and including the influence of the other subchannels, was calculated by the preceding bounding analyses to be 0.019.

This uncertainty applies at beginning of life. The effect of irradiation-induced swelling of rod, wire and duct was analyzed and was found to result in reduced temperatures in the hot channel. Therefore, it is conservative to apply the above uncertainty throughout life.

There is a tendency for thermally-induced bowing to cause all of the rods to bow toward the hottest channel. However, the thermal compressive force was calculated to be negligible compared with the experimentally determined bundle compressive forces. Therefore, thermal bow will not significantly change the subchannel flow area.

In evaluating the corresponding film temperature drop hot channel factor, it was found that the effect of the decrease in the unit cell hydraulic diameter was dominant with respect to the effect of the decrease in the Nusselt number. The effect of the change in pitch-to-diameter ratio on the circumferential temperature distribution was minimal. Thus, a higher value of the film heat transfer coefficient and consequently, a film subfactor less than 1.0 will result. Conservatively, a value equal to unity was adopted.

3.1.9 Film Heat Transfer Coefficient

Liquid metal heat transfer data for parallel flow through rod bundles were reviewed in Reference 19. A conservative design correlation was selected in Reference 19 for the rod pitch-to-diameter ratio range $1.2 \leq P/D \leq 1.3$ corresponding to that in CRBRP fuel assemblies. The data base is shown in Figures 3.14 to 3.16 together with the design correlation which is designated Curve 1. A 3σ uncertainty of 0.12 was recommended based on the deviations of the data points overpredicted by the correlation.

The analysis was repeated taking into account the variation among investigators, which reduced the number of data sets to $n = 6$. However, it was found that applying Equation (2.8), the new analysis resulted in lower cladding temperatures at PEOV conditions and lower fuel centerline temperatures than the correlation recommended in Reference 19. Therefore, the latter correlation is conservative and will still be used.

As a further indication of the conservatism in the correlation, it may be noted that in the range of interest, the correlation results in lower heat transfer coefficients than the theoretical lower limit calculated for the case of turbulent flow through unbaffled rod bundles, under conditions of uniform heat flux at the inside surface of the cladding, with heat transfer by molecular conduction only through the sodium[20].

1630 059

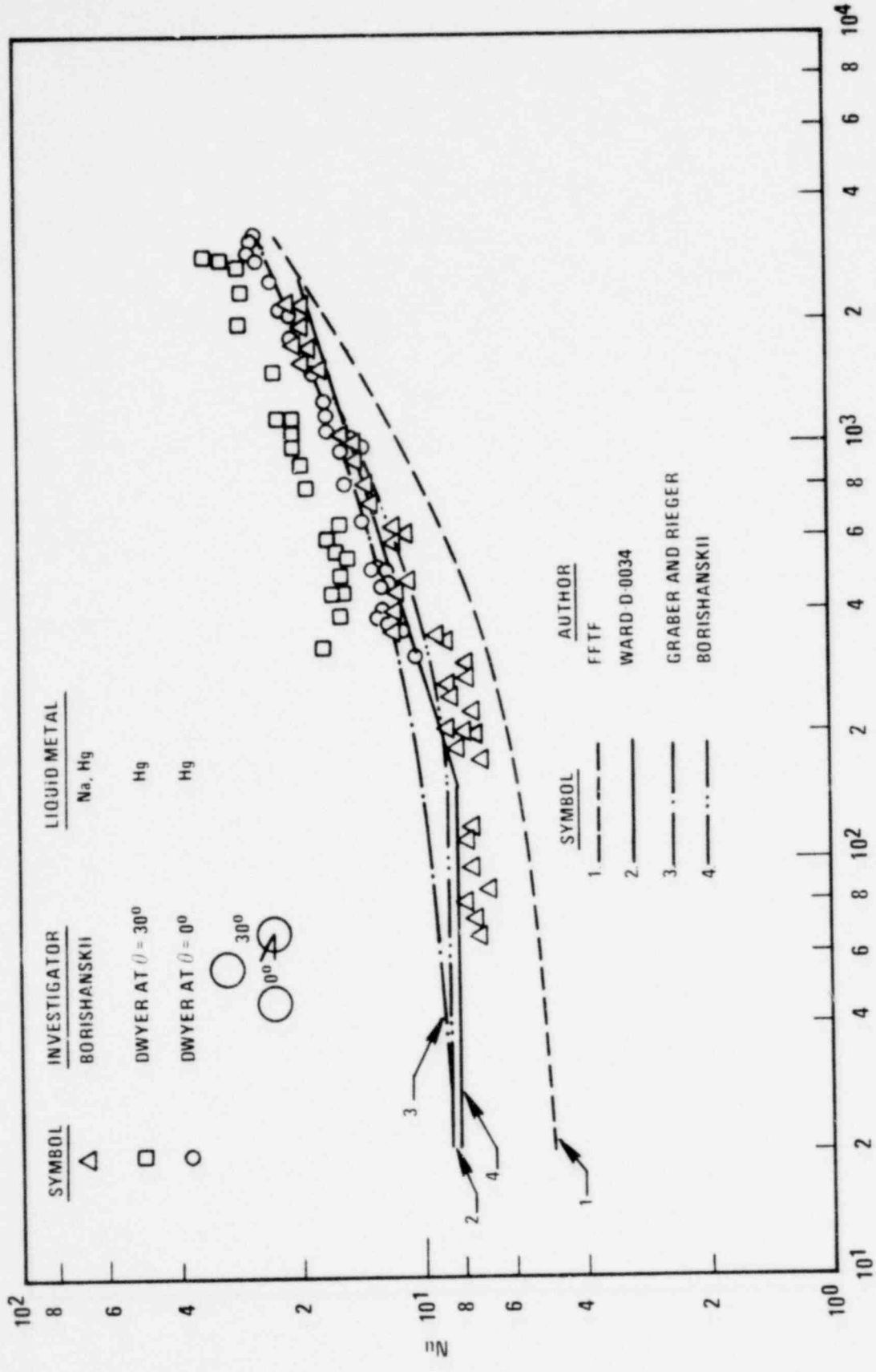

Figure 3-14. Comparison of Predicted and Experimental Results for P/D = 1.3

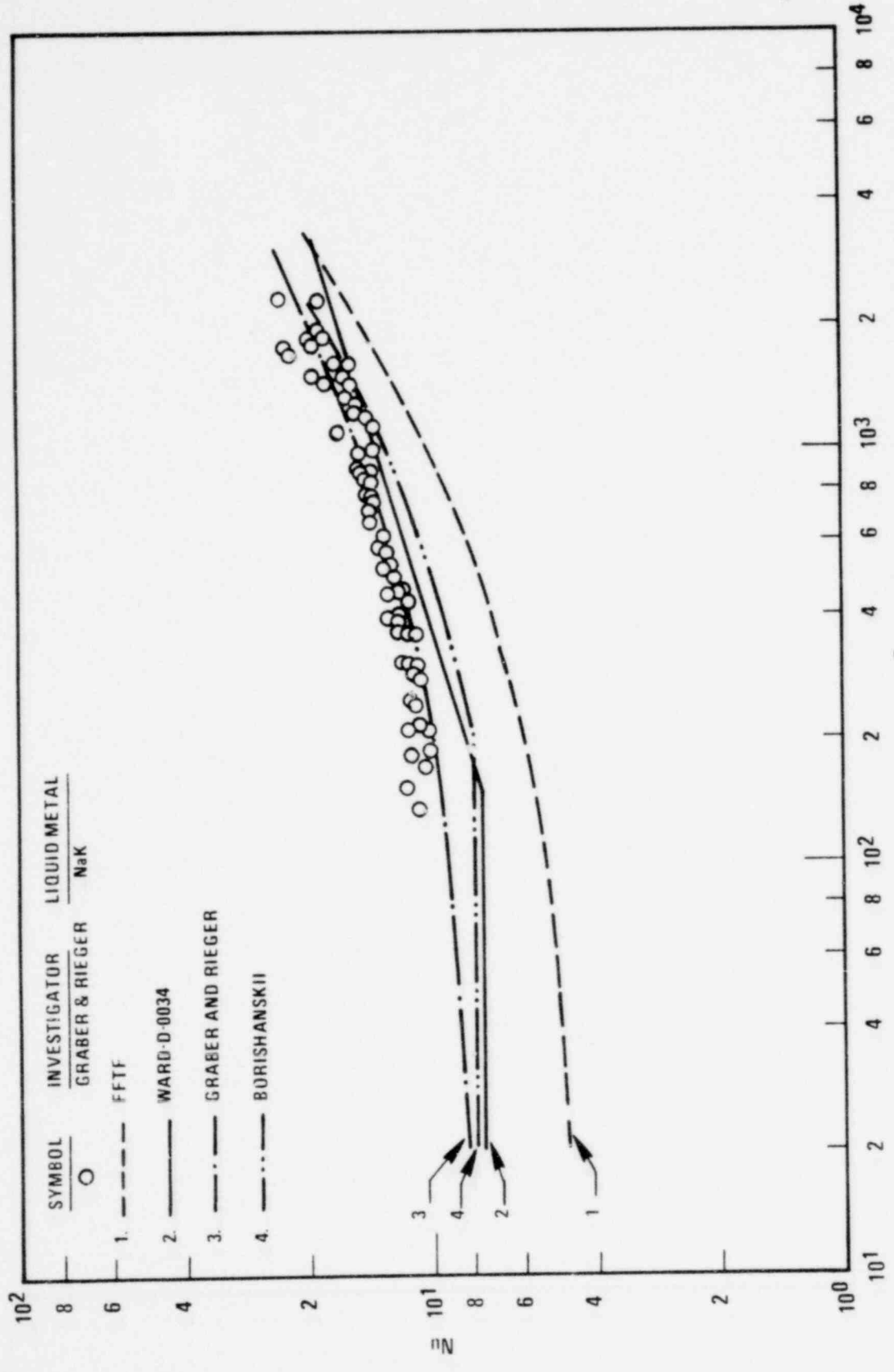

Figure 3-15. Comparison of Predicted and Experimental Results for P/D = 1.25

9926-16

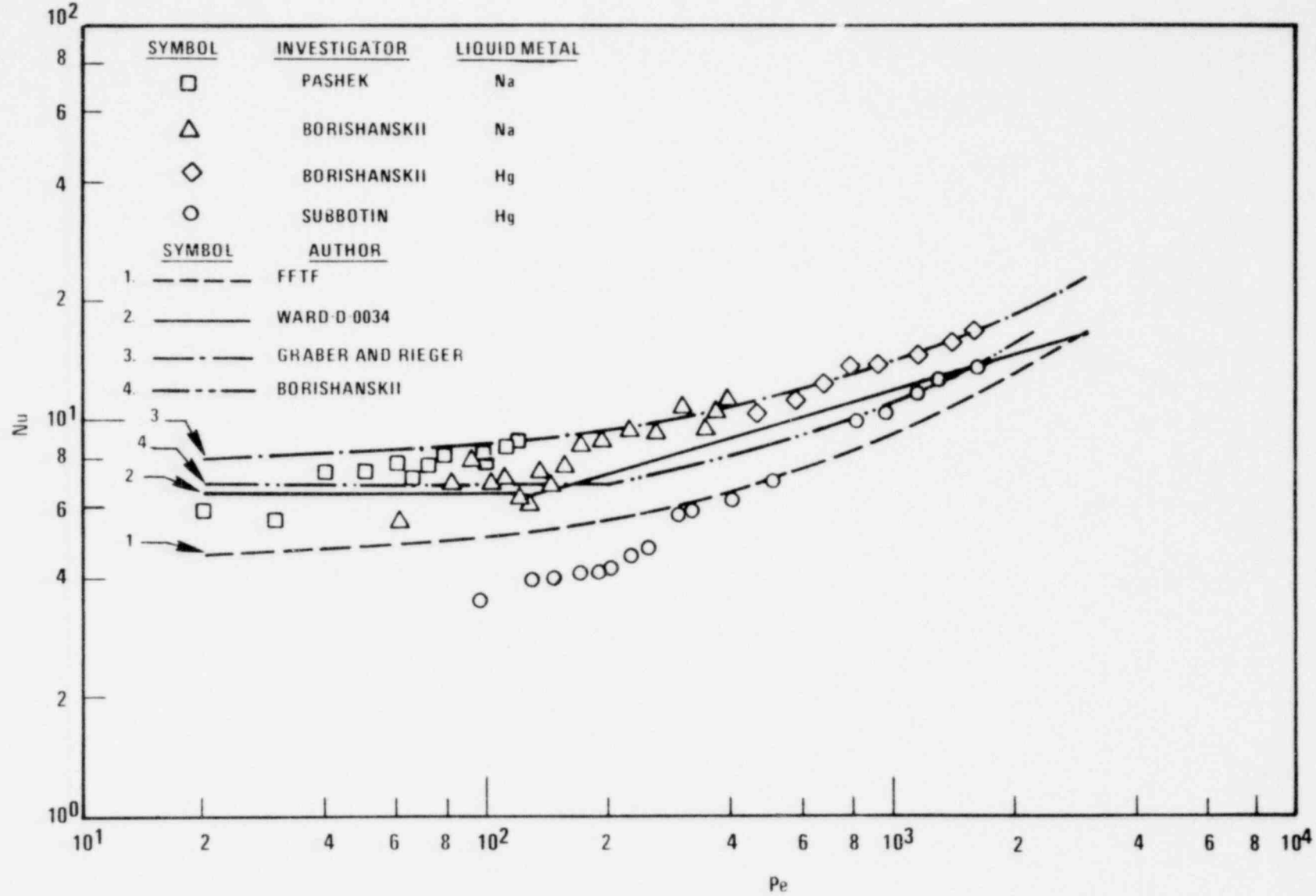

Figure 3-16. Comparison of Predicted and Experimental Results for P/D = 1.2

3.1.10 Pellet-Cladding Eccentricity

An eccentric position of the fuel pellet within the cladding will give rise to an increased heat flux in the area of minimum gap with consequent increases in temperature rise through the coolant film and the cladding. Analyses indicated that the effect on the fuel temperature would be to shift the position of the maximum fuel temperature from the centerline; the value of the maximum fuel temperature being actually lower for eccentric than for nominal, concentric conditions. Conservatively, a value equal to 1.0 was selected for power-to-melt analyses (Section 3.2).

The effect of pellet-cladding eccentricity on the film and cladding temperature drops was calculated assuming conservatively that pellet-cladding contact will occur, but at some random circumferential orientation. For a typical fresh fuel rod, the circumferential variation in heat flux as a result of pellet-cladding eccentricity was calculated using the LIFE-III correlation for gap conductance. The axial variation of local cladding midwall temperature beneath the wire wrap for a centered pellet, and of coolant temperature were obtained from a NICER run. The results were combined to determine the maximum cladding midwall temperature anywhere along the rod for each direction of pellet displacement. This provided a probability distribution of maximum cladding midwall temperature. The resulting bounding uncertainty in film and cladding temperature drops was the combination of a direct factor of 1.14 and a 3σ statistical factor of 1.174.

These factors apply only at beginning of life and decrease to unity at about 0.5 to 1.5 atom % burnup.

It may be noted that the orientation of the fresh Fuel Assembly during shipping can result in the pellets tending to be displaced in the direction which is downward during shipping. Specifying the fresh fuel assembly orientation during shipping so as to avoid any increase in the pellet-cladding eccentricity factor due to improper orientation is under consideration.

3.1.11 Cladding Thickness and Conductivity

The thermal conductivity of 316 SS is given in Reference 21 together with the data base used. The values are based on unirradiated data. The estimated uncertainty[21] is $\pm$ 5%.

The correlation used in the design analysis yields results which are 5% below the data given in Reference 21 i.e., the uncertainty is already conservatively included as a direct factor.

For maximum fuel temperature (power-to-melt) analyses, the worst case occurs at beginning of life and no additional correction for irradiation effects is required. The effect of cladding ID and OD tolerances results in a $[2(\frac{.0005}{.0150})^2]^{\frac{1}{2}}\sqrt{3} = 0.08$ (3σ) uncertainty in temperature drop through the cladding. However, the combined statistical uncertainties in thermal conductivity and in cladding thickness have a smaller effect on the temperature drop than does the direct factor of 1.05 built into the design correlation. Therefore no additional uncertainty factor is required for maximum fuel temperature calculations.

Maximum cladding midwall or ID temperatures are used for fuel rod lifetime analyses. Minimum fuel rod lifetime occurs when cladding thickness is at its minimum value, which also corresponds to minimum temperature drop through the cladding. Therefore, it is conservative to assume nominal cladding thickness for the temperature calculation.

The effect of irradiation is accounted for by noting that for the most highly irradiated fuel assembly at the end-of-life, volumetric swelling at the cladding hot spot is approximately 1.0% $\pm$ 0.5%, based on the correlation of swelling test data given in Reference 21. Since swelling represents dispersed porosity (vacancies) in the cladding, the effect of irradiation swelling at the cladding hot spot is calculated from the Maxwell-Eucken equation[22] to be 1.015 $\pm$ 0.008. In addition, a decrease in conductivity would be expected due to interstitial lattice defects produced and remaining when vacancies are also produced. Reference 23 gives some experimental data for the effect of irradiation on the electrical conductivity of cold-worked 347 stainless steel, which is expected to be similar to the effect on the thermal conductivity of the cold-worked 316 stainless steel cladding. There was a reduction in conductivity of 1-2% at low neutron exposures (10^{18} to 10^{19} fast nvt) and low temperatures. At higher exposure there was a smaller change. At higher irradiation temperature ($\sim$300°C) the change was reduced by about 50%. Based on this, an additional direct factor of 1.02 was conservatively applied. The irradiation swelling direct factor of 1.015, the interstitial lattice defect direct factor of 1.02, and the combined statistical uncertainties in

irradiation swelling and in thermal conductivity have a smaller effect on the temperature drop than does the direct factor of 1.05 built into the design correlation. Therefore no additional uncertainty factor is required for maximum cladding temperature calculations.

3.1.12 Coolant Properties

The enthalpy and the density of sodium are parameters used in the energy and momentum balance for the heated coolant channels to determine the local coolant temperatures. The correlations are obtained from Reference 24.

The recommended correlation for enthalpy was based on the data of Ginnings, et al.[25] They report a probable error of the mean from 0.01 to 0.03% (depending on the temperature). Taking into consideration their estimate of systematic errors, they estimate the probable error of the enthalpy to be between 0.1 and 0.2% and the probable error of the heat capacity to be between 0.3 and 0.4%. For hot spot analyses, coolant temperature changes are large and the uncertainty associated with enthalpy rather than with heat capacity is more appropriate. The upper estimate 0.2% probable error (errors equally likely to be greater as smaller) converts to a 0.9% 3σ uncertainty.

More recent measurements by Fredrickson and Chasanov[26] showed excellent agreement with Ginnings' data. For a typical 400°F temperature rise in CRBRP, Fredrickson's correlation gives an enthalpy rise within 0.01% of that obtained with the recommended correlation.

The density correlation was derived by Stone, et al.[27] from the data of References 27 to 33. The deviations of these data and those of Gol'tsova[34] from the recommended correlation are shown in Table 3.7. For the five investigators covering the present range of interest (References 30, 31(B), 32, 33, 34),

$$\text{RMS \% Avg. Dev.} = 0.674$$

$$\text{\% Avg. Dev. of Mean} = \frac{0.674}{\sqrt{5}} \times \frac{\sqrt{5}}{\sqrt{4}} = 0.337$$

The average deviation of the mean of 0.337% converts to a 1.5% "3σ" uncertainty. The effect of the small number of data points on the overall tolerance interval is negligible as shown in Section 2.4. The statistically combined enthalpy and density subfactors yield a sodium properties factor of $(0.9^2 + 1.5^2)^{1/2} = 1.7\%$.

TABLE 3.7

SUMMARY OF DENSITY MEASUREMENTS FOR LIQUID SODIUM

Investigator	Temp. Range (°F)	% Average Deviation: Observed - Correlation / Correlation
NRL[29]	mp to 503	±0.08
Jackson[30]	937 to 1314	-0.74
Rinck[32]	804 to 1183	+0.15
Hagen[28]	mp to 336	±0.05
NRL[27]	1577 to 2491	±0.17
Novikov[31] (A)	248 to 505	-0.14
(B)	275 to 1324	+0.71
Nishibayoshi[33]	486 to 1580	±1.09
Gol'tsova[34]	802 to 2754	±0.11

1630 066

3.1.13 Nuclear Uncertainties

The total power or burnup uncertainty is composed of nuclear design methods uncertainties and/or biases (based on comparisons of calculations and measurements of isotopic fission and capture rates and gamma heating in ZPPR-7), CRBRP design uncertainties relating primarily to absolute power normalization and fissile content variations, and a general class of modeling uncertainties. In the fuel, the power uncertainty is broken down into a statistical part which is combined in quadrature (root-mean-square) with other statistical uncertainties, and a nonstatistical bias and uncertainty which is applied directly to envelope the upper limits of the peak power density. Due to the limited scope of the available blanket data, only a nonstatistical uncertainty is developed. Uncertainties are provided for the fuel, inner blanket and radial blanket assemblies. Where a basis exists for such, a spatial distribution of the uncertainty is provided (e.g., adjacent to, and removed from, the influence of inserted control rods, and by assembly-row in the radial blanket).

Experimental verification of the calculational methods and data used to predict the power distributions in CRBRP is provided by the measurements performed in the ZPPR critical facility. ZPPR is a zero power critical mockup of the CRBRP consisting of a matrix of rectangular drawers containing fuel, steel, and sodium plates loaded to simulate the average compositions of the CRBRP core and blanket regions. CRBRP design methods are verified, and design bias factors and uncertainties are derived, by direct comparison of calculated and measured ZPPR parameters. These parameters include isotopic fission and capture rate and gamma heating distributions in support of power distribution predictions. The design (methods) bias factors and uncertainties are subsequently applied to the calculation of these parameters in CRBRP which are predicted with the same calculational tools and data.

1630 067

The results presented herein are based primarily on the analysis of ZPPR-7 (Phases A-E) measurements. ZPPR-7 modeled the basic characteristics of a heterogeneous CRBRP core with annular rings of inner blanket assemblies.

Tables 6.1B and 6.2B list the statistical and nonstatistical uncertainties applicable to the predictions of both local and rod- or assembly-integrated power density in the core fuel assemblies. The uncertainties are divided into those applicable to fuel regions directly adjacent to the partially inserted row 7 corner (R7C) control rods, and those applicable to all other core locations. The uncertainties for fuel assemblies adjacent to inserted R7C control rods are shown for both the side adjacent to the R7C control rod and the far side. Uncertainty values are presented for the heat flux at the peak power position (peak power density near the core midplane), the heat flux at the top of the core (power density at the core/upper axial blanket (UAB) interface) and the channel coolant (rod-channel integrated power) in Table 6.1B and the assembly mixed mean outlet temperature (assembly integrated power) in Table 6.2B.

The peak and integrated power densities in the fuel are well predicted with the standard 2D-synthesis nuclear design techniques. However, the power density at the top of the core is relatively poorly predicted due to difficulties in simultaneously modeling the behavior in this region while preserving the integral and peak (core midplane) power in two dimensions. In addition, the accuracy of few group diffusion theory is poorer in the presence of the steep flux gradient and in the region of the core/UAB material discontinuity.

These factors are reflected in the larger "heat flux at top of core" uncertainty.

The statistical uncertainties consist of experimental uncertainties (fission rates and gamma heating) at the 3σ level, criticality and control rod insertion uncertainties, and local fuel fissile content variations.

3.1.13.1 Experimental

The experimental power uncertainty consists primarily of Pu-239 and U-238 fission rate and gamma heating uncertainties. The experimental (statistical) power uncertainty is derived from the +2% (1σ) root-mean-square deviation

1630 068

between calculated and measured core fission rate (Pu-239, U-235) distributions in ZPPR-7 covering a variety of reactor critical configurations. There is an observed radial tilt in the calculation-to-experiment ratios for Pu-239 fission in Phases A and B of ZPPR-7 which tends to overestimate (by 3-5%) the Pu-239 fission rate in the area of the fuel "islands" in rows 7, 8 and 9, and specifically around the R7C control locations, in the beginning-of-life configuration. This overprediction, coupled with the application of a $+3\sigma$ power uncertainties, would result in an overly high estimate of the peak power in these locations. Consequently, the beginning-of-life (BOC1, BOC3, BOC5) power in the rows 7, 8, 9 region of the core is biased downward in Table 6.1B (footnote 4) by 1-3% to remove the basic tilted characteristics in the fission rate (power shape). This radial tilt was not observed in the Phase C or D ZPPR-7 experiments with plutonium loaded in the inner blankets, so the aforementioned bias is not applied to the end-of-life power shape.

The analysis of the ZPPR-7 experimental U-238 fission rate distribution showed substantial fluctuations in the calculation-to-experiment ratios between fuel and inner blanket assemblies, possibly attributable to the infinite medium cross-section preparation scheme. Based on these ZPPR-7 results, a one-sided +20% U-238 fission uncertainty is indicated in the core fuel assemblies (although U-238 fission only accounts for about 6% of the total power in the fuel so that this uncertainty accounts for approximately 1% on the high-side of the total power uncertainty).

Analysis of the preliminary ZPPR-7 gamma heating measurements shows a scatter of $\pm$10% in the calculation-to-experiment (C/E) ratios in the core regions and a consistent 15-20% underprediction in the radial blanket. There was some evidence in the ZPPR-4 gamma heating measurements, however, that this underprediction behavior at the core/blanket interface is at least in part an anomaly caused by the comparison of homogeneous (cell-average) calculated heating rates with point-measured values in regions of substantial gamma fine structure. This uncertainty is therefore considered an upper bound. Gamma heating accounts for about 10% of the total fuel assembly power, so the $\pm$10% uncertainty accounts for approximately $\pm$1% of the total fuel assembly power uncertainty.

The direct combination of ±6% (3σ) plutonium fission rate uncertainty (≈85% of the total core power), ±20% U-238 fission rate uncertainty (≈6% of the total core power, and ±10% gamma heating uncertainty (≈10% of the totalcore power) results in a ±7% (approximately 3σ) total experimental power uncertainty in the fuel, in addition to the space-dependent beginning-of-life bias discussed earlier. This uncertainty applies equally to the local pellet, rod, and fuel assembly power predictions. Due to the slight space-dependent trends in the C/E distributions, this uncertainty is not statistically reducible for small groups of fuel assemblies.

The experimental fission rate uncertainties are based on well over 100 foil measurements in ZPPR-7.

3.1.13.2 Criticality Uncertainty

The uncertainty in the prediction of the hot critical state of the reactor results in an uncertainty in the depth of primary control rod insertion which, in turn, affects the local power distribution (principally the radial and axial distributions in the immediate vicinity of the inserted control rods, and to a lesser extent throughout the remainder of the core). This uncertainty is derived from a (3σ) statistical value of the criticality uncertainty of ±0.5%Δk developed from the 4 unrodded critical configurations in ZPPR-7. The resulting power uncertainty is derived parametrically by varying the control rod bank insertion by an amount corresponding to the ±0.5%Δk to produce power perturbation maps. The criticality power uncertainty applies approximately equally to the beginning and end-of-cycle power distributions due to a partial cancellation between the lesser influence of the nearly-withdrawn primary control rods and the larger magnitude of the criticality uncertainty which includes burnup reactivity swing uncertainties near the end-of-cycle. This criticality (rod insertion) uncertainty results in a ±1% power uncertainty throughout the core with the exception of those assemblies directly adjacent to the inserted control rods. The power distribution in the fuel assemblies directly adjacent to the inserted control rods is strongly influenced by the position (depth of insertion) of those rods so that the criticality uncertainty in these assemblies is both larger and space-dependent across the assemblies as indicated in footnote (3) to Table 6.1B.

1630 070

3.1.13.3 Pellet Fissile Content Tolerance

The specified fuel pellet fissile content (manufacturing) tolerance results in a local fission rate bounding uncertainty of ±3%. Because the pellets are fabricated in batches, this uncertainty is not reduced for groups of pellets comprising a single fuel rod or a single fuel assembly. Very large numbers of fuel assemblies are, however, subject to a smaller specified ±0.5% fissile content tolerance. For a rectangular probability profile, the ±3% uncertainty results in a 3σ uncertainty of 5.2%.

3.1.13.4 Modeling Uncertainties

Specific model uncertainties in the CRBRP core power distribution predictions include parametric uncertainties arising from 3D effects (bounding), rod-power interpolation (bounding) and radial and axial burnup modeling (engineering judgement). The aforementioned modeling uncertainties are derived parametrically, so no specific σ level can be assigned. The values quoted do, however, generally cover the range of variations noted. Modeling uncertainties are combined with other nonstatistical uncertainties directly rather than statistically.

CRBRP power, burnup and reaction rate distributions are predicted by a two-dimensional (2D) synthesis technique whereby "radial" shape factors, F_R^N, derived from hexagonal calculations, and axial shape factors F_Z^N, derived from RZ calculations, are superimposed on average power conditions to result in the three-dimensional (3D) power distribution throughout the core and blankets. A benchmark calculation with consistent 3D and 2D-synthesis models has been used to infer the geometric modeling biases introduced by the 2D-synthesis technique at the beginning-of-life. In general, the agreement between the two models is good (with the exception of the regions strongly influenced by the partially inserted R7C control rods as noted in Table 6.1B) with the peak power density predicted within the range of ±3% and rod- or assembly-integrated power predicted within ±1% in the core. The polynomial fit to power-by-rod, performed with input from 24 mesh-per-assembly 2DB hexagonal calculations, introduces an additional uncertainty of ±1% in the radial power shape within an assembly. Burnup modeling in the core generally introduces little error in the power distribution in high-power locations, although some uncertainty is necessarily

introduced in the end-of-life axial power shapes due to smoothing. The axial peak-to-average power has been shown to be nominally overpredicted by 2% in ZPPR-4 and in ZPPR-7 The net peak power density modeling uncertainty throughout the core (with the exception of assemblies directly influenced by inserted control rods) is therefore ±2% (±3% 3D effect plus ±1% intra-assembly radial power shape uncertainty less 2% axial peak-to-average overprediction). This value increases to +10% on the high-side for the "heat flux at the top of the core" with the inclusion of the 5% fall-off in the prediction of the axial power shape indicated in the ZPPR-4 and -7 experiments, and with some additional uncertainty in the tail of the axial power shape. The ±2% integrated rod power uncertainty is made up of ±1% 3D effect plus the ±1% radial shape uncertainty, whereas the ±1% total assembly power modeling uncertainty is entirely 3D effect.

The radial and axial power shapes in the vicinity of inserted control rods are particularly sensitive to control rod modeling. Partially inserted control rods in the CRBRP are modeled with an "effective" amount of control volume fraction which results in the same reactivity worth inserted in the 2D hexagonal calculations as would result from an explicit 3D representation. This technique results in a good representation of the average power in the surrounding fuel assemblies, but necessarily introduces some spatial bias in the radial power shape very close to the inserted control rods. In addition, the axial power shape is selected to best represent the assembly-average power so that the shape is somewhat more perturbed in the region of the fuel pins directly adjacent to the inserted control rod, and likewise somewhat less perturbed on the side of the assembly farthest from the inserted rod. The combination of these radial and axial shape perturbations, derived primarily from the 3D-2D synthesis comparison, results in a space-dependent modeling bias (uncertainty) which varies across the assembly as indicated in Table 6.1B (footnote 1).

3.1.13.5 Control Rod Banking

The maximum control rod out-of-bank specified tolerance of ±1.5 inches introduces a potential power asymmetry in the core. The bounding power uncertainty resulting from the control insertion asymmetry is found from full-core parametric calculations to be ±2% except directly adjacent to the inserted rods where the bounding uncertainty is increased to ±4%.

3.2 Power-To-Melt Uncertainty Factors for Fuel Assemblies

3.2.1 Introduction

This section presents a preliminary analysis of the uncertainties in power-to-melt calculations for the heterogeneous core. The results will be refined and updated for the FSAR based on further analysis and additional experimental data. The primary data used for this work were the results of the short-time, (low burnup) HEDL-P19 and P-20 tests[35,36] which were integral experiments designed to provide thermal performance information.

The LIFE-III code was used as the calculational tool. The code is a detailed model for describing the thermal and mechanical behavior of fast reactor oxide fuel pins and has been calibrated and verified with the HEDL P-19 and P-20 tests in addition to a number of intermediate and high burnup pins. Figure 3.17 and Table 3.8 show how well the code represents the P-19 and P-20 data. The code was used to calculate the power-to-melt of the CRBRP AFMS fuel and blanket rods, and the sensitivities to variations in fuel pin parameters used for uncertainty analysis.

In the subsequent sections for fuel applications, the uncertainties in the code predictions of the power-to-melt arising from data scatter and the overall accuracy of measurements in the EBR-II are first analyzed. The uncertainties which occur when applying the code to the CRBRP conditions are then evaluated. The factors considered here include the tolerances on fabrication parameters and reactor instrumentation and thermal hydraulic and systematic uncertainties. The individual uncertainties were determined by calculating the power-to-melt for the nominal peak rod conditions and design parameters followed by calculating the effect of a variation in each parameter on the nominal code result.

All the individual uncertainties are then statistically combined and the probability distribution for the reactor power-to-melt determined. The design criterion can then be measured by determining if the 115% of nominal power is three standard deviations below the power-to-melt.

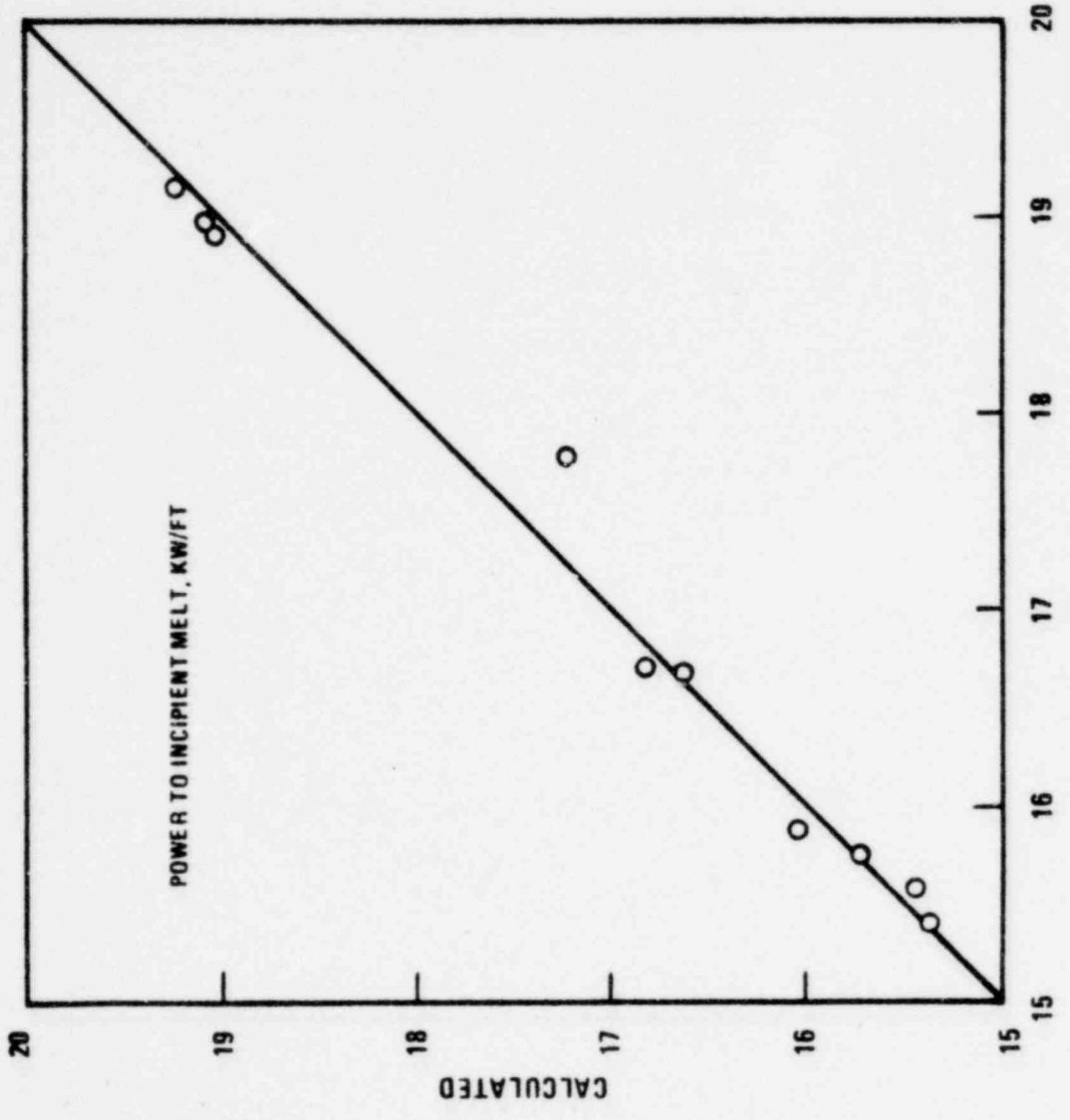

Figure 3-17. LIFE-III Thermal Calibration T18/6000

90-6-18

1630 074

TABLE 3.8

CENTER TEMPERATURES AND POWERS-TO-MELT OF INCIPIENT MELT SECTIONS
AS COMPUTED BY LIFE-III CALIBRATION T18/6000

Pin No.	Calculated T_{max} °F (°C)	Calculated Power-to-Melt kW/ft (kw/m)	Observed Power-to-Melt kW/ft (kw/m)
P19-35	5009 (2765)	16.62 (54.5)	16.69 (54.6)
P19-02	4978 (2748)	16.04 (52.6)	15.89 (52.1)
P19-24R	5024 (2773)	15.44 (50.6)	15.59 (51.1)
P19-27R	4990 (2754)	19.23 (63.1)	19.16 (62.8)
P19-28	4966 (2741)	19.02 (62.4)	18.82 (61.8)
P19-30	5070 (2799)	17.22 (56.5)	17.79 (58.3)
P19-08	5006 (2763)	15.36 (50.4)	15.40 (50.5)
P20-07	5004 (2762)	15.72 (51.7)	15.75 (51.7)
P20-30	4985 (2752)	16.82 (55.2)	16.70 (54.8)
P20-33	4982 (2750)	19.07 (62.5)	18.98 (62.2)

Average T = 5001 ± 28°F
(2761 ± 16°C)

r.m.s error
= 0.21 kw/ft (.69 kw/m)

std. dev.*
= 0.24 kw/ft (.77 kw/m)

*Two degrees of freedom lost in calibrating LIFE-III parameters.

1630 075

3.2.2 EBR-II Factors

The factors associated with EBR-II experiments which contribute to uncertainties in power to melt measurements are listed and defined below:

1. σ_{fab} (σ is the standard deviation) is due to variation in fuel pin fabrication parameters from their nominal values.

2. σ_{PIE} is due to uncertainty in post-irradiation examination (PIE) measurements.

3. σ_{space} is due to uncertainties in the spatial dependence of neutronics calculations and local inhomogenieties in the EBR-II core.

4. σ_{time} is due to uncertainty on overall power level due to variations in EBR-II instrumentation and the uncertainty in the neutronics calculation for a given core loading. This uncertainty causes random fluctuations in quoted power level that vary with time.

5. σ_{sys} is due to a difference between actual and quoted overall EBR-II power that doesn't change with time. It is known that a systematic shift in EBR-II power level exists and a correction is made by experimenters. An estimate is required of the uncertainty on this correction for this analysis which is identified here as σ_{sys}. This uncertainty does not show up as scatter in the data. Such a systematic uncertainty would show up in the scatter of data comparing different reactors.

The evaluation of each of these uncertainties will now be discussed.

σ_{time}

The major contribution to this uncertainty results from fluctuations in the primary and secondary EBR-II coolant loop heat balance. This yields a 2% standard deviation[37]. Neutronic calculation of γ precursors in the P-19 test introduce a further uncertainty of less than 1%[38] and a value of 0.8% was used. Accordingly this factor was evaluated as

$$\sigma_{time} \cong \sqrt{2\%^2 + 0.8\%^2} = 2.2\% \qquad (3.8)$$

1630 076

This uncertainty would not show up as fluctuations in results from a single subassembly since all pins would have been subjected to the same errors in overall power determination during the same times.

σ_{sys}

A detailed analysis of the P-19 test indicated that a correction factor of 0.94 must be applied to the calculated EBR-II power level[38]. This factor has been used in all reported analysis of these results and those of the P-20 test and was used for the LIFE-III calibration. Subsequent work suggested a factor of 0.91[37], while recent analysis by the EBR-II Project indicates 0.96. As an interim position, the 0.94 factor is being retained. An evaluation of the recent analysis by the EBR-II Project will be performed when their report is issued. In addition, burnup analysis data will be evaluated with respect to this factor. The EBR-II Project also estimated that further systematic bias should be no more than $\pm 2\%$. For work in this document an uncertainty, σ_{sys}, of 3% is used which covers both the .91 and .96 power factors and is more conservative than the 2% estimate by EBR-II.

σ_{space}

The spatial uncertainties in pin powers arise from uncertainties in neutron transport calculations. Calculations have been checked by comparison of measurements of control rod worth[38]. Table 3.9 and Figure 3.18 show the resulting percentage difference between measured and calculated flux, which has a standard deviation, σ''_{space}, of 1.7%. In addition local flux peaks produce an estimated uncertainty σ'_{space} of about 0.5%. Finally in the highly enriched fuel of P19, differences in the γ absorption can produce a +0.7% to -0.7% variation in pin power going from the center to the outside of the assembly. This introduces a standard deviation of $.7/\sqrt{3} \cong 0.4\%$. Combining these,

$$\sigma_{space} \cong \sqrt{1.7^2 + .5^2 + .4^2} = 1.8\% \qquad (3.9)$$

1630 077

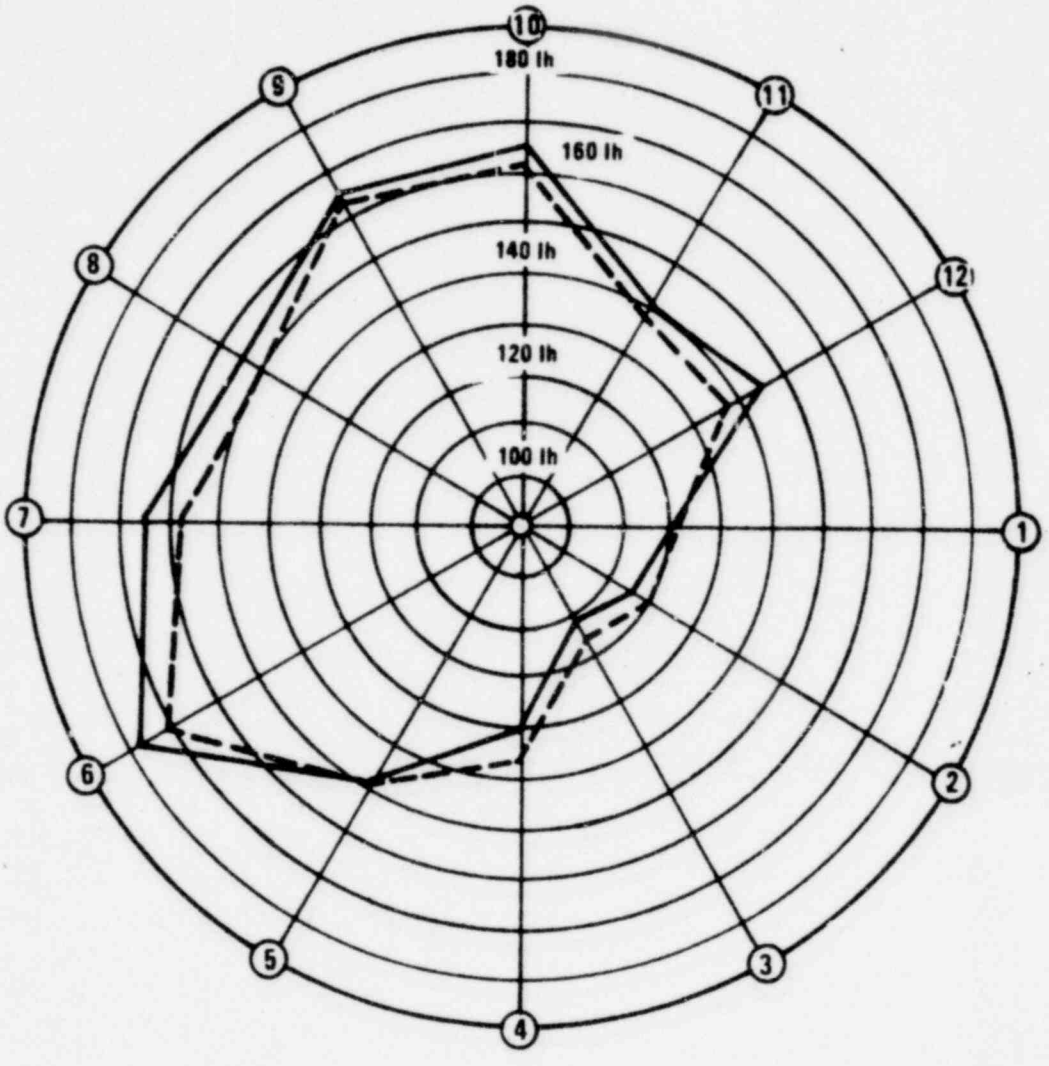

Figure 3-18. Control-Rod Worths for EBR-II Run 27A

9926-19

1630 078

TABLE 3.9

SPATIAL DEPENDENCE OF POWER UNCERTAINTY
CALCULATED FROM COMPARISON OF MEASURED
AND CALCULATED CONTROL ROD WORTHS

Control Rod Number	Calculated Minus Measured Power (%)
1	- .67
2	-1.75
3	-1.8
4	-2.35
5	0.
6	1.85
7	2.25
8	1.5
9	.45
10	1.2
11	.7
12	2.25

Average Δ Power = .3%
Standard Deviation = 1.7%

1630 079

σ_{fab}

The scatter in burnup measurements as compared to values calculated from EBR-II powers has been analyzed and found to be $\sigma_{BU} \tilde{=} 1.1\%$. This analysis is from individual subassemblies, and since pins in a subassembly are in the reactor for the same time, they would not reflect the uncertainties σ_{time} and σ_{sys}. The scatter in the burnup data includes a combination of EBR-II power uncertainties and uncertainty in the burnup measurement technique.

$$\sigma_{BU} \tilde{=} 1.1\% \tilde{=} \sqrt{\sigma'^{2}_{space} + \sigma^{2}_{fab} + (0.5\%)^{2}} \qquad (3.10)$$

where the 0.5% is the estimated burnup measurement accuracy of the mass spectrometry. The spatial uncertainty $\sigma'_{space} \sim .5\%$ is that for an individual subassembly and not the entire core. The burnup uncertainty has also been calculated by HEDL to be 3% (1σ). In this work a single power factor for all subassemblies was used. The data scatter due to power fluctuation with time, σ_{time}, and core wide spatial uncertainty, σ_{space}, would therefore apply and the 3% standard deviation obtained can be attributed to

$$3\% \tilde{=} \sqrt{\sigma^{2}_{time} + \sigma^{2}_{space} + \sigma^{2}_{fab} + (0.5\%)^{2}} \qquad (3.11)$$

Using the previously determined values for σ_{time}, σ_{space} and σ'_{space} in equations (3.10) and (3.11) the two self-consistent values for σ_{fab} are respectively obtained.

$$\sigma_{fab} = .85, .82\% \qquad (3.12)$$

σ_{PIE}

The scatter of the P-19 and P-20 experiments relative to the LIFE calibration has been calculated (see Table 3.8 and Figure 3.17). The standard deviation is about 1.3%. It is interesting to note that only one pin in this group was significantly outside this standard deviation, and that was P-19-30. If P-19-30 had been excluded, the standard deviation would have been 0.8%.

It might be more reasonable to use 0.8%, but to be conservative, 1.3% will be used. The scatter in P19 and P20 data reflect uncertainties in fabrication, local spatial fluctuations and post irradiation examination measurement uncertainty. Since P20 powers were normalized to P19 results, P20 is not an independent experiment at a separate time and σ_{time} does not apply. So

$$\sigma_{P19/P20} \sim 1.3\% \approx \sqrt{\sigma_{fab}^2 + \sigma'^2_{space} + \sigma_{PIE}^2} \qquad (3.13)$$

Equation (3.13) then gives

$$\sigma_{PIE} = 0.9\% \qquad (3.14)$$

Values of the above uncertainties are summarized in Table 3.10.

Total Uncertainty

The total uncertainty is a combination of all the components

$$\sigma_{tot} = \sqrt{\sigma_{fab}^2 + \sigma_{PIE}^2 + \sigma_{space}^2 + \sigma_{time}^2 + \sigma_{sys}^2} = 4.3\% \qquad (3.15)$$

Resolution of the EBR-II power factor is expected to reduce the systematic uncertainty to 2%, and σ_{tot} will drop to 3.7%.

σ_{tot} represents the scatter and uncertainty in the power to melt data. The uncertainty in the average of these data is given by the standard deviation of the mean. The standard deviation of the mean takes into account the number of data points N, and is given by $\sigma/\sqrt{N}$. In the various components of σ_{tot}, a separate measurement toward determining σ_{sys} would require use of a different reactor; a separate measurement for σ_{time} would require an experiment done at a different time and a separate measurement for σ''_{space} would require another experiment done in a different position in EBR-II. As explained above, P19 and P20 cannot be counted as being done at different times or different positions. So for σ_{sys}, σ''_{space} and σ_{time} N = 1. For the other components N = 10, the number of rods used. Thus

$$\sigma_{mean} = \sqrt{\sigma_{sys}^2 + \sigma_{time}^2 + \sigma''^2_{space} + (\sigma_{fab}^2 + \sigma_{PIE}^2 + \sigma'^2_{space})/10} = 4.1\% \qquad (3.16)$$

1630 081

TABLE 3.10

VALUES OF UNCERTAINTIES IN EBR-II

	%
σ_{space}	1.8
σ_{time}	2.2
σ_{fab}	0.8
σ_{PIE}	0.9
σ_{sys}	3.0
σ_{tot}	4.3
σ_{mean}	4.1

σ_{mean} is dominated by σ_{sys} and σ_{time} with the other components making a small contribution. The mean of the power to melt data is represented by the LIFE-III calibration and the uncertainty on this mean is given by σ_{mean}.

3.2.3 Power-to-Melt in CRBRP

The probability of melting in CRBRP must be evaluated. To do this the LIFE-III calibration will be extrapolated from P19/P20 to CRBRP conditions. The power-to-melt margin is lowest near beginning of fuel life. Since we are considering only fresh and very low burnup fuel and this is the burnup range covered by P19/P20, the extrapolation is small and it is assumed that no biases are introduced. The additional uncertainty comes from the use of fuel with 33% Pu enrichment instead of 25% enrichment used in the calibration. An estimate of the values and uncertainties of power-to-melt in CRBR with reference fuel can be made. Then the uncertainties in the CRBR power-to-melt are statistically added to the P19/P20 σ_{mean} uncertainty and to the extrapolation uncertainty to define a probability of melting.

1. CRBRP Design Uncertainties

The uncertainties in a CRBRP power-to-melt due to the factors listed in Table 3.11 will be considered. Fabrication and irradiation uncertainties arise from design tolerances and uncertainties in neutron physics and thermal hydraulic calculations. These uncertainties can be estimated from the design tolerances by computing their effect on power-to-melt using LIFE-III. The design tolerances will be for pellet density, cladding I.D., enrichment, instrumentation and pellet diameter. There is also a tolerance on fuel weight per length which prevents certain combinations of density and diameter. To simplify analysis and add the conservatism of not taking credit for this weight per length restriction, it will be neglected. Tolerances lead to fabrication of parts whose means may lie with approximately uniform probability anywhere within the fabrication tolerance bounds. The bounds of such a rectangular distribution correspond to $\pm \sqrt{3}\sigma$. The tolerances are listed in Table 3.11. Actual distributions of dimensions and fuel density are expected to be available for use in the FSAR hot channel factor analyses.

TABLE 3.11

CRBRP FUEL ROD TOLERANCES AND UNCERTAINTIES

UNCERTAINTIES REPRESENT $\sqrt{3}\,\sigma$

	Nominal	$\sqrt{3}\,\sigma_1$
Fuel Pellet Diameter	.1935	± .0015 in.
Cladding Inside Diameter	.200	± .0005 in.
Fuel Pellet Density	91.3	±1.6% TD
Reactor Power*		±5.07%
Cladding O.D. Temperature Near Midplane**		±15.6°F

* Statistical combination of nuclear data, criticality, and fissile fuel maldistribution uncertainties.

** Due to thermal hydraulic uncertainties not including uncertainties in power.

1630 084

3.2.4 Typical Power-to-Melt Analysis

LIFE-III runs are made to analyze the effect of variations in the parameters of Table 3.11 on the melting of the peak power pin. A programmed reactor startup is specified by giving the steady state reactor power as a function of time, REPOW (t). REPOW (t) is the total reactor power as determined by the reactor control settings, and Q (t) is the corresponding linear power including direct factors of the peak pin near its axial midplane at the location of peak centerline fuel temperature. The reactor power units are normalized to a value of 1.0 at nominal full power, i.e. REPOW (t) is 1.0 when the nominal power of the peak pin at X/L = .45, Q(t), is 12.73 kw/ft. This reactor power history remains the same for all the runs considered below. The power-to-melt is defined in LIFE-III by ramping the reactor power up until melting starts in the peak pin. This is done at various times during the steady state irradiation to obtain the burnup dependence. The programmed startup assumed for this study is illustrated in Figure 3.19.

3.2.4.1 LIFE-III Runs

A code run with the nominal conditions of Table 3.11 and the power history of Figure 3.19 defines the mean reactor power-to-melt for the nominal peak pin as follows:

$$\overline{REPOW}_M \text{ (nominal,t)} = \frac{1}{CP_o} \overline{Q}_M \text{ (nominal,t)}$$

where $\overline{Q}_M$ is the peak pin linear power at X/L = .45 when the LIFE-III centerline temperature reaches the fuel melting point and $\overline{REPOW}_M$ is the reactor power at that time. CP_o = 12.73 kw/ft because of the normalization of units chosen for reactor power. $\overline{REPOW}_M$ is labeled the mean reactor power-to-melt (signified by the bar) since the mean of P19/P20 has been used to calibrate LIFE-III and the P19/P20 power uncertainty will be subsequently added.

Code runs were also made for small perturbations of the design parameters to determine the sensitivity of power-to-melt to variations in each parameter. The sensitivites are shown in Table 3.12 and the corresponding standard deviations in power-to-melt obtained from the standard deviations in the parameters from Table 3.11 are shown in Table 3.13.

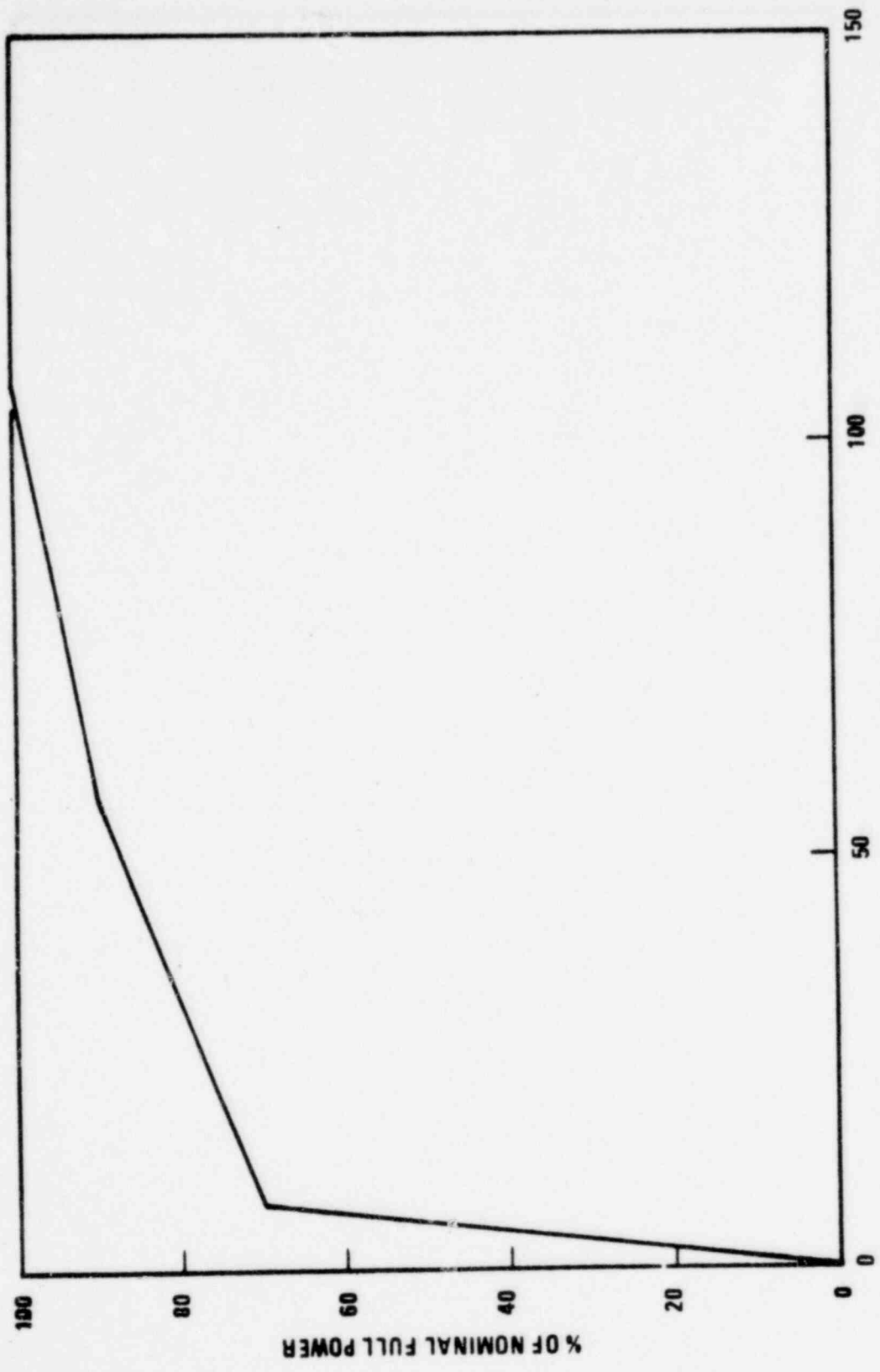

Figure 3-19. Power History Used in the Evaluation of Power-To-Melt Uncertainties

9926-20

1630 086

It is assumed that reactor power-to-melt can be approximated by a linear function of each parameter about the nominal point. This assumption was checked for pellet diameter variations for which the greatest non-linearities would be expected. Figure 3.20 shows the actual variations of power-to-melt with pellet diameter and the assumed linearizations which were selected to give a close fit over the range where power-to-melt was below nominal.

3.2.4.2 Extrapolation Uncertainty

The melting temperature of $(U,25\%Pu)O_2$ is 2760°C (5000°F) with a bounding 3σ uncertainty of $\pm$60°C (108°F). The melting temperature is based on an extensive review of all published data and a thorough analysis of the techniques and data has been included in the Nuclear Systems Materials Handbook[21]. The uncertainty was conservatively estimated from a review of the original data. It is not necessary to use an uncertainty on melting temperature when the LIFE-III code is employed to analyze $(U,25\%Pu)O_2$ since the code was calibrated with fuel with this plutonium content. The nominal melting point value was used for calibration. Since the current CRBRP fuel contains 33% PuO_2, extrapolation of this code to predict the power-to-melt requires consideration of additional uncertainties due to increased Pu content. Based on the calibrated melting point of 2760°C for 25% PuO_2 fuel, and considering the $\pm 3\sigma$ uncertainty of $\pm$60°C for the entire range of $(U,Pu)O_2$ solid solutions, the uncertainty in extrapolating from 25% to 33% PuO_2 was determined by estimating the uncertainty of the slopes. The 3σ uncertainty in extrapolation is 2 x 60/100 = 1.2°C per wt% PuO_2 or 9.6°C in extrapolating from 25% to 33% PuO_2 fuel (i.e., melting point uncertainty σ_{TM} = 9.6 x 1.8/3 = 5.8°F). This uncertainty is applied to the nominal melting point for 33% PuO_2. The sensitivity of power-to-melt changes in melting point.

$$\partial \overline{REPOW}_M / \partial T_{MP}$$

is calculated from the nominal LIFE-III run, and this is used to convert the uncertainty on melting temperature to uncertainty on power-to-melt

$$\sigma_{extrap} = \partial \overline{REPOW}_M / \partial T_{MP} \; \sigma_{TM}$$

1630 087

3.2.4.3 Combining P19/P20, Extrapolation and CRBRP Uncertainties

$REPOW_M$ is the mean reactor power-to-melt. To get the probability distribution for the reactor power-to-melt, the uncertainty in the P19/P20 experiments

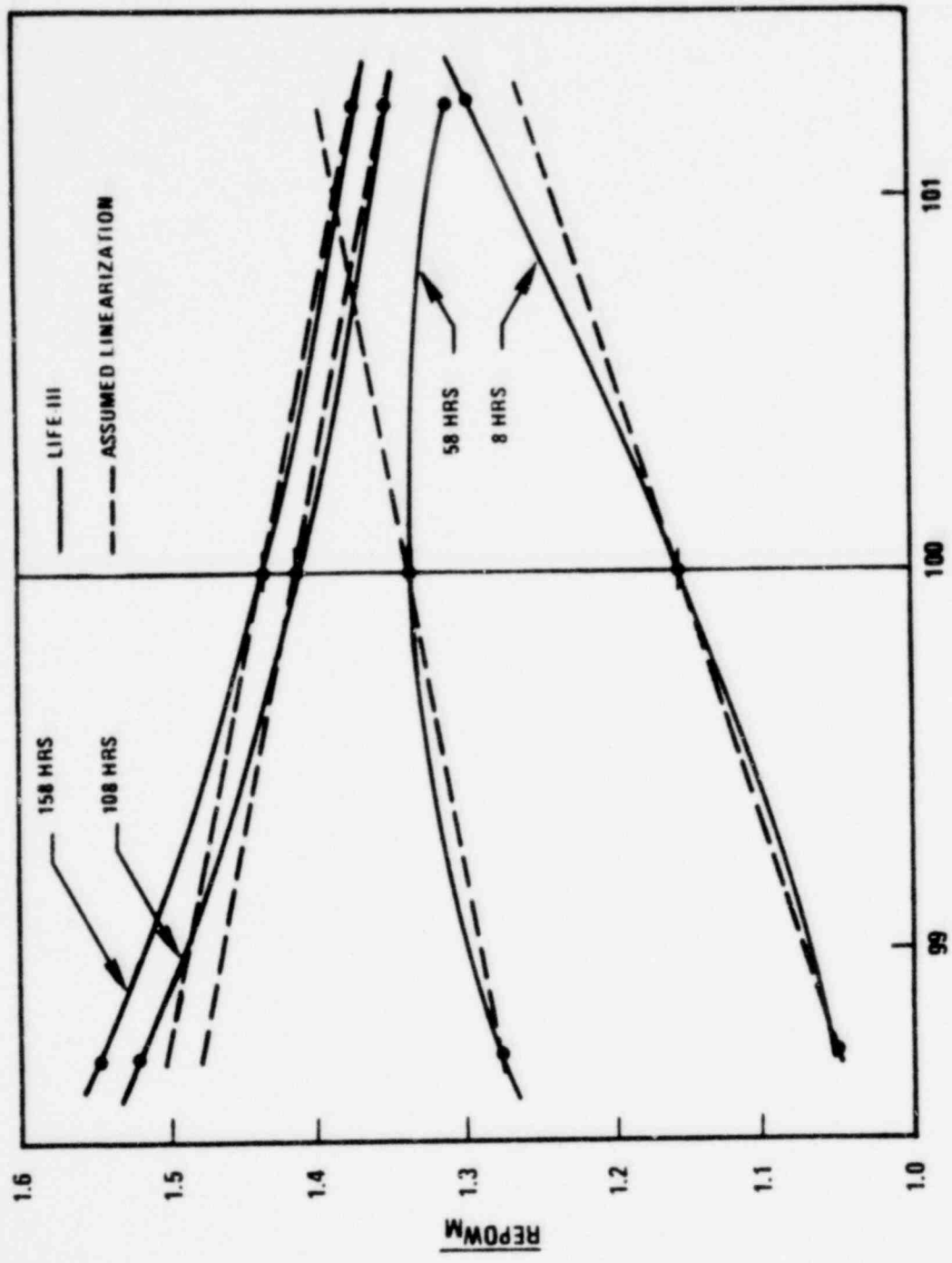

Figure 3-20. Variation of Power-to-Melt with Pellet Diameter

1630 088

(σ_{mean}) and the extrapolation uncertainties (σ_{extrap}) are added to the CRBRP design uncertainties ($\sigma_{\overline{R}}$), resulting in the probability distribution for reactor power-to-melt with standard deviation

$$\sigma_{REPOW}(t) = \sqrt{\sigma_{\overline{R}}(t)^2 + \sigma_{mean}^2 + \sigma_{extrap}^2}$$

and a mean of $\overline{REPOW}_M$ (nominal,t), where t is time-in-life.

3.2.4.4 Design Criterion

The design criterion is that the reactor control settings be low enough so that

$$1.15 * REPOW(t) < \overline{REPOW}_M (nominal,t) - 3\sigma_{REPOW_M}(t)$$

for all time, or that a 15% overpower is three standard deviations below melting power.

3.2.4.5 Results of CRBRP Power-to-Melt Uncertainties

The results of the analysis outlined above are summarized in Tables 3.12 through 3.15. In Table 3.12, the derivatives of the power-to-melt with respect to the different parameters are calculated. In Table 3.13, these are used to convert design uncertainties into uncertainties on power-to-melt which are then statistically combined.

The uncertainty on melting point due to extrapolation to a Pu enrichment different from P19/P20 is given in Table 3.14. The nominal LIFE II run is used to find the effect of a change in melting point on power-to-melt. This is used to convert the uncertainty of melting point into an uncertainty on power-to-melt.

In Table 3.15, the uncertainties from the measured power-to-melt (converted to reactor power units), the extrapolation to CRBRP conditions, and the CRBRP design uncertainties are statistically combined, and the design criterion for melting is examined to see if it is fulfilled for the programmed reactor startup chosen.

1630 089

The positive margin at all times shows that the power-to-melt criterion is met by the selected programmed startup.

Applying Equation (2.8) to take into account the number of data points used in obtaining $\sigma_{P19/P20}$ and σ''_{space} does not significantly affect the results.

TABLE 3.12

SENSITIVITY OF POWER-TO-MELT TO DESIGN UNCERTAINTIES

TIME, t hrs.	REPOW	CHANGE IN POWER-TO-MELT FOR ONE PERCENT CHANGE IN DESIGN UNCERTAINTY [$\partial REPOW_M / \partial(\%X_i)$]				
X_i:		ρ_{pel}	D^*_{pel}	D_{clad}	Power	T_{clad}
8	0.7	-.0040	.112	-.098	-.0107	-.00092
58	0.9	-.0017	.043	-.062	-.0027	-.00069
108	1.0	-.0051	-.051	.060	-.0093	-.00081
158	1.0	-.0051	-.050	.060	-.010	-.00081

*Derivative taken from Figure 3.20.

1630 091

TABLE 3.13

STATISTICAL COMBINATION OF POWER-TO-MELT
UNCERTAINTIES DUE TO DESIGN UNCERTAINTIES

TIME, t hrs.	REPOW	ONE SIGMA POWER UNCERTAINTY RESULTING FROM DESIGN UNCERTAINTY $[\sigma_i \, \partial \overline{REPOW}_M / \partial X_i]$					STATISTICAL COMBINATION
		ρ_{pel}	D_{pel}	D_{clad}	Power	T_{clad}	$\sigma_{\overline{R}}$
8	0.7	-.0041	.050	-.014	-.0337	-.0036	.062
58	0.9	-.0017	.019	-.0089	-.0085	-.0027	.023
108	1.0	-.0052	-.023	.0087	-.0294	-.0032	.039
158	1.0	-.0052	-.022	.0087	-.0315	-.0032	.040

1630 092

TABLE 3.14

EFFECT OF MELTING POINT UNCERTAINTY OF
σ_{TM}=5.8°F ON UNCERTAINTY OF POWER-TO-MELT

t(hrs)	$\partial\bar{Q}_M/\partial T_M$ kw/ft/°F	σ_{extrap} (kw/ft)	σ_{extrap} (REPOW Units)
8	0.0095	.055	.0043
58	0.0069	.040	.0031
108	0.0061	.035	.0027
158	0.0058	.034	.0026

1630 093

TABLE 3.15

TOTAL UNCERTAINTY ON CRBRP REACTOR POWER-TO-MELT
IN REACTOR POWER UNITS WHERE NOMINAL FULL POWER IS 1.0

t (hrs)	REPOW	$\sigma_{\overline{R}}$	σ_{mean}	σ_{extrap}	TOTAL σ_{REPOW_M}	$\overline{REPOW}_M$ (nominal,t)	$\overline{REPOW}_M - 3\sigma_{REPOW_M}$ -1.15 REPOW
8	0.7	.062	.047	.0043	.078	1.152	.113
58	0.9	.023	.055	.0031	.060	1.335	.120
108	1.0	.039	.058	.0027	.070	1.415	.055
158	1.0	.040	.059	.0026	.071	1.437	.074

3.3 Coolant Exit Mixed Mean Hot Spot Factors for Fuel Assemblies

This Section discusses the hot spot factors which apply to the average coolant temperature (or enthalpy) rise for a single assembly.

Essentially, the same individual factors discussed in Section 3.1 for the enthalpy rise of the hot rod contribute to the coolant exit temperature; however, integrated values over the assembly must be considered for the assembly mixed mean exit.

The hot spot factors for evaluation of CRBRP fuel assemblies mixed mean exit temperature are presented in Tables 6.2A and 6.2B.

3.4 Fission Gas Plenum Pressure Uncertainty Factors for Fuel Assemblies

This Section discusses the uncertainties which apply to calculations of the fuel rod fission gas plenum pressure. The fission gas plenum pressure is calculated through the perfect gas law:

$$p = nRT/V$$

and consequently, depends on uncertainties affecting the rated value of:

- plenum volume
- plenum temperature
- amount of gas released to the plenum, which depends on burnup (i.e., amount of gas produced) and fractional release.

The fission gas release model, its calibration against experimental data from irradiation of mixed oxide fuels in EBR-II and the associated uncertainty analysis will be documented in a separate report for the FSAR.

With regard to plenum volume, the minimum volume considering all the geometrical tolerances is conservatively assumed for all plenum pressure calculations.

Finally, an uncertainty analysis of the various factors contributing to the plenum temperature and burnup was conducted. Hot spot factors are reported in Tables 6.3A and 6.3B. Since the analysis is used for fuel lifetime calculations, the hot channel factors are evaluated for plant expected operating conditions.

Essentially, the same individual factors discussed in Section 3.1 for the enthalpy rise of the hot rod are considered, keeping in mind that for plenum

pressure calculations integrated values over the rod length and assembly residence time must be considered. The various subfactors are discussed in the following.

3.4.1 Power Level Measurement and Control System Dead Band

The power measurement bounding uncertainty including calorimetric power measurement error, setting instrumentation error and drift in instrumentation and electronics is 1.65% (2σ). This appears in Table 6.3A as a 1.025 (3σ) factor on burnup. The temperature effect appears as part of the reactor Δ^T and inlet temperature variation factor.

The integrated effect of the $\pm$ 2% control system dead band over the assembly lifetime is estimated to be zero. The control rod stop which limits the combined power level and control dead band uncertainty to a maximum of $\pm$3% will conservatively be neglected.

3.4.2 Flow Distribution Calculational Uncertainty

Two fuel assembly analyses were performed using COTEC with different mixing parameters. These results showed the uncertainty factor on coolant temperature rise in the core region to be greater than the uncertainty on average plenum temperature. It will be conservatively assumed that the factor for the plenum temperature is equal to that for the core region as discussed in Section 3.1.6.

3.4.3 Subchannel Flow Area

The uncertainty will be less than that in the core region as discussed in Section 3.1.8 because the gas plenum temperature is the average of the six neighboring subchannels and because temperature uncertainties in the core region are reduced by coolant mixing in the gas plenum region. However, for the present analysis the uncertainty will be conservatively assumed to be the same as for the core region.

3.4.4 Remaining Factors

The remaining uncertainty factors are the same as for the hot rod, as discussed in Section 3.1.

4.0 BLANKET ASSEMBLIES HOT SPOT FACTORS

The inner and radial blanket hot spot factors are evaluated similarly to the corresponding fuel hot spot factors even though the actual numerical value may be different, since a different type of assembly is considered. The detailed discussion in Section 3 is still valid and therefore, it not repeated here; only the major differences are discussed in this Section.

4.1 Fuel Rod Cladding and Coolant Temperatures Hot Spot Factors for Blanket Assemblies

The hot spot factors for evaluation of CRBRP inner and radial blanket assemblies rod cladding and channel coolant temperatures are presented in Tables 6.4A and 6.4B.

4.1.1 Cladding Circumferential Temperature Variation

Analyses of the blanket rod cladding circumferential temperature variation using the FATHØM-360 computer program[1] showed that the hot spot factor is in the range of 3.0 to 3.3 across the film (depending upon assembly operating conditions), approximately 0.6 from cladding OD to midwall and approximately 0.7 from cladding OD to ID. A detailed analysis is performed for the lifetime-limiting assembly in each flow zone. In addition, a 20% bounding uncertainty is applied to the deviations from the nominal case to conservatively account for uncertainties resulting from finite-difference modeling, flow distribution uncertainties and flow mixing uncertainties.

4.1.2 Inlet Flow Maldistribution

Inlet flow maldistribution subfactors are the same as for Fuel Assemblies (Section 3.1.5) with the following exceptions. Manufacturing tolerances (excluding the rod bundle region which is considered separately in the Subchannel Flow Area analysis) resulted in a bounding 3σ flow uncertainty of 0.023 for the Radial Blanket. For the Inner Blanket, the same value was conservatively used as for the Fuel Assemblies.

IPFM test data for Fuel Assemblies also apply for Inner Blanket Assemblies. Test data for Radial Blanket LIM's are given in Table 4.1. A statistical analysis of the four-run average flow for each LIM showed a variation of

0.0294 based on 26 data points. This was increased to 0.04 on the basis of engineering judgement to allow margin to envelope possible differences between homogeneous and heterogeneous core configurations. This is considered to be conservative since based upon the observed differences between fuel assembly and radial blanket assembly LIM flow variations in the IPFM test, heterogeneous core radial blanket LIM's are expected to show less scatter than homogeneous core radial blanket LIM's.

The 3σ uncertainty in blanket assembly flow due to fuel assembly systematic error interation is calculated to be 0.011 by a similar analysis to that discussed in Section 3.1.5.

An additional uncertainty occurs in the Radial Blanket because the number of orifices in the LIM is varied to achieve the goal assembly pressure drop. This step-wise approximation of the pressure drop requirements results in a bounding 3σ flow uncertainty of 0.043.

The remaining Inlet Flow Maldistribution subfactors are the same as for the Fuel Assemblies. The 3σ subfactors for the Inner Blanket and the Radial Blanket are listed in Table 4.2. The overall factor calculated as the root-mean-square of the subfactors is also shown.

TABLE 4.1

RESULTS OF FOUR IPFM FLOW
DISTRIBUTION TESTS AT ~100% FLOW, 3 LOOPS

	FLOW DEVIATION FROM AVERAGE, %			
LIM	RUN 1	RUN 2	RUN 3	RUN 4
D17	.62	-.53	-.19	-.48
D12	-.00	.41	.07	.52
E1	-.95	-.91	-.84	-.52
E24	-1.37	-.66	-1.10	-.32
E23	1.05	.99	.95	1.70
E22	1.52	1.88	2.48	1.50
E21	.06	-.16	-.43	-.42
E20	-.38	-.94	-.23	-.61
E19	1.08	.10	1.02	.22
E18	-.83	-.88	-.80	-.56
E17	-.66	-.49	-.42	-.14
E16	.67	1.44	1.53	1.94
E15	1.42	.97	.19	1.03
E14	-.10	-.02	-.05	.29
E13	.29	-.17	-.03	.01
E12	-2.15	.79	-.38	-1.56
E11	-2.19	.89	.15	-.84
E10	-1.19	-.77	-.63	-1.35
E9	.22	-.22	.18	.42
E8	.64	-.98	-1.61	-1.36
E7	-2.65	-1.88	-1.84	-1.74
E6	1.68	1.32	1.35	.93
E5	2.36	1.39	1.12	1.31
E4	-.87	-1.49	-1.43	-1.22
E3	1.77	.13	.78	1.08
E2	-.02	-.21	.15	.16

1630 099

TABLE 4.2

BLANKET ASSEMBLY INLET FLOW MALDISTRIBUTION SUBFACTORS (3σ)

	Inner Blanket	Radial Blanket
Hydraulic Characteristics		
Systematic	1.018	1.018
Random	1.045	1.045
Manufacturing Tolerances	1.013	1.023
Orificing Inflexibility	-----	1.043
Configuration		
Among LIM's	1.02 (33)*	1.04 (26)*
Among Assemblies	1.024 (7)*	1.024 (7)*
Systematic Error Interation	1.011	1.011
Overall (3σ)	1.060	1.084

*Number of data points shown in parentheses.

1630 100

4.1.3 Flow Distribution Calculational Uncertainty

The flow distribution calculational uncertainty for the blankets was based on extrapolating from the analysis for the fuel assemblies (Section 3.1.6). The value of the coefficient C in Equation (3.8) was increased to 0.6945×10^{-3} in^{-1} to account for a possible bundle size effect. The value was obtained empirically by interpolating between HEDL 217-rod[9] and ORNL 19-rod[6] data. The value of the CØTEC empirical cross flow parameters were determined from data from experiments in diverse geometries[6-11].

The uncertainty analysis was performed as for the fuel assemblies (Section 3.1.6) and the largest hot channel factors were found to occur in the peak skew assemblies. The value at the cladding peak temperature elevation was 1.199 (3σ). This was combined with the flow split uncertainty of 1.04 (3σ) for a 61-rod bundle (Section 3.1.6) to give an overall statistical uncertainty of 1.203 (3σ).

In addition, a direct factor of 1.03 is applied. This includes the direct flow split factor of 1.01 for a 61-rod bundle (by the same method as in Section 3.1.6) as well as additional margin which based on previous experience with sodium heat transfer experiments in rod bundles is judged to be sufficient to cover the testing biases and uncertainties which might be uncovered during the heat transfer testing of a prototypic rod bundle in sodium since the blanket analysis is based on the extrapolation of non-prototypic rod bundle mixing tests.

In a recent study[39], the flow split was measured in a nearly prototypic blanket geometry using the isokinetic sampling technique. The ratio of interior-to-average subchannel velocity at the maximum flow rate tested was reported to be 0.88. This study is being evaluated and may require modification of the flow split used in CØTEC blanket analyses and recalculation of AFMS assemblies flow distribution and temperatures.

Test data are forthcoming which will provide a more direct measure of the code calibration and uncertainties for the FSAR analyses (See Table 6.11). A 5:1 scale test at ARD of a sector of a blanket rod bundle using air will provide detailed crossflow data. Heat transfer tests in sodium are being performed at ARD on a prototypic blanket rod bundle covering a range of power levels, flow rates, and power skews typical of blanket operating conditions in CRBRP.

4.1.4 Subchannel Flow Area

COBRA IV[40] analyses, similar to those discussed in Section 3.1.8 for the fuel rod bundle, were performed for the blanket rod bundle. In addition to the nominal case, runs were made for the cases of a) a single nested subchannel, b) the hot subchannel and three adjacent subchannels all nested, c) maximum duct ID and minimum rod and wire OD, and d) minimum duct ID.

From these results, the overall bounding 3σ uncertainty in hot channel coolant temperature rise due to uncertainties in rod, wire and duct dimensions and rod spacings, and including the influence of the other subchannels, was calculated to be 0.053. The uncertainty was increased to 0.07 based on engineering judgement to account for calculational uncertainties.

This uncertainty applies at the beginning of life. The effect of irradiation-induced swelling of rod wire and duct was analyzed for a homogeneous core radial blanket assembly assuming maximum distortion rates and resulted in a direct factor of 1.020 at end-of-life. Using homogeneous core fuel assembly swelling calculations, the heterogeneous core inner blanket direct factor was estimated to be 1.029 at end-of-life. Because of the uncertainty in extrapolating from homogeneous to heterogeneous core conditions, a direct factor of 1.05 at end-of-life will be used based on engineering judgement for both inner and radial blankets until the corresponding analyses are performed for heterogeneous core conditions which will be done for the FSAR.

4.1.5 Film Heat Transfer Coefficient

A conservative design correlation was selected in Reference 19 for the rod pitch-to-diameter ratio range $1.05 \leq P/D \leq 1.15$ corresponding to that in CRBRP blanket and control assemblies. The data base is shown in Figures 4.1 to 4.3, together with the design correlation which is designed Curve 2. A 3σ uncertainty of 0.21 was recommended based on the deviations of the data points overpredicted by the correlation.

As an indication of the conservatism of the correlation, it may be noted that in the range of interest, the correlation results in lower heat transfer coefficients than the theoretical lower limit calculated for the case of turbulent flow through unbaffled rod bundles, under conditions of uniform heat flux at the inside surface of the cladding, with heat transfer by molecular conduction only through the sodium[20].

4.1.6 Pellet-Cladding Eccentricity

The pellet eccentricity factor was assumed the same as for the fuel assemblies. Since it differs from unity only at beginning of life, it does not significantly affect blanket assembly lifetime.

4.1.7 Nuclear Uncertainties

Tables 6.4B and 6.5B list the uncertainties applicable to the predictions of local and rod or assembly-integrated power uncertainties in the inner and radial blanket assemblies. Blanket uncertainties are divided into beginning and end-of-life values primarily as a result of the large change in isotopic fission rates. Values are presented for the heat flux (power density) uncertainty near the midplane at the location of the peak linear power and near the top of the 36-inch "core" (the approximate location of the peak clad temperature), and the channel coolant uncertainty (the rod-channel integrated power uncertainty for application to the total channel enthalpy rise and to the total rod burn-up) in Table 6.4B, and for the assembly-integrated power uncertainty (for the mixed mean coolant outlet temperature) in Table 6.5B. The blanket uncertainties have been derived to best fit the respective high power locations.

1630 103

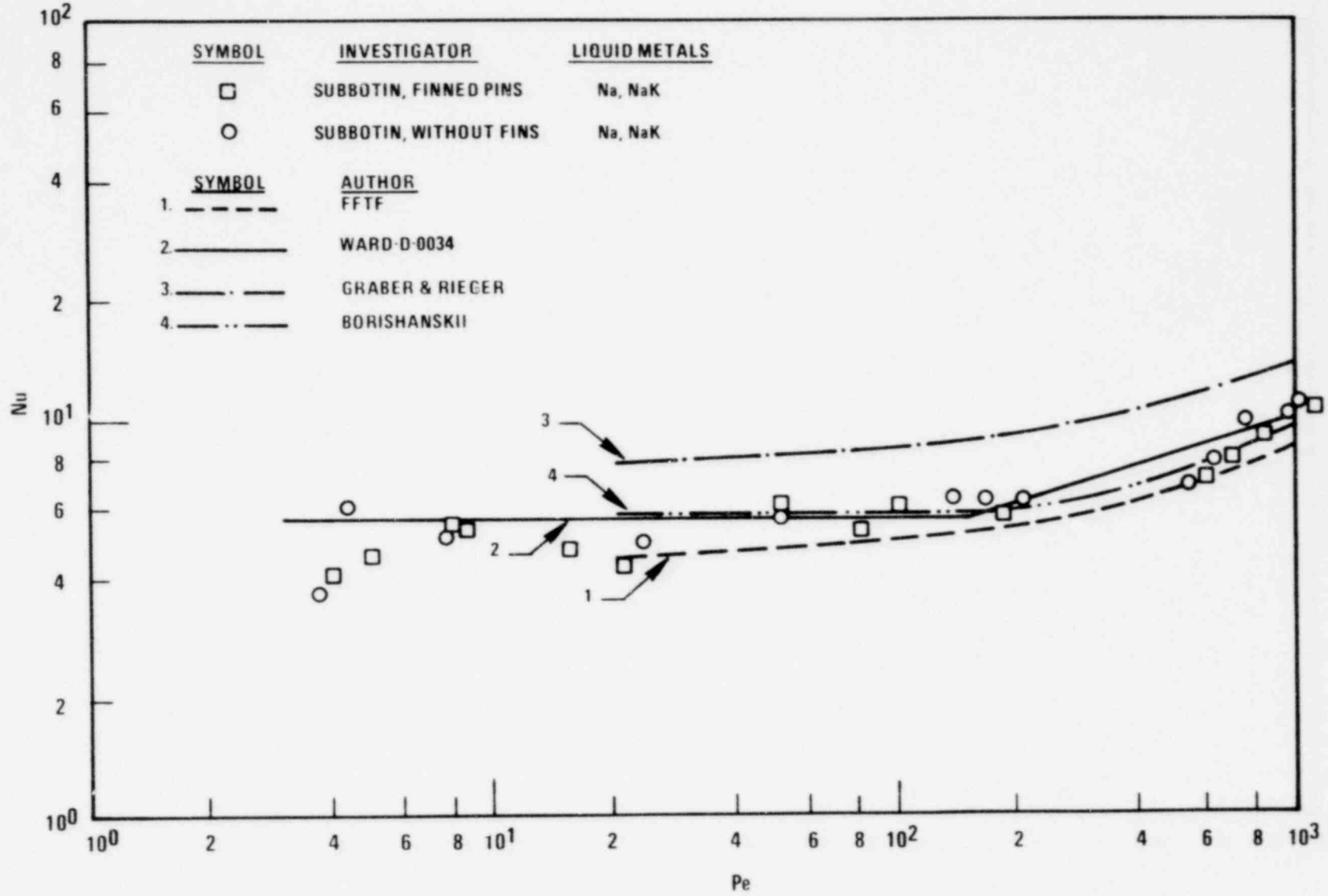

Figure 4-1. Comparison of Predicted and Experimental Results for P/D = 1.15

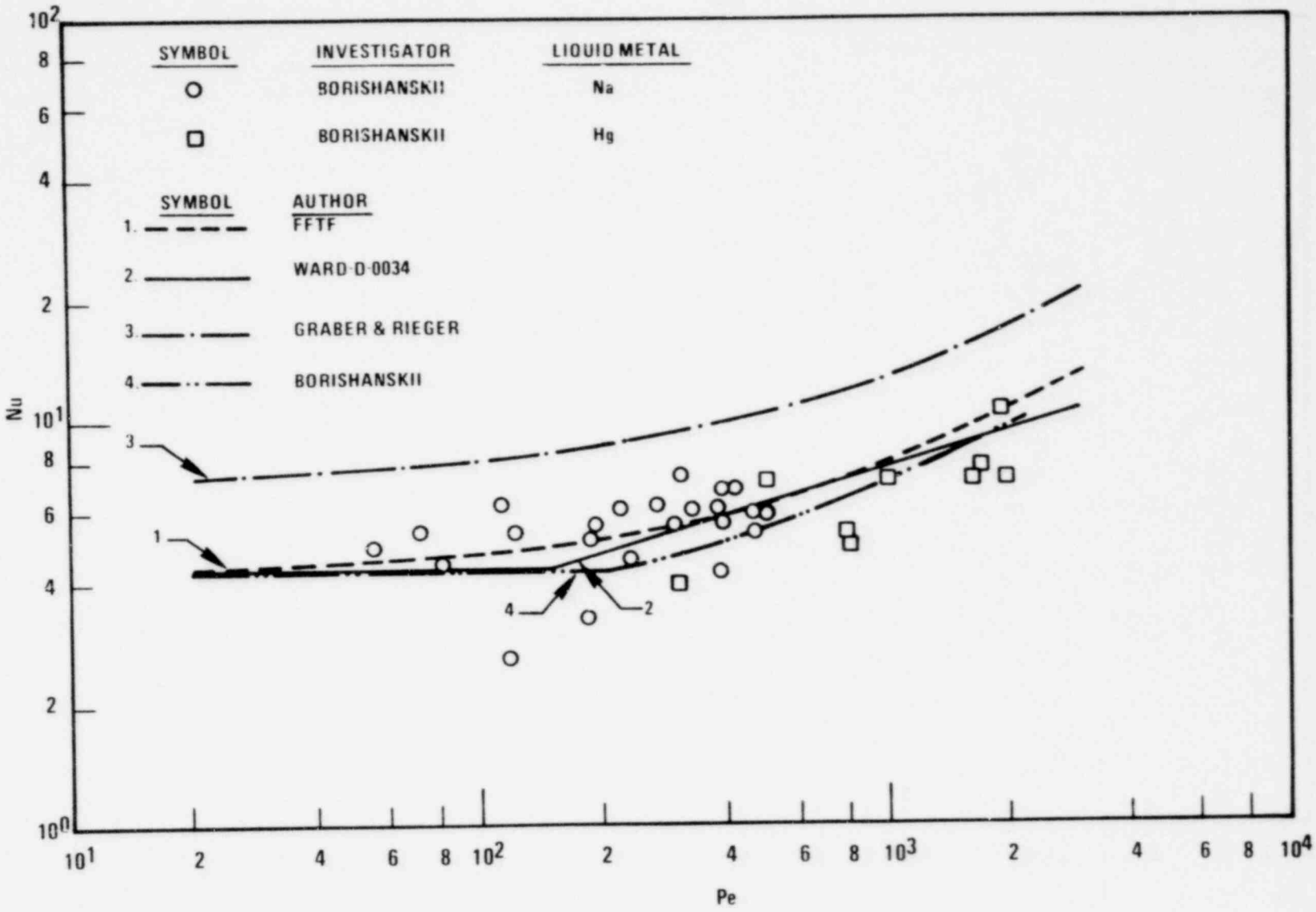

Figure 4-2. Comparison of Predicted and Experimental Results for P/D = 1.1

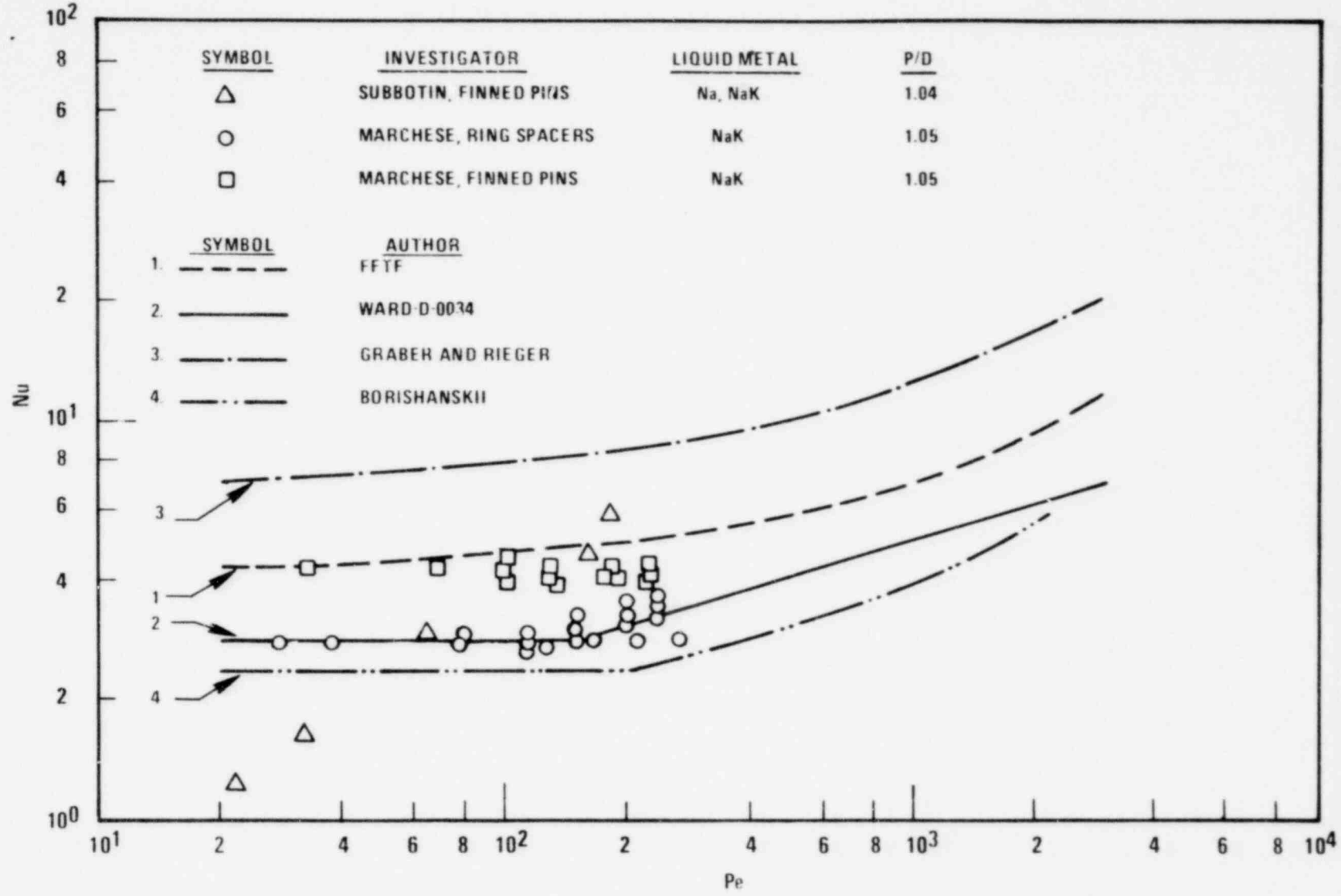

Figure 4-3. Comparison of Predicted and Experimental Results for P/D ≤ 1.05

4.1.7.1 Experimental

Due to the somewhat limited scope of the measured blanket data in Phases A-E of ZPPR-7, it is recommended that the experimental fission and capture rate and gamma heating uncertainty component be combined directly (rather than in quadrature as with the purely statistical uncertainties) with the other uncertainties in the inner blanket assemblies, which is a conservative approach. The experimental uncertainty component is defined to be three times the root mean square combination of the Pu-239 fission rate, U-238 fission rate, U-238 capture rate and gamma heating rate deviations, weighted by their respective fractions of the total inner blanket power for any particular location and for any particular time in life.

The beginning-of-life inner blanket power experimental uncertainty is dominated by the statistical $\pm$10% (3σ) uncertainty in U-238 fission rate which contributes nearly 60% of the total fresh blanket power (compared to less than 30% of the end-of-life power in the burned blankets). The remaining uncertainty at the beginning-of-life results from the 15-20% uncertainty in the predicted blanket gamma heating which constitutes nearly 40% of the beginning-of-life blanket power and about 20% of the end-of-life blanket power. Pu-239 fission calculation-to-experiment ratios vary $\pm$3% to $\pm$5% (3σ) at beginning and end-of-life, respectively, in the inner blankets. In addition, the U-238 capture rate (Pu-239 production rate) is substantially (9 $\pm$ 4%) overpredicted, necessitating the application of an end-of-life fission rate bias of less than unity. Pu-239 fission comprises roughly 50% of the end-of-life inner blanket power. The 2% overprediction of axial peak-to-average power, as well as the $\sim$5% underprediction of power density at the extremities of the (36") "core", are biased out of the inner blanket experimental uncertainties in Table 6.4B. Combining the aforementioned reaction rate and gamma heating uncertainties with their fractional contributions to the total blanket power results in the time-dependent biases and uncertainties shown in Table 6.4B. In particular, the peak power density uncertainty is $\pm$10% at beginning-of-life and -5 $\pm$ 5% at end-of-life.

1630 107

The radial blanket calculation-to-experiment ratios of fission and capture rate data in ZPPR-7 exhibit a characteristic space dependence, falling-off of the order of 10% in the radial direction from the core-blanket interface out to the blanket-reflector interface. Due to the limited number of radial blanket measurements and the space-dependent nature of the data, the radial blanket experimental uncertainties are treated non-statistically for each blanket row. The radial blanket experimental power uncertainty is derived from the limits of the observed variations in blanket fission and capture rates and gamma heating. It is assumed that the observed variation limits represent 1.5σ limits so that 3σ equivalent empirical uncertainties can be obtained by doubling the maximum deviation from the mean of the Pu-239 fission rate, U-238 fission rate, U-238 capture rate and gamma heating rate variation limits weighted by their respective fractions of the total blanket power at any particular radial location and for any particular time in life.

The beginning-of-life row 1 radial blanket power experimental uncertainty is again dominated by the empirical +6 $\pm$ 8% uncertainty in U-238 fission rate which constitutes approximately 60% of the fresh blanket power. In the second row, the beginning-of-life U-238 fission rate empirical uncertainty is +23 $\pm$ 20% due to an apparent mis-prediction of the blanket spectral gradient. The remaining uncertainty results from the $\pm$20% uncertainty in the blanket gamma heating rate which constitutes about 40% of the fresh blanket power. The 2% over-prediction of axial peak-to-average power, as well as the $\sim$5% underprediction of the power density at the extremities of the 36 inch "core", are biased out of the radial blanket experimental uncertainties. The net resultant beginning-of-life radial blanket peak power density experimental uncertainties are therefore +2 $\pm$ 9% (row 1) and +10 $\pm$ 14% (row 2).

At the end-of-life, the U-238 fission rate (15-25% of the total radial blanket power) uncertainty increases to +13 $\pm$ 12% (row 1) and +33 $\pm$ 20% (row 2). The U-238 capture rate (Pu-239 production rate) is again overpredicted (+10 $\pm$ 8% in the first row and +4 $\pm$ 8% in the second row). Additionally, the end-of-life Pu-239 fission rate uncertainty is $\pm$4% (row 1) and +7 $\pm$ 4% (row 2). The U-238 capture rate (buildup) and Pu-239 fission rate uncertainties are both

applied to the 60-70% of the end-of-life radial blanket power attributable to Pu-239 fission. Combining the Pu-239 fission rate, U-238 capture rate, U-238 fission rate and gamma heating rate uncertainties with their fractional contributions to the total radial blanket power, and applying the aforementioned 2% axial peak-to-average bias, results in the time and space-dependent experimental biases and uncertainties in Table 6.4B. The resulting net end-of-life radial blanket peak power density experimental empirical uncertainty is -4 $\pm$ 7% in the first row and +5 $\pm$ 8% in the second row.

4.1.7.2 Manufacturing Tolerances

The $\pm$1% blanket heavy metal theoretical density tolerance gives rise to a similar bounding $\pm$1% uncertainty in blanket power generation. The U-235 content tolerance in the depleted uranium blanket feed material results in a small ($\pm$1%) uncertainty in the beginning-of-life blanket power, and a negligible uncertainty in the end-of-life power where U-235 fission contributes only about 2% of the total blanket power.

4.1.7.3 Modeling Uncertainties

Blanket modeling bounding uncertainties consist of power-by-rod interpolation uncertainties, intra-assembly burnup uncertainties, axial power shape and buildup uncertainties and 3D geometric effects. The least-squares fit to power-by-rod in the inner blankets is performed with input from 24 mesh-per-assembly 2DB calculations. Pin-by-pin burnup does not substantially increase the peak end-of-life power in the highest power assemblies. The fitting uncertainty in the inner blankets is assumed to be $\pm$5% at beginning-of-life (where the fresh blanket power is sensitive to both the total flux and neutron spectrum gradients), and $\pm$1% of the end-of-life (where the peak inner blanket power is relatively flat and less fast-spectrum sensitive). The axial peak-to-average power shape uncertainty, deduced from RZ burnup calculations, is $\pm$1% near the core midplane and $\pm$5% at the top of the 36 inch "core" region, primarily due to smoothing at the end-of-life. Additional three-dimensional effects to not contribute a substantial uncertainty in the inner blankets ($\pm$1 to 2%).

Radial blanket modeling uncertainties consist of power and burnup-by-rod (PUMA) uncertainties, axial power and buildup uncertainties and 3D geometric effects. The rod-fitted flux, cross-section and gamma heating and the resulting composite power and burnup (buildup) distribution uncertainties are taken to be ±5% at the beginning-of-life of ±2 to ±3% at the end-of-life based on PUMA benchmark verification calculations. The axial power shape uncertainty in the radial blankets is +1% at the core midplane at the beginning-of-life, ±2% at the core midplane at the end-of-life based on a chopped cosine approximation, and ±5% at the top of 36 inch "core" region due to smoothing of the burnup distribution at end-of-life. The 2D power synthesis is arranged to best predict the radial blanket power (±1%) near the highest power locations on the sides of the assemblies closest to the core. The net blanket modeling uncertainty is ±7%.

4.1.7.4 Criticality and Control Rod Banking Uncertainties

Criticality and control rod banking bounding uncertainties primarily influence the inner blanket power distributions. In addition to the effect of criticality uncertainties on control rod insertion, and hence, on power distribution as discussed earlier, the uncertainty in fuel enrichment specification results in a flux level uncertainty which ultimately results in a ±1% plutonium buildup and end-of-life blanket power uncertainty.

1630 110

4.2 Power-to-Melt Uncertainty Factors For Blanket Assemblies

4.2.1 Extrapolation Uncertainty

The LIFE-III Code's thermal analysis has been well calibrated against low-burnup (<1.1%) fuel pin PIE measurements. Blanket pin irradiation tests are in progress and additional tests are planned (see Table 4.3), but PIE data to verify the code are not currently available. Therefore, application of the LIFE-III Code to radial blanket pins involves extrapolation of fuel pin data. Three basic types of possible errors are involved.

1. Errors due to the larger diameter of radial blanket pins, i.e., if any model contains an incorrect dependency on length (e.g., the thermal-gradient dependency of pore velocity may not be linear as assumed), there will be an error which will show up in the thermal analysis of a radial blanket pin even though the calibration corrects for this error in fuel pins;
2. Errors due to uncertain dependencies of various fuel properties on PuO_2 content;
3. Errors due to extrapolation of thermal fuel pin data to higher burnups (≈1.6%) and/or times (≈13,000 hours) that characterize blanket pins when their power is at a maximum.

Each of these three potential error sources is evaluated below.

The present analysis uses the specifications and operating conditions of 1B/A 128, pin 27. Gamma heating was taken explicitly into account. However, the approximation was made that it all occurs in the fuel and not in the cladding and sodium. This is a conservative assumption. The pin studied has the highest center temperature of any radial blanket pin. The section at X/L = 0.466 was run since a preliminary study showed that this value of X/L has the highest fuel center temperature. A power ramp was imposed on the normal operating history at the end of Cycle 4, at which time the power is highest, to determine the power-to-melt. The results of the LIFE-III runs are given in Figure 4.4 for initial diametral gaps varying from 4 to 9 mils. The powers-to-melt are all about 23.8 kW/ft (39% over-power) with very little dependence on initial gap size. The latest (Revision 5)

TABLE 4.3

BLANKET IRRADIATION TESTS

DRS NO.	FACILITY	TEST	SCHEDULE FOR COMPLETION	PURPOSE
31.3.03	EBR-II	WBA-20	9/80	Power Jump Test
		WBA-21	9/83	2σ Limit Test
31.3.04	FFTF	WBA-40	9/87	RB/A Proof Test
		WBA-41	9/85	IB/A 2σ Limit Test
		WBA-45/46	9/85	Instrumented Natural Circulation Test; Power-to-Melt Test

1630 112

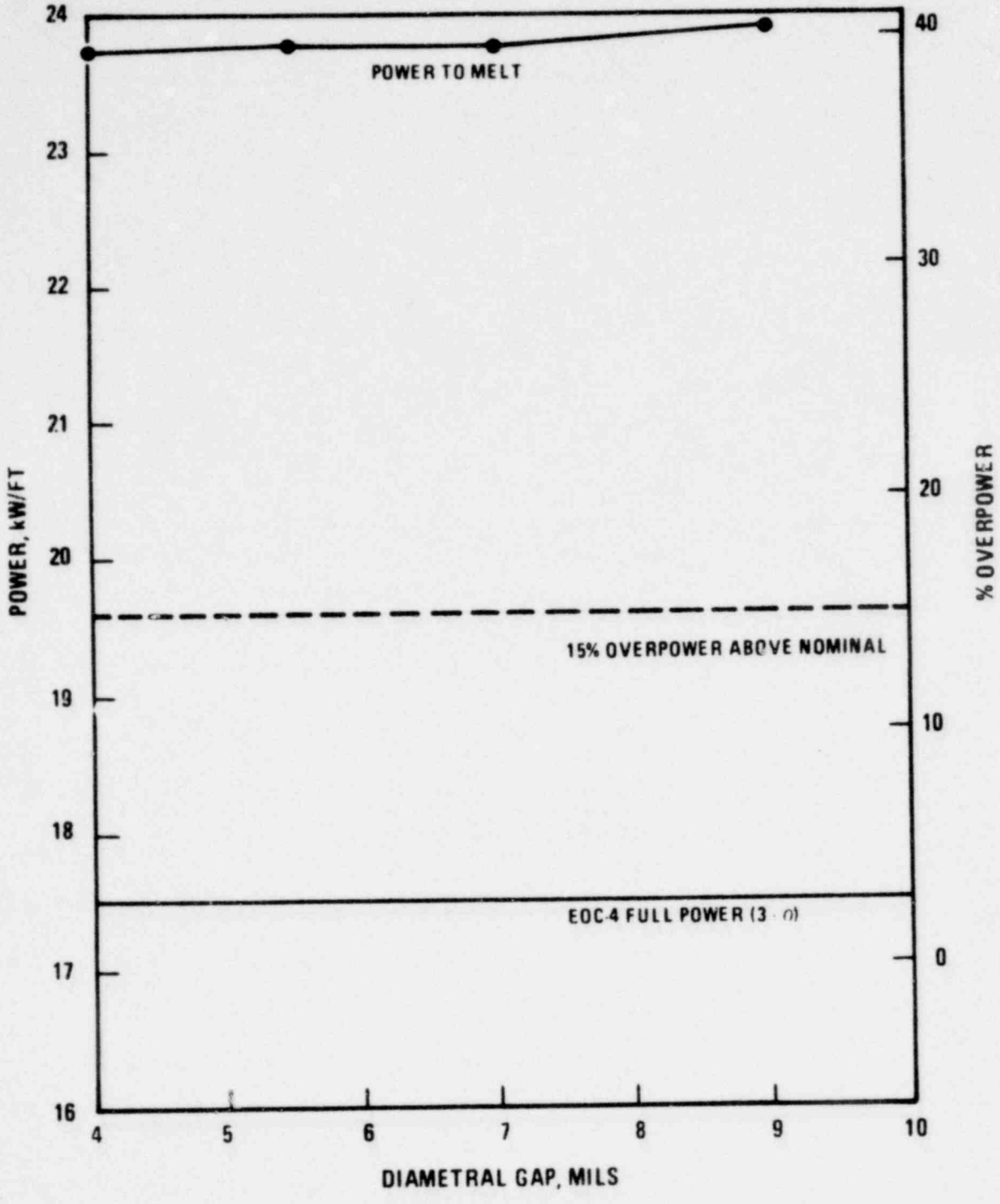

Figure 4-4. Power-To-Melt Study, IB A 128, Pin 27 X/L = 0.466 EOC-4 3-σ Operating Conditions.

0926-25

1630 113

cladding swelling equation was used, with a nominal τ of 6.3. The NSMH[21] fuel melting temperature (solidus) was used. It takes burnup and PuO_2 content explicitly into account. A PuO_2 content at the end of Cycle 4 of 4.5 wt.% was used. This gives a fuel melting temperature of 5057°F.

Error Source (1)

There are three possibilities for errors of this type:

(a) In addition to microscopic roughness, the surface roughness term in the gap conductance equation includes "waviness" and "errors of form" which are likely to be proportional to the fuel pellet diameter even though LIFE-III assumes this roughness to be independent of pellet diameter. To evaluate this error, it was assumed that the worst possible case of zero microscopic fuel surface roughness applies and that the entire fuel surface roughness is composed of waviness and errors of form. Thus, the surface roughness term for radial blanket rods should be increased by the ratio of the blanket pellet diameter to the fuel pellet diameter (2.36). The effect of this change on radial blanket power-to-melt was found to be a reduction from 23.58 to 23.31 kW/ft., i.e., by 1.6% of nominal full power (16.86 kW/ft). The evidence as to the basic character of the surface roughness is in favor of it being composed of microscopic roughness which is determined by the grinding operation (and hence independent of pellet diameter). LIFE-III uses roughness values characteristic of grinding operations.

(b) The pore velocity equation may not be linear in thermal gradient as assumed. This is highly improbable, however, because all known mechanisms for pore migration (surface diffusion, volume diffusion, vapor-phase transport) are all known to be linear in thermal gradient.

(c) The fuel swelling rate may not properly model changes in scale. Thus, there is an uncertainty in the state of the fuel-cladding gap. In the nominal case the gap is open by 0.17 mils (radial) at the start of the power ramp (at the end of Cycle 4). Because of uncertainty, however, the possibility of a significantly larger gap exists. To evaluate the uncertainty in power-to-melt resulting from the uncertainty

in fuel swelling, the swelling rate was reduced by a factor of 10 to represent a bounding 3σ uncertainty. This produced a start-of-jump gap of 0.60 mils, but it increased the power-to-melt to 24.1 kw/ft. The reason for this result is that the fuel ran hotter during its lifetime and consequently increased the central hole from 9.4 mils to 16.2 mils.

The fuel swelling rate was then increased by a factor of 10 to cause the gap to be closed at the start of the power jump. This left the central hole essentially unchanged and reduced the power-to-melt to 23.46 kw/ft. This sensitivity yields a bounding uncertainty of 0.71% of nominal full power. Since further fuel swelling rate increases cannot reduce the gap further, this uncertainty represents essentially the maximum that can be obtained.

Error Source (2)

Consider first the dependence of fuel thermal conductivity, K_f, on PuO_2 content. To take account of the lower PuO_2 content (4.5% at end-of-life) of the radial blanket pins relative to the 25% PuO_2 content of the calibration pins, the nominal value of K_f was increased by 3.2% in accordance with the accepted dependence[41] of K_f on PuO_2 content. To estimate the 3σ error involved in this extrapolation to lower PuO_2 content, it was assumed that the 3σ error in the gradient in the K_f vs. PuO_2 function is ±100%. Thus, the most negative uncertainty in K_f is -3.2%. This produces a reduction in power-to-melt of 3.1% of nominal full power.

Next, consider the dependence of gap conductance, Hg, on PuO_2 content. There is no obvious reason why gap conductance should be dependent on PuO_2 content in any but very minor ways. UO_2-PuO_2 hardness may be somewhat dependent on PuO_2 content. However, since the stainless steel cladding is the softer material, the hardness of the fuel does not enter the gap conductance equation. Pore migration velocities depend on PuO_2 content by virtue of the different diffusivity and vapor pressure of PuO_2. The difference between the vapor pressure of PuO_x and UO_x gaseous species over solid UO_2-PuO_2 at a given temperature is very small however. Thus, pore migration velocities should be only slightly dependent on PuO_2 content. This conclusion is further supported by the fact that the rate of pore migration is controlled by the migration rate of the least-mobile species. Thus, over a wide range

of PuO_2 contents, only very little variation in pore-migration velocity is expected. Therefore, uncertainties from this source are taken as negligibly small in this analysis.

Error Source (3)

The LIFE-III thermal analysis was calibrated and checked-out against fuel pin PIE data that extended out to burnups of 1.1% and times of about 1,000 hours. Radial blanket pins of interest here have peak burnups of about 1.6% and operating times of about 13,000 hours. Thus, extrapolations outside the calibration-checkout data base are implied by LIFE-III thermal analyses of the radial blanket pins. There are four basic extrapolations to be evaluated here:

(a) Melting temperature extrapolation

An uncertainty in radial blanket power-to-melt calculations arises from the uncertainty in melting temperature. This uncertainty has two components:

(a) the uncertainty in the UO_2-PuO_2 solidus temperature, and

(b) the uncertainty in the effect of burnup on melting temperature.

The 1σ uncertainty values for these items are 25[42] and 24.5°C[43] respectively. A statistical combination of these yields a net 1σ uncertainty of 35°C. This temperature uncertainty translates into a power uncertainty of 1.05 kW/ft. (3σ), i.e., 6.2% of nominal full power.

(b) Gap Conductance Extrapolation

Gap conductance, Hg, changes with time because the gap surface roughness is reduced by creep (which causes an increase in Hg.) LIFE-III does not model this creep-relaxation and hence predicts no increase in Hg due purely to time. Hg does change with burnup, however, due to (1) fission gas dilution of the plenum gas and (2) the buildup of solid fission products in the gap.

Fission gas dilution of the plenum gas is determined by the amount of fission gas released and the initial moles of helium fill-gas. The fission gas release model has been calibrated against fuel pins covering a wide range of burnups and times as part of the calibration of the mechanical

analysis of LIFE-III. However, there is some question as to the direct applicability of this model to radial blanket pins. As an estimate of the 3σ uncertainty associated with applying the present LIFE-III fission gas release model to radial blanket pins, the nominal fission gas release rate was decreased by a factor of 100. This reduced the overall fission gas release from 85 to 41% which is considered to be about as large an error in fission gas release that differences between fuel and blanket pins could conceivably cause. This was found to reduce the power to melt by 0.36 kW/ft. i.e. by 2.13% of nominal full power (16.86 kW/ft.). The effect of a given amount of fission gas dilution of the plenum gas on gas thermal conductivity has been accurately measured over the full range of gas compositions by Von Ubish, Hall, and Srivastav[44]. The small uncertainties in the Von Ubish et al measurements are negligible in comparison with the remaining uncertainties.

The buildup of solid fission products in the fuel-cladding gap is modeled only quasi-empirically by using what is referred to as the "CRUDFIL" factor. To simulate the burnup dependence of this factor, the rate of transfer of solid fission products to the gap is taken to be directly proportional to the rate of release of gaseous fission products from the fuel.

The in-reactor behavior of UO_2 or UO_2 with lower PuO_2 contents (blanket fuel) is very similar to core fuel (~25% PuO_2-UO_2). Thus, it is expected that the "CRUDFIL" factor derived from core fuel experiments should apply to blanket fuel. However, there is some uncertainty concerning the exact value.

As a bounding estimate of the 3σ uncertainty associated with this model, it is assumed that the rate of transfer of solid fission products to the gap in a radial blanket pin is only 1/4 of the nominal rate used in LIFE-III for fuel pins. The basis for this assumption is that for this and smaller values, it was found that fuel temperatures in mechanical calibration pins become so high, that the fuel becomes too soft to strain the cladding or develop a center hole as observed in the experiments. Using 1/4 the nominal CRUDFIL factor on radial blanket pin 27 of IB/A 128 is found to reduce the power-to-melt from 23.58 kw/ft to 22.89 kw/ft, representing a reduction of 4.1% of nominal full end-of-life power (16.86 kw/ft).

(c) Restructuring Rate Extrapolation

Restructuring is a function only of time and temperature. The best single indicator of the overall rate of restructuring is the central hole size. The LIFE-III calculation of central hole size has been calibrated not only against low time, low burnup pins in the thermal calibration, but also against a wide range of burnups and times in the calibration of the mechanical analysis. The agreement between calculation and measurement is good over a wide range of burnups (0-16.5%) and times (0-21,000 hours). This is shown in Figures 4.5 and 4.6. The standard deviation for the 37 comparisons was found to be 1.7 mils. This results in a 3σ uncertainty of about 5.1 mils.

To relate the uncertainty in central hole radii to a corresponding error in power-to-melt, the power-to-melt of several high temperature fuel pins was determined with various central hole radii obtained by varying the assumed activation energy for as-fabricated pore migration. It was found that the power-to-melt changed by 0.06 to 0.08 kW/ft per 1-mil change in central hole radius. Thus a 5.1 mil uncertainty in central hole radius results in an uncertainty of 0.31 to 0.41 kW/ft in power-to-melt. For a nominal full power of 13.72 kW/ft this uncertainty is equivalent to 2.3 to 3.0% of nominal full power. This uncertainty of 3% (3σ) of nominal full power was applied to the blanket.

(d) Thermal Conductivity Extrapolation

Fuel thermal conductivity (K_f) changes with time due to fuel restructuring which changes the porosity. It also changes with burnup due to the buildup of fission products within the fuel. Because of the good correlation of computed and measured central hole radii over a wide range of times and burnups it is unlikely that the extrapolation of the porosity-dependent factor in the LIFE-III equation for K_f to a burnup of about 1.6% involves any significant error.

The effect of fission product buildup on K_f has been measured out to only 0.16 atom percent burnup[45]. No change in thermal conductivity

1630 118

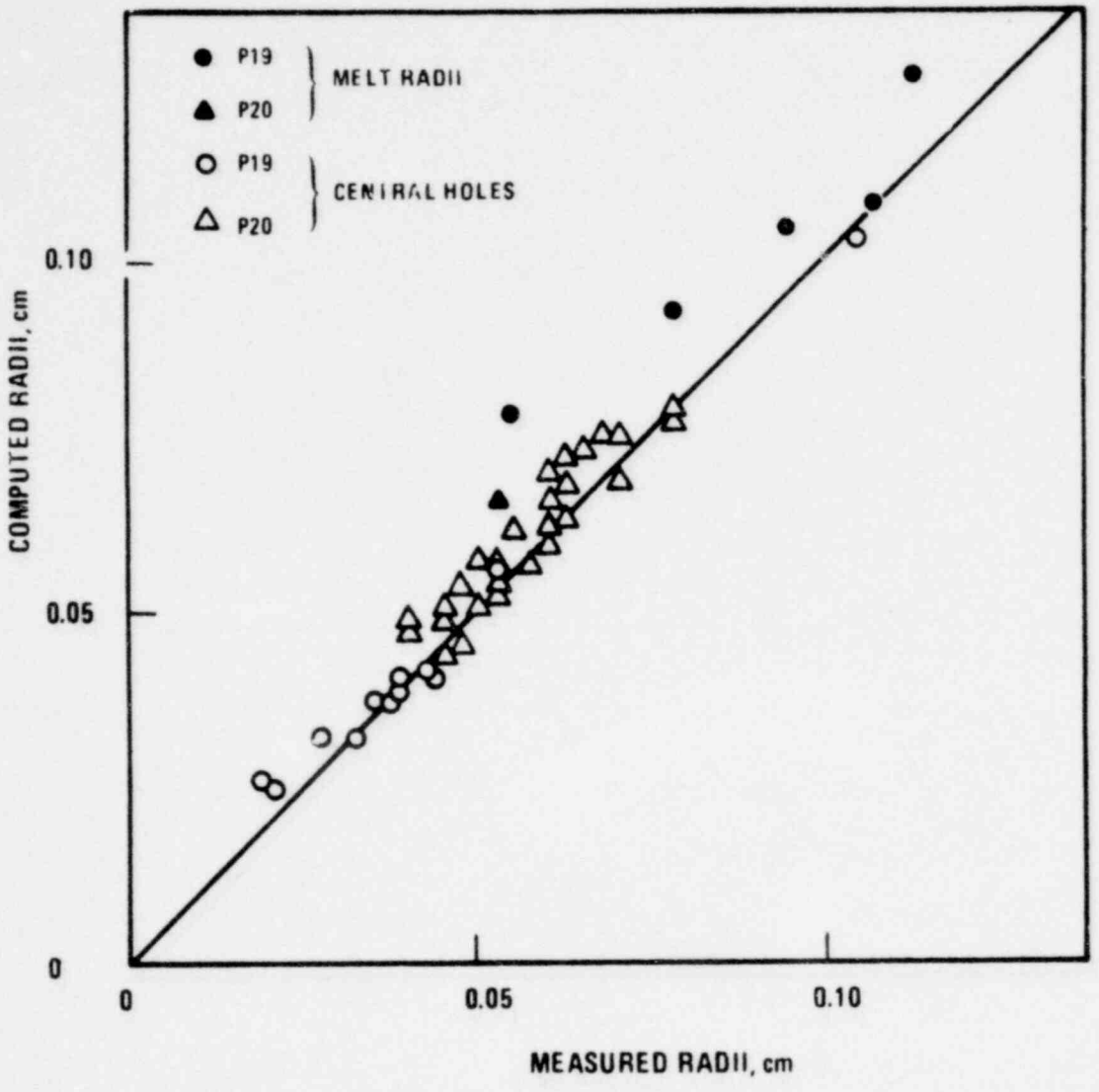

Figure 4-5. Comparison of Computed and Observed Central Hole Radii and Melt Radii

9926-26

1630 119

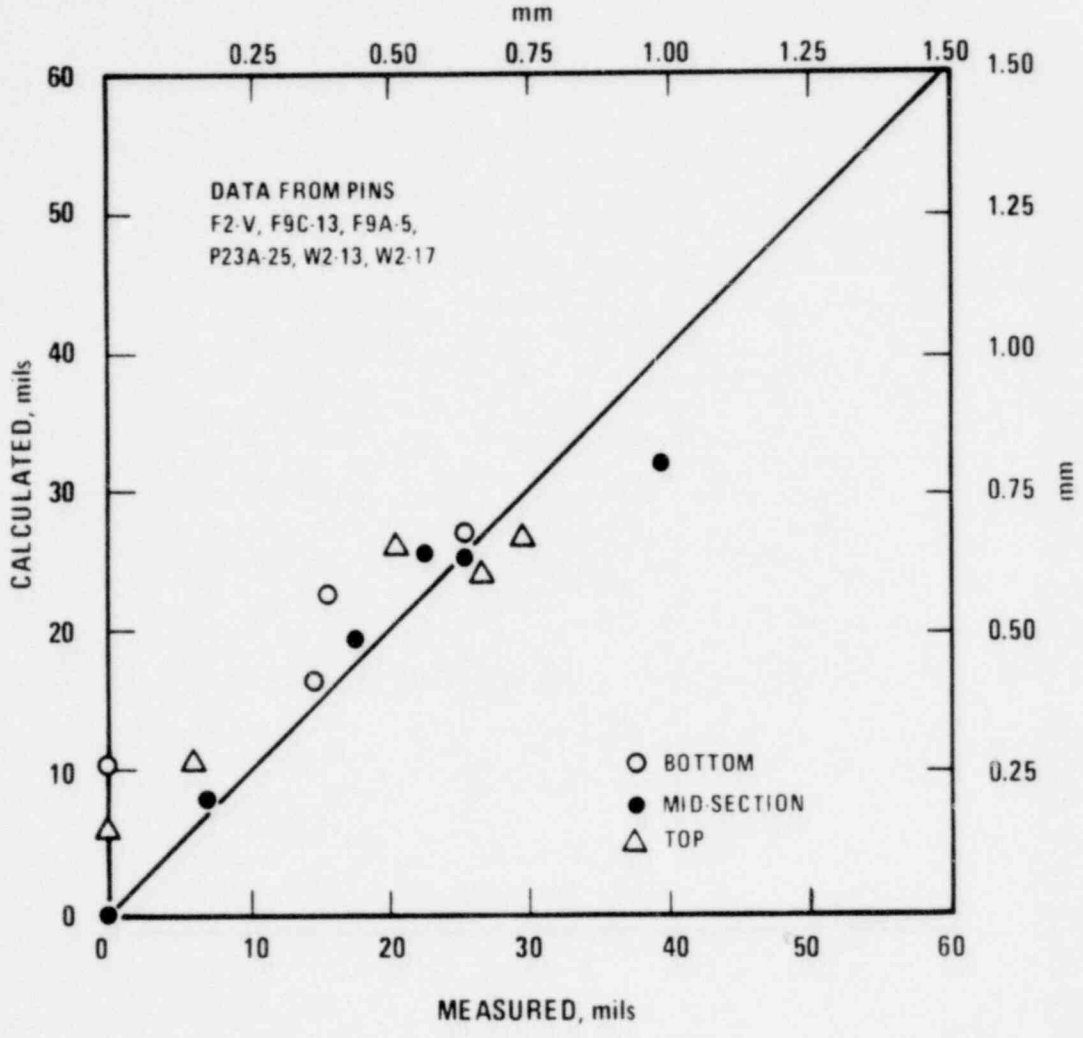

Figure 4-6. Comparison of Calculated and Predicted Center Hole Radii for Mechanical Calibration Pins.

9926-27

1630 120

was observed. For this preliminary analysis, a worst case estimate was made by assuming that one hole percent of fission products is equivalent to one percent of porosity. In the low-porosity limit one percent porosity changes K_f by 1.5%[46] (which is about three times the effect of PuO_2.) The porosity created by the 0.246 atoms per fission of Xe and Kr is already considered in the LIFE-III calculation of K_f. This leaves 2.0 - .246 = 1.754 fission product atoms per fission to be accounted for. At a burnup of 1.6 a/o burnup this worst-case approximation treatment yields a reduction in K_f of 4.2% (1.6 x 1.75 x 1.5). Such a reduction in K_f is found to reduce power-to-melt by about 4.0% in IB/A 128, pin 27. This is equivalent to a reduction of 5.6% of nominal full power (16.86 kw/ft).

(e) Cladding Swelling

The uncertainty in the cladding swelling equation used is expressed as an uncertainty in the parameter τ. The empirical worst value of τ is 5.0 (3σ), relative to a nominal (best fit) value of 6.3. A LIFE-III run with τ = 5.0 and a diametral cold gap of 4 mils resulted in a reduction in power-to-melt of 2% of nominal full power.

SUMMARY

As stated previously, extrapolating the LIFE-III code, which has been calibrated against fuel pin data, to radial blanket pins involves three basic types of uncertainties:

(I) Geometry effects;
(II) PuO_2 effects;
(III) Burnup extrapolation effects

Each of these three categories has been further resolved into its primary components and these have been analyzed and estimates of the associated uncertainties made. These are now summarized in Table 4.4.

1630 121

4.2.2 CRBRP Blanket Rod Design Uncertainties

As had been done for the fuel rods, the uncertainties introduced by fabrication tolerances and irradiation uncertainties are estimated by LIFE-III runs in which a parameter is varied within its tolerance to see its effect on power-to-melt. Table 4.5 lists the tolerances considered. Table 4.6 shows the sensitivity of power-to-melt to variations in each parameter. These results are then used to connect the fabrication and irradiation tolerances into uncertainties on power-to-melt which are statistically combined to give the CRBR design contribution to power-to-melt uncertainty, $\sigma_{\overline{R}}$, which is also shown in Table 4.6.

4.2.3 Total Blanket Rod Uncertainty and Design Criteria

Using the same analysis procedure as for fuel, the EBR-II data base uncertainty σ_{mean}, the uncertainty due to extrapolation to CRBRP conditions, σ_{extrap}, and the design tolerance uncertainties are combined in Table 4.7 to give the total uncertainty in blanket rod power-to-melt, σ_{REPOWM}. Application of the design criterion of no melting at 115% of nominal full power at a 3σ level of confidence shows that the design criterion is satisfied, and an additional margin of 4.9% in power remains.

1630 122

TABLE 4.4

EXTRAPOLATION UNCERTAINTIES FOR BLANKET RODS

	$3\sigma_1$
(I) GEOMETRY EFFECTS:	
(A) Gap conductance fuel-surface roughness	1.6 % NFP
(B) Pore velocity	≈ 0 % NFP
(C) Fuel swelling (Gap size)	0.71 % NFP
(II) PuO_2 EFFECTS	≈3.1 % NFP
(III) BURNUP EXTRAPOLATION EFFECTS:	
(A) Melting Temperature extrapolation	6.2 % NFP
(B) Gap Conductance extrapolation	4.6 % NFP
(C) Restructuring Rate extrapolation	3.0 % NFP
(D) Thermal Conductivity extrapolation	5.6 % NFP
(E) Cladding Swelling	2.0 % NFP

A statistical combination of the above uncertainties yields 10.8% at a 3σ level for the total extrapolation uncertainty associated with applying LIFE-III to radial blanket pins.

1630 123

TABLE 4.5

CRBRP Blanket Rod Tolerances and Uncertainties

Uncertainties represent $\sqrt{3}\sigma$

	Nominal	$\sqrt{3}\sigma_i$
Fuel Pellet Diameter	.470	± .001 in.
Cladding Inside Diameter	.4760	± .0005 in.
Fuel Pellet Density	95.6	± 1.0%
Reactor Power*		0
Cladding O.D. Temperature Near Midplane**		25°F

* All power uncertainties included as direct factors in "nominal" rod power.

** Due to thermal hydraulic uncertainties not including uncertainties in power.

1630 124

TABLE 4.6

Blanket Rod Sensitivities of Power-to-Melt to Design Uncertainties; Power-to-Melt Uncertainties due to Individual Design Uncertainties; and the Statistical Combination of These Power-to-Melt Uncertainties

(a) Change in Power-to-Melt for one percent change in Design Uncertainty, $[\partial\overline{REPOW}_M/\partial(\%X_i)]$

(b) One Sigma Power Uncertainty Resulting From Design Uncertainty, $[\sigma_i \partial\overline{REPOW}_M/\partial X_i]$

X_i	ρ_{pel}		D_{pel}		D_{clad}		Power		T_{clad}		Statistical Combination $\sigma_{\overline{R}}(t)$
	(a)	(b)	(a)	(b)	(a)	(b)	(a)	(b)	(a)	(b)	
	-.0019	-.0011	-.025	-.0031	.0095	.0006	-.0073	0.0	0.0	0.0	.0033

TABLE 4.7

Total Uncertainty on CRBRP Reactor Power-to-Melt for Blanket Rod in Reactor Power Units where Nominal Full Power is 1.0

$\sigma_{\overline{R}}$	σ_{mean}	$\sigma_{extrap.}$	total σ_{REPOW_M}	$\overline{REPOW}_M$ (nominal,t)	$\overline{REPOW}_M - 3\sigma_{REPOW_M}$ -1.15 REPOW
.0033	.057	.036	.067	1.400	.049

4.3 Coolant Exit Mixed Mean Hot Spot Factors for Blanket Assemblies

The blanket assemblies mixed mean hot spot factors are evaluated similarly to the corresponding fuel assemblies factors (Section 3.3 and Tables 6.2A and 6.2B). The various subfactors are presented in Tables 6.5A and 6.5B. As previously pointed out in Section 4.1.7, different nuclear uncertainties must be considered depending on the assembly radial position and time-in-life.

4.4 Fission Gas Plenum Pressure Hot Spot Factors for Blanket Assemblies

The blanket assemblies fission gas plenum pressure hot spot factors are evaluated similarly to the corresponding fuel assemblies factors (Section 3.4 and Tables 6.3A and 6.3B). The remarks in Section 3.4 also applies to this set of hot spot factors.

The various subfactors accounted for in evaluating the CRBRP blanket assemblies rod fission gas pressure are presented in Tables 6.6A and 6.6B.

5.0 PRIMARY CONTROL ASSEMBLIES HOT SPOT FACTORS

Primary control assemblies (PCA) hot spot factors currently being used for design analyses are shown in Tables 6.7 through 6.10. These factors currently in use were developed for the homogeneous core, and are being updated for the heterogeneous core. Table 5.2 shows a comparison between the current uncertainties and a preliminary updating, which shows that the current uncertainties give overall conservative results. The PCA factors are generally more conservative than those which have been adopted for fuel and blanket assemblies because of the less advanced status of the primary control assemblies design. The factors will be updated for the FSAR analyses as the design progresses, and more data such as those from the test listed in Table 6.11 are obtained.

The primary control assemblies hot spot factors are evaluated in a similar fashion to the fuel assemblies hot spot factors discussed in Section 3, with four exceptions. One difference is the introduction of three separate hot spot factors to account for uncertainties in heat flux through the absorber, the cladding and the coolant. This is due to the fact that, while in the fuel and blanket rods approximately 98% of the heat is generated in the fuel pellet, a sizeable amount (~20%) of heat is generated in the much thicker cladding of the control rod and in the coolant. A second major difference between control and fuel assemblies is the introduction of a new factor to account for uncertainties in prediction of the flow split between absorber bundle and bypass; in fact, only the fraction of coolant flowing through the absorber bundle acts as an effective heat removal medium. A third difference is the inclusion of separate gap and absorber uncertainties, which were combined in the equivalent fuel and blanket pin power-to-melt analyses. A fourth difference is the need for a Lifetime Structural Calculations Uncertainty Factor which will be discussed in Section 5.4.

5.1 Absorber Pin Temperatures Hot Spot Factors for Primary Control Assemblies

5.1.1 Power Level Measurement and Control System Dead Band

This factor is 1.03 and is identical to that for the fuel assembly as discussed in Section 3.1.1.

5.1.2 Inlet Flow Maldistribution

1630 128

The coolant enthalpy rise factor is taken as a direct factor of 1.08.

An analysis similar to those for the fuel and blanket assemblies (Section 3.1.5 and 4.1.3) was performed, and the results given in Table 5.1. The resulting

TABLE 5.1

CONTROL ASSEMBLY INLET FLOW MALDISTRIBUTION SUBFACTORS (3σ)

Hydraulic Characteristics	
Systematic	1.018
Random	1.045
Manufacturing Tolerances	1.023
Configuration	
Among LIM's	1.02
Among Assemblies	1.00
Systematic Error Interaction	1.011
Overall (3σ)	1.058

1630 129

bounding uncertainty factor of 1.058 (3σ) is less than the assumed direct factor of 1.08, and therefore the assumed factor is conservative.

More data will be forthcoming from the PCA hydraulic test (see Table 6.11) and will be used for the FSAR analyses.

5.1.3 Assembly Flow Maldistribution Calculational Uncertainties

A direct factor of 1.08 is taken, which based on available wire-wrapped rod bundle data (see Sections 3.1.6 and 4.1.3), is judged to be sufficient to account for uncertainties in the THI-3D[47] calculations of subchannel temperature distributions. A film coefficient uncertainty of 1.075 is conservatively adopted, even though the correlation shows no variation with flow in this range (Figure 4.3). This value includes the uncertainties in inlet flow (previous Section) and bundle/bypass flow split (next Section).

5.1.4 Bundle/Bypass Flow Split

The control assembly flow splits into absorber assembly and bypass flow components; only the former contributes directly to absorber element cooling. The uncertainty in predicting the absorber assembly fraction of control assembly flow is estimated to be 10% on the following bases: a) the theoretical flow split prediction shows[48] a maximum under-estimate of 6% when compared with HEDL data; b) since the HEDL data were for a 61-rod bundle, based on engineering judgement an additional 4% was included to account for extrapolation to a 37 rod bundle. Future flow testing of the reference control assembly (see Table 6.11) will reduce this uncertainty.

5.1.5 Cladding Circumferential Temperature Variation

The analysis of cladding circumferential temperature variation was performed by a similar method to that for the fuel pin. The factor was found to be 1.286 at the cladding midwall. This was increased to 1.40 on the basis of engineering judgement to allow for calculational uncertainties. This analysis will be updated for the FSAR.

5.1.6 Reactor ΔT and Inlet Temperature Variation

Statistical factors (3σ) of 1.02 for inlet temperature variation and 1.04 for reactor ΔT variation are assumed at Plant Expected Operating Conditions. In addition, the assembly inlet temperature is increased by 16°F.

As discussed in Sections 3.1.3 and 4.1.4, the factor should be about 1.14 (3σ) together with a 7.4°F (3σ) uncertainty in inlet temperature due to loop temperature imbalance. Therefore, the assumed factors are not sufficiently conservative. However, it will be shown in Section 5.1.16 that the updated total uncertainty is less than that assumed in the analysis. Therefore, the overall results are conservative even though the factors for reactor ΔT and inlet temperature variation are not sufficiently conservative.

5.1.7 Absorber Maldistribution and Conductivity

FFTF calculated the statistical hot channel factor for temperature drop through the pellet due to mechanical deviations to be 1.033. The uncertainty on local absorber heat generation is equal to the uncertainty on pellet temperature drop due to mechanical deviations. (Pellet temperature drop due to conductivity and restructuring is considered in a separate subfactor). The above uncertainty value was adopted, pending further analysis for the specific conditions of CRBRP control assemblies (37 vs. 61 pin design, hence larger diameter absorber pellets) which will be done for the FSAR.

A 2% uncertainty is assumed for coolant enthalpy rise since approximately 20% of the coolant enthalpy rise is due to cladding gamma heating and since the axially integrated effect of local absorber heating variation will be less than the 3.3% maximum local value.

The thermal conductivity of the B_4C absorber in the control assemblies was taken from Reference 14 and is valid for

$$\text{B-10 captures} > 5 \times 10^{20} \text{ captures/cc}$$
$$440 < T < 180°F$$

The maximum uncertainty was reported in Reference 48 to be in the range of 6 to 9%. To conservatively accommodate this possible variation, a bounding uncertainty value of 10% (3σ) has been incorporated in the thermal and structural analyses of the absorber pin. Also, the use of an expression based on burnup levels greater than 5×10^{20} captures/cc provided further conservatism, since for lower burnup, the B_4C thermal conductivity is much higher than that expressed by the equation.

Since the absorber centerline temperature is of the order of 2000°F, a slight extrapolation of the correlation is necessary.

5.1.8 Wire Wrap Orientation

The maximum statistical variation in the hot channel ΔT is estimated to be 1% based on the discussion in Section 3.1.7.

5.1.9 Subchannel Flow Area

A COBRA analysis which reduced to a minimum the area and rod to rod gaps of only the hot channel was compared to a nominal case. The result was a hot channel subfactor of 1.059. In addition to the subfactor for dimensional variation, a value of 1.062 was included statistically to account for pin diametral increase consistent with FFTF analyses. The statistically combined value of dimensional variation and pin diametral increase is 1.086.

Since the film coefficient actually increases, a value of 1.00 is conservatively taken for the film uncertainty.

Associated with the minimum channel area is a reduction in gamma heat consequent to the reduced subchannel volume. For conservatism, a value of 1.00 is assumed for coolant heat flux.

5.1.10 Film Heat Transfer Coefficient

An uncertainty factor of 1.21 for film heat transfer coefficient was used consistently with the data and recommendations of Reference 19.

5.1.11 Pellet-Cladding Eccentricity

The phenomena accompanying pellet-cladding eccentricity in control assembly absorber rods are similar to those discussed in Section 3.1.10 for fuel rods. At the beginning of life with hot absorber pellet and cladding dimensions, the case of maximum absorber pellet to cladding eccentricity in the control assembly rods resulted in film and cladding subfactors of 1.374 and 1.386, respectively. The film and cladding subfactors are local and, as such, do not apply to fuel temperature calculations. Fuel and gap subfactors of 1.0 were assumed for conservatism (see discussion in Section 3.1.10).

1630 132

5.1.12 Cladding Thickness and Conductivity

A 1.10 uncertainty factor on irradiated cladding thermal conductivity in addition to a 2.2% dimensional variation combines statistically to give a 1.10 hot spot subfactor for cladding ΔT. This is conservative as discussed in Section 3.1.11.

The cladding dimensional variations result in a 1.044 subfactor for local cladding gamma heat generation and a subfactor less than 1.01 for coolant enthalpy rise since gamma heating is only about 20% of the total heating.

5.1.13 Gap Thickness and Conductivity

An empirical 10% uncertainty in thermal conductivity of the gap gas combined statistically with a bounding 8.1% statistical uncertainty on hot gap thickness results in a 1.128 value for the subfactor.

The uncertainty on hot gap thickness includes the thermal expansion uncertainties and cold dimensional tolerances of the cladding I.D. and the absorber pellet O.D. at beginning of life. The absorber pellets always swell faster than the cladding, so swelling, even with swelling uncertainties included, always results in gap closure and reduced gap ΔT. Thus, the hot spot gap ΔT is maximum at the beginning of life when the fluence induced swelling is negligible.

5.1.14 Coolant Properties

The statistical coolant properties variation in the control assemblies is identical to that discussed in Section 3.1.12 for fuel assemblies.

5.1.15 Nuclear Uncertainties

Uncertainties due to physics analysis calculational methods (15% on coolant enthalpy rise and on absorber, cladding and coolant heat generation) are applied directly on nuclear radial peaking factors.

5.1.16 Overall Uncertainty

As an example, assume a nominal plant expected coolant temperature rise of 300°F in the hot channel. Table 5.2 shows a comparison of the coolant temperature rise for the cases of current uncertainties from Table 6.7 and updated

TABLE 5.2

COMPARISON OF HOT SPOT COOLANT TEMPERATURES CALCULATED USING CURRENT UNCERTAINTIES AND UPDATED UNCERTAINTIES

Assume Nominal Plant Expected Coolant ΔT = 300°F

Direct		Current Uncertainties (Table 6.7)	Preliminary Updated Uncertainties
Power Level Measurement and Control System Dead Band		1.03	1.03
Inlet Flow Maldistribution		1.08	1.02
Assembly Flow Maldistribution Calculational Uncertainties		1.08	1.08
Bundle/Bypass Flow Split		1.10	1.10
Statistical (3σ)			
Inlet Flow Maldistribution		---	1.058
Inlet Temperature Variation		1.02	1.146
Reactor ΔT Variation		1.04	
Absorber Maldistribution and Conductivity		1.02	1.02
Wire Wrap Orientation		1.01	1.01
Subchannel Flow Area		1.09	1.09
Cladding Thickness and Conductivity		1.01	1.01
Coolant Properties		1.01	1.017
Loop Temperature Imbalance		---	1.025
TOTAL	2σ	1.413	1.402
	3σ	1.459	1.479

Coolant ΔT, °F, above nominal inlet:		Current Uncertainties	Preliminary Updated Uncertainties
	2σ:	(1.413)(300) = 424	(1.402)(300) = 421
	Inlet:	16	---
	Total	440	421
	3σ:	(1.459)(300) = 438	(1.479)(300) = 444
	Inlet:	16	---
	Total:	454	444

uncertainties from the preceeding Sections. The updated inlet temperature uncertainty of 7.4°F due to loop temperature imbalance has been converted to an equivalent uncertainty of 1.025 on coolant temperature rise. The coolant temperature rise above nominal inlet is found to be 440°F (2σ) and 454°F (3σ) using current uncertainties, as compared with 421°F (2σ) and 444°F (3σ) using updated uncertainties. Therefore, the current uncertainties give overall conservative results.

5.2 Coolant Exit Mixed Mean Hot Spot Factors for Primary Control Assemblies

The control assemblies mixed mean hot spot factors are evaluated similarly to the corresponding fuel assemblies factors previously discussed in Section 3.3.

The various subfactors are presented in Table 6.8. No flow split uncertainty factor is considered in evaluation of the mixed mean outlet temperature, as the flow is judged to be fully mixed at the assembly exit.

5.3 Fission Gas Plenum Pressure Hot Spot Factors for Primary Control Assemblies

Table 6.9 summarizes the hot spot factors applied in evaluation of the primary control assembly absorber rod gas plenum pressure.

In addition, the minimum plenum volume and the HEDL recommended fission gas release design correlation[49] are conservatively considered in plenum pressure calculations.

5.4 Primary Control Assemblies Lifetime Structural Calculations Uncertainty Factor

In performing the cladding stress/strain mechanical analyses, proper consideration must be given to swelling of B_4C pellets and cladding during the absorber lifetime. Reference 49 reported that the diametral growth of the B_4C pellet is directly proportional to burnup but inversely proportional to the irradiation temperature. To assure conservative evaluations: a) hot spot factors on burnup corresponding to the ones developed for the plenum pressure calculations are used; b) due to the inverse relationship between pellet growth and temperature, the uncertainties affecting the absorber temperature are such as to yield its minimum value.

Table 6.10 details the uncertainty factors for lifetime structural calculations. The various factors considered in Table 6.10 correspond to the lower bound of the uncertainty range with the following exceptions:

- Uncertainties affecting heat generation have been selected for consistency at the higher level, since they are the same uncertainties affecting the burnup.

- Uncertainties have been integrated over the lifetime (hence, for example, elimination of the control system dead band effect) and over the pin volume (hence, elimination of the cladding circumferential temperature variation and pellet-cladding eccentricity factors).

- In the case of the bundle/bypass flow split, the fact that CRAB and CRSSA hydraulic model slightly overpredicts the bundle flow was taken into account.

- In the case of the subchannel flow area, it was judged that the two effects of increase in flow area due to tolerances and decrease due to pin deformation were counterbalancing.

Plant Expected Operating conditions in conjunction with hot spot factors outlined in Table 6.10 are used in lifetime structural calculations.

6.0 SUMMARY OF PRELIMINARY RESULTS AND FUTURE TESTS

The hot channel factors used in calculations of the coolant temperature, cladding temperature, and gas plenum pressure for the CRBRP fuel, blanket, and primary control assemblies which were discussed in the preceding sections are summarized in Tables 6.1A through 6.10.

For convenience, the uncertainties associated with the fuel and blanket assemblies, are grouped according to engineering (table numbers with the "A" suffix) and nuclear considerations (table numbers with the "B" suffix). Note that 3σ statistical values are applied to the plant thermal-hydraulic design conditions when performing safety analyses. The 2σ level is applied to plant expected operating conditions when calculating parameters such as cladding temperature and pressure, which are input to replaceable core assembly lifetime analyses. The hot channel factors in this report are applicable at full power steady state conditions. The 3σ uncertainties associated with the thermal-hydraulic values are conservatively used as the initial conditions for emergency and faulted transient and safety analyses.

The hot channel factors reported in Tables 6.1A through 6.10 are considered to be conservative. This will be further established as additional data becomes available from tests which are planned or in progress. These include: additional irradiation experiments on fuel, blanket, and primary control rods; engineering mockup critical experiments in the ZPPR; pressure drop tests of fuel, blanket, and control assemblies and orifice configurations; heat transfer tests on a 61 fuel rod bundle in sodium; cross-flow measurements in a 5:1 scale blanket rod bundle sector in air; and heat transfer tests in sodium on a prototypic blanket rod bundle. These data will be included in the FSAR analyses. A more detailed tabulation of the forthcoming T&H tests is given in Table 6.11.

TABLE 6.1A

CRBRP FUEL ASSEMBLIES ROD TEMPERATURE ENGINEERING UNCERTAINTY FACTORS

	COOLANT	FILM	CLADDING
DIRECT(o)			
Power Level Measurement and Control System Dead Band	1.03(1.0)	1.03(1.0)	1.03(1.0)
Inlet Flow Maldistribution (Direct Bias)	1.02		
Flow Distribution Calculational Uncertainty (Simulation Bias)	1.03	1.006	
Cladding Circumferential Temperature Variation		$1.0^{(+)}{}_{\sim}1.7\text{-}2.1^{(d)}$	$1.0^{(+)}{}_{\sim}0.8^{(*,d)}{}_{\sim}0.9^{(e,d)}$
Pellet-Cladding Eccentricity		$1.14^{(*,\phi)}$	$1.14^{(*,\phi)}$
STATISTICAL (3σ)(o)			
Reactor ΔT and Inlet Temperature Variation	$1.0(\sim 1.14)^{(a)}$	1.016	
Inlet Flow Maldistribution	1.059		
Loop Temperature Imbalance	(b)		
Wire Wrap Orientation	1.01		
Subchannel Flow Area	1.019	1.0	
Film Heat Transfer Coefficient		1.12	
Pellet-Cladding Eccentricity		$1.0^{(+)}{}_{1.174}{}^{(*,\phi)}$	$1.0^{(+)}{}_{1.174}{}^{(*,\phi)}$
Cladding Thickness and Conductivity			1.00(c)
Coolant Properties	1.017		
Flow Distribution Calculational Uncertainty (Calibration)	1.058	1.005	

(*) For cladding midwall temperature calculations.
(+) For fuel temperature calculations
(ϕ) Applies to BOL conditions
(o) Nuclear Uncertainty Factors are given on Table 6.1B
(a) For given coolant ΔT, HCF (3σ) = $1 + (3/\Delta T)\ (0.002304\Delta T^2 - 0.384\Delta T + 121)^{1/2}$
(b) Maximum 3σ uncertainty of 7.4°F in inlet temperature
(c) Direct factor of 1.05 included in design correlation
(d) Calculated for lifetime-limiting assembly in each flow zone with FATHØM. Includes 20% uncertainty in HCF-1.
(e) For cladding ID temperature calculations.

NOTE: Same values of subfactors apply to both Plant T&H and Expected Operating conditions except when two values are given; in this case, the parenthesized values apply to Plant Expected Operating conditions while the non-parenthesized values apply to T&H Operating conditions.

TABLE 6.1B

CRBRP FUEL ASSEMBLIES ROD TEMPERATURE NUCLEAR UNCERTAINTY FACTORS

WITH AND WITHOUT CONTROL ASSEMBLY INFLUENCE

	COOLANT	HEAT FLUX
DIRECT(o)		
Physics Modeling	1.02(1)	(*)1.02(1.10)(1)
Control Rod Banking	1.02(2)	1.02(2)
ZPPR-7 Flux Tilt	1.0(4)	1.0(4)
STATISTICAL (3σ)(o)		
Experimental (Nuclear)	1.07	1.07
Criticality	1.01(3)	1.01(3)
Fissile Fuel Maldistribution	1.052	1.052

If assembly is influenced by adjacent R7C control rod, replace with:

		COOLANT		HEAT FLUX			
				"PEAK POWER POSITION"		"TOP OF CORE"	
		BOL	EOL	BOL	EOL	BOL	EOL
1) Physics Modeling	Adjacent	1.04	1.02	1.03	1.02	1.15	1.15
	Far Side	1.01	1.02	.95	1.02	1.30	1.15
2) Control Rod Banking	Adjacent	1.04	1.02	1.04	1.02	1.01	1.01
	Far Side	1.02	1.02	1.02	1.02	1.01	1.01
3) Criticality	Adjacent	1.04	1.04	1.04	1.04	1.0	1.0
	Far Side	1.01	1.01	1.01	1.01	1.03	1.03

4) ZPPR-7 Flux Tilt - Assy's. 9, 10, 13, 14, 15, 16, 17, 23, 25, 37, 38, 41, 42, 43, 44, 45, 51, 53 (0.97 @ BOL, 1.0 @ EOL). Assy's. 12, 18, 19, 40, 46, 47 (0.99 @ BOL, 1.0 @ EOL).

(*) Non-parenthesized value applies at the peak power position (i.e., core midplane). Parenthesized value applies at the core lower/upper axial blanket interface except as superseded by note (1).

(o) Engineering Uncertainty Factors are given on Table 6.1A

TABLE 6.2A

CRBRP FUEL ASSEMBLIES MIXED MEAN EXIT TEMPERATURE ENGINEERING HOT CHANNEL FACTORS

DIRECT(o)	
Power Level Measurement and Control System Dead Band	1.03(1.0)
Inlet Flow Maldistribution (Direct Bias)	1.02
STATISTICAL (3σ)(o)	
Reactor ΔT and Inlet Temperature Variation	1.0(∿1.14)(a)
Inlet Flow Maldistribution	1.059
Loop Temperature Imbalance	(b)
Coolant Properties	1.017

(a) For given coolant ΔT, $HCF(3\sigma) = 1+(3/\Delta T)(0.002304\Delta T^2-0.384\Delta T+121)^{1/2}$
(b) Maximum 3σ uncertainty of 7.4°F in inlet temperature
(c) Nuclear uncertainty factors are given in Table 6.2B

NOTE: Same values of subfactors apply to both Plant T&H and Expected Operating conditions except when two values are given; in this case, the parenthesized values apply to Plant Expected Operating Conditions while the non-parenthesized values apply to T&H Operating conditions.

1630 140

TABLE 6.2B

CRBRP FUEL ASSEMBLIES MIXED MEAN EXIT TEMPERATURE NUCLEAR UNCERTAINTY FACTORS

	ASSEMBLY EXIT
DIRECT(o)	
Physics Modeling	(*)1.01(1.02 @ BOL,1.01 @ EOL)
Control Rod Banking	(*)1.02(1.03 @ BOL,1.02 @ EOL)
ZPPR-7 Flux Tilt	1.0 (4)
STATISTICAL (3σ)(o)	
Experimental (Nuclear)	1.07
Criticality	(*)1.01(1.02)
Fissile Fuel Maldistribution	1.052

(4) ZPPR-7 Flux Tilt - Assy's. 9, 10, 13, 14, 15, 16, 17, 23, 25, 37, 38, 41, 42, 43, 44, 45, 51, 53 (0.97 @ BOL, 1.0 @ EOL). Assy's. 12, 18, 19, 40, 46, 47 (0.99 @ BOL, 1.0 @ EOL).

(*) Non-parenthesized values are applied for assemblies not adjacent to R7C control assemblies. Parenthesized values are applied for the control assembly effect fo. assemblies adjacent to R7C control assemblies.

(o) Engineering uncertainty factors are given on Table 6.2A.

TABLE 6.3A

CRBRP FUEL ASSEMBLIES PLENUM PRESSURE

ENGINEERING UNCERTAINTY FACTORS

	PLENUM TEMPERATURE	BURNUP
DIRECT[o]		
Inlet Flow Maldistribution (Direct Bias)	1.02	
Flow Distribution Calculational Uncertainty (Simulation Bias)	1.03	
STATISTICAL (3σ)[o]		
Power Level Measurement and Control System Dead Band	1.0	1.025
Inlet Flow Maldistribution	1.059	
Loop Temperature Imbalance	(b)	
Reactor ΔT and Inlet Temperature Variation	$\sim$1.14[a]	
Wire Wrap Orientation	1.01	
Subchannel Flow Area	1.019	
Coolant Properties	1.017	
Flow Distribution Calculational Uncertainty (Calibration)	1.058	

[o] Nuclear Uncertainty Factors are given on Table 6.3B

(a) For given coolant ΔT, HCF (3σ) = $1 + (3/\Delta T)\ (0.002304\Delta T^2 - 0.384\Delta T + 121)^{1/2}$

(b) Maximum 3σ uncertainty of 7.4°F in inlet temperature

NOTE: Values of subfactors apply to plant expected operating conditions.

TABLE 6.3B

CRBRP FUEL ASSEMBLIES PLENUM PRESSURE NUCLEAR UNCERTAINTY FACTORS

WITH AND WITHOUT CONTROL ASSEMBLY INFLUENCE

	PLENUM TEMPERATURE	BURNUP
DIRECT(o)		
Physics Modeling	1.02(1)	1.02(1)
Control Rod Banking	1.02(2)	1.02(2)
ZPPR-7 Flux Tilt	1.0(4)	1.0(4)
STATISTICAL (3σ)(o)		
Experimental (Nuclear)	1.07	1.07
Criticality	1.01(3)	1.01(3)
Fissile Fuel Maldistribution	1.052	1.052

If assembly is influenced by adjacent control rod, replace with:

		BOL	EOL
1) Physics Modeling	Adjacent	1.04	1.02
	Far Side	1.01	1.02
2) Control Rod Banking	Adjacent	1.04	1.02
	Far Side	1.02	1.02
3) Criticality	Adjacent	1.04	1.04
	Far Side	1.01	1.01

(4) ZPPR-7 Flux Tilt - Assy's. 9, 10, 13, 14, 15, 16, 17, 23, 25, 37, 38, 41, 42, 43, 44, 45, 51, 53 (0.97 @ BOL, 1.0 @ EOL). Assy's. 12, 18, 19, 40, 46, 47 (0.99 @ BOL, 1.0 @ EOL).

(o) Engineering Uncertainty Factors are given on Table 6.3A.

TABLE 6.4A

CRBRP INNER/RADIAL BLANKET ASSEMBLIES ROD TEMPERATURES ENGINEERING UNCERTAINTY FACTORS

	COOLANT	FILM	CLADDING
DIRECT(o)			
Power Level Measurement and Control System Dead Band	1.03(1.0)	1.03(1.0)	1.03(1.0)
Irradiation Swelling	1.00(ϕ) 1.05(f)		
Inlet Flow Maldistribution (Direct Bias)	1.02		
Flow Distribution Calculational Uncertainty (Simulation Bias)	1.03	1.008	
Cladding Circumferential Temperature Variation		1.0(+) ~3.4-3.8(g)	1.0(+) ~0.7(*,g) ~0.8(h,g)
Pellet-Cladding Eccentricity		1.14(*,ϕ)	1.14(*,ϕ)
STATISTICAL (3σ)(o)			
Reactor ΔT and Inlet Temperature Variation	1.0(~1.14)(a)		
Inlet Flow Maldistribution	1.060(d) 1.084(e)	1.018(d) 1.025(e)	
Loop Temperature Imbalance	(b)		
Wire Wrap Orientation	1.01		
Subchannel Flow Area	1.07(ϕ) 1.0(f)	1.0	
Film Heat Transfer Coefficient		1.21	
Pellet-Cladding Eccentricity		1.0(+) 1.174(*,ϕ)	1.0(+) 1.174(*,ϕ)
Cladding Thickness and Conductivity			1.0(c)
Coolant Properties	1.017		
Flow Distribution Calculational Uncertainty (Calibration)	1.203	1.006	

(*) For cladding midwall temperature calculations.
(+) For fuel temperature calculations
(ϕ) Applies to BOL conditions
(f) Applies to EOL conditions
(o) Nuclear Uncertainty Factors are given on Table 6.4B
(a) For given coolant ΔT, HCF (3σ) = 1 + (3/ΔT) $(0.002304\Delta T^2 - 0.384\Delta T + 121)^{1/2}$
(b) Maximum 3σ uncertainty of 7.4°F in inlet temperature
(c) Direct factor of 1.05 included in design correlation
(d) Inner Blanket
(e) Radial Blanket
(g) Calculated for lifetime-limiting assembly in each flow zone with FATHOM. Includes 20% uncertainty in HCF-1.
(h) For cladding ID temperature calculations.

NOTE: Same values of subfactors apply to both Plant T&H and Expected Operating conditions except when two values are given; in this case, the parenthesized values apply to Plant Expected Operating conditions while the non-parenthesized values apply to T&H Operating conditions.

TABLE 6.4B

CRBRP INNER/RADIAL BLANKET ASSEMBLIES ROD TEMPERATURE NUCLEAR UNCERTAINTY FACTORS

	INNER BLANKET		RADIAL BLANKET			
			Row 1		Row 2	
	COOLANT	HEAT FLUX	COOLANT	HEAT FLUX	COOLANT	HEAT FLUX
DIRECT (BOL)(o)						
Physics Modeling	1.06	(*)1.07(1.11)	1.07	(*)1.07(1.02)	1.03	(*)1.07(0.99)
Control Rod Banking	1.02	1.02	1.02	1.02	1.02	1.02
Experimental (Nuclear)	1.12	(*)1.10(1.17)	1.13	(*)1.11(1.18)	1.27	(*)1.24(1.32)
Criticality	1.02	1.02	----	----	----	----
Heavy Metal	1.01	1.01	1.01	1.01	1.01	1.01
U-235	1.01	1.01	1.01	1.01	1.01	1.01
DIRECT (EOL)(o)						
Physics Modeling	1.02	(*)1.04(1.12)	1.01	(*)1.07(1.05)	1.01	(*)1.07(1.02)
Control Rod Banking	1.02	1.02	1.02	1.02	1.02	1.02
Experimental (Nuclear)	1.03	(*)1.00(1.07)	1.05	(*)1.03(1.10)	1.15	(*)1.13(1.21)
Criticality	1.01	1.01	----	----	----	----
Heavy Metal	1.01	1.01	1.01	1.01	1.01	1.01
U-235	----	----	----	----	----	----

(*) Non-parenthesized values apply at the peak power position (i.e., near core midplane). Parenthesized values apply at core upper/lower axial blanket interface extension.

(o) Engineering Uncertainty Factors are given on Table 6.4A

TABLE 6.5A

CRBRP INNER/RADIAL BLANKET ASSEMBLIES MIXED MEAN EXIT TEMPERATURE

ENGINEERING UNCERTAINTY FACTORS

DIRECT(o)	
Power Level Measurement and Control System Dead Band	1.03(1.0)
Inlet Flow Maldistribution (Direct Bias)	1.02
Irradiation Swelling	1.00(e) 1.05(f)
STATISTICAL (3σ)(o)	
Reactor ΔT and Inlet Temperature Variation	1.0(≈1.14)(a)
Inlet Flow Maldistribution	1.060(c) 1.084(d)
Loop Temperature Imbalance	(b)
Coolant Properties	1.017

(o) Nuclear Uncertainty Factors are given in Table 6.5B.
(a) For given coolant ΔT, HCF (3σ) = 1 + (3/ΔT) $(0.002304\Delta T^2 - 0.384\Delta T + 121)^{1/2}$
(b) Maximum 3σ uncertainty of 7.4°F in inlet temperature.
(c) Inner Blanket
(d) Radial Blanket
(e) Applies to BOL conditions
(f) Applies to EOL conditions

NOTE: Same values of subfactors apply to both plant T&H and expected operating conditions except when two values are given; in this case, the parenthesized values apply to plant expected operating conditions while the non-parenthesized values apply to T&H operating conditions.

TABLE 6.5B

CRBR INNER/RADIAL BLANKET ASSEMBLIES MIXED MEAN EXIT TEMPERATURE NUCLEAR UNCERTAINTY FACTORS

	INNER BLANKET	RADIAL BLANKET	
		Row 1	Row 2
	ASSEMBLY EXIT	ASSEMBLY EXIT	ASSEMBLY EXIT
DIRECT (BOL)(o)			
Physics Modeling	1.01	1.02	1.02
Control Rod Banking	1.02	1.02	1.02
Experimental (Nuclear)	1.12	1.13	1.27
Criticality	1.02	----	----
Heavy Metal	1.01	1.01	1.01
U-235	1.01	1.01	1.01
DIRECT (EOL)(o)			
Physics Modeling	1.01	1.02	1.02
Control Rod Banking	1.02	1.02	1.02
Experimental (Nuclear)	1.03	1.05	1.15
Criticality	1.01	----	----
Heavy Metal	1.01	1.01	1.01
U-235	----	----	----

(o) Engineering uncertainty factors are given on Table 6.5A.

TABLE 6.6A

CRBRP INNER/RADIAL BLANKET ASSEMBLIES PLENUM PRESSURE

ENGINEERING UNCERTAINTY FACTORS

	PLENUM TEMPERATURE	BURNUP
DIRECT(o)		
Inlet Flow Maldistribution (Direct Bias)	1.02	
Flow Distribution Calculational Uncertainty (Simulation Bias)	1.03	
Irradiation Swelling	1.00(e) 1.05(f)	
STATISTICAL (3σ)(o)		
Power Level Measurement and Control System Dead Band	1.0	1.025
Inlet Flow Maldistribution	1.060(c) 1.084(d)	
Loop Temperature Imbalance	(b)	
Reactor ΔT and Inlet Temperature Variation	≈1.14(a)	
Wire Wrap Orientation	1.01	
Subchannel Flow Area		
Coolant Properties	1.017	
Flow Distribution Calculational Uncertainty (Calibration)	1.203	

(o) Nuclear Uncertainty Factors are given on Table 6.6B

(a) For given coolant ΔT, HCF $(3\sigma) = 1 + (3/\Delta T)\ (0.002304\Delta T^2 - 0.384\Delta T + 121)^{1/2}$

(b) Maximum 3σ uncertainty of 7.4°F in inlet temperature

(c) Inner Blanket

(d) Outer Blanket

(e) Applies to BOL conditions

(f) Applies to EOL conditions

NOTE: Values of subfactors apply to plant expected operating conditions.

TABLE 6.6B

CRBRP INNER/RADIAL BLANKET ASSEMBLIES PLENUM PRESSURE NUCLEAR UNCERTAINTY FACTORS

	INNER BLANKET		RADIAL BLANKET			
			Row 1		Row 2	
	PLENUM TEMPERATURE	BURNUP	PLENUM TEMPERATURE	BURNUP	PLENUM TEMPERATURE	BURNUP
DIRECT (BOL)(o)						
Physics Modeling	1.06	1.06	1.07	1.07	1.03	1.03
Control Rod Banking	1.02	1.02	1.02	1.02	1.02	1.02
Experimental (Nuclear)	1.12	1.12	1.13	1.13	1.27	1.27
Criticality	1.02	1.02	----	----	----	----
Heavy Metal	1.01	1.01	1.01	1.01	1.01	1.01
U-235	1.01	1.01	1.01	1.01	1.01	1.01
DIRECT (EOL)(o)						
Physics Modeling	1.02	1.02	1.01	1.01	1.01	1.01
Control Rod Banking	1.02	1.02	1.02	1.02	1.02	1.02
Experimental (Nuclear)	1.03	1.03	1.05	1.05	1.15	1.15
Criticality	1.01	1.01	----	----	----	----
Heavy Metal	1.01	1.01	1.01	1.01	1.01	1.01
U-235	----	----	----	----	----	----

(o) Engineering uncertainty factors are given on Table 6.6A

TABLE 6.7

CRBRP PRIMARY CONTROL ASSEMBLIES PIN TEMPERATURES HOT CHANNEL/SPOT FACTORS

		Coolant	Film	Cladding	Gap	Absorber	Heat Generation: Absorber	Heat Generation: Cladding	Heat Generation: Coolant
DIRECT(+)									
Power Level Measurement and Control System Dead Band		1.03					1.03	1.03	1.03
Inlet Flow Maldistribution		1.08							
Subassembly Flow Maldistribution			1.075						
Calculational Uncertainties		1.08							
Bundle/Bypass Flow Split		1.10							
Cladding Circumferential Temperature Variation			1.0(0) (Note 1)	1.0(0)					
STATISTICAL (3σ)(o)									
Inlet Temperature Variation		1.02(♦) 1.0(†)							
Reactor ΔT Variation		1.04(♦) 1.0(†)							
Absorber Maldistribution and Conductivity		1.02				1.10	1.03		
Wire Wrap Orientation		1.01							
Subchannel Flow Area		1.09	1.0						1.0
Film Heat Transfer Coefficient			1.21						
Pellet-Cladding Eccentricity			1.37(*)	1.39(*)					
Cladding Thickness and Conductivity		1.01		1.10				1.04	
Gap Thickness and Conductivity					1.13				
Coolant Properties		1.01							
TOTAL	2σ	1.413(♦) 1.484(†)	1.23(0) 1.38(*)	1.07(0) 1.27(*)	1.09	1.07	1.051	1.057	1.03
	3σ	1.458 1.445	1.30 1.53	1.10 1.40	1.13	1.10	1.061	1.071	1.03

(+) Uncertainties due to physics analysis calculational methods (15% on coolant enthalpy rise and on absorber, cladding and coolant heat generation) are applied directly on nuclear radial peaking factors.

(*) For local cladding temperature calculations.

(0) For average cladding, absorber temperature calculations.

(o) In addition, the assembly inlet temperature will be increased by 16°F, to account for primary loop temperature coolant uncertainties.

(♦) Applies to Plant Expected Operating Conditions.

(†) Applies to Plant T&H Design Conditions

(Note 1) Under the wire wrap local hot spot factors are 3.17, 1.40 and 1.20, for the cladding OD, midwall and ID, respectively. Applies to the nominal temperature drop between cladding and bulk coolant.

TABLE 6.8

CRBRP PRIMARY CONTROL ASSEMBLIES MIXED MEAN EXIT TEMPERATURE HOT CHANNEL FACTORS

DIRECT(+)		
Power Level Measurement and Control System Dead Band		1.03
Inlet Flow Maldistribution		1.08
STATISTICAL (3σ)(o)		
Inlet Temperature Variation		$1.03^{(\phi)}1.0^{(+)}$
Reactor ΔT Variation		$1.04^{(\phi)}1.0^{(+)}$
Absorber Maldistribution		1.02
Cladding Thickness		1.01
Coolant Properties		1.01
TOTAL	2σ	$1.154^{(\phi)}1.130^{(+)}$
	3σ	$1.175^{(\phi)}1.140^{(+)}$

(+) Uncertainties due to physics analysis calculational methods (15% for both assembly and chimney exit) are applied directly on nuclear radial peaking factors.
(ϕ) Applies to Plant Expected Conditions.
(+) Applies to Plant T&H Design Conditions.
(o) In addition, the assembly inlet temperature will be increased by 16°F (assembly exit) or 10°F (chimney exit), to account for primary loop temperature control uncertainties.

1630 151

TABLE 6.9

CRBRP PRIMARY CONTROL ASSEMBLIES PLENUM PRESSURE
HOT CHANNEL FACTORS

		Plenum Temperature	Burnup
DIRECT(+)			
Power Level Measurement		1.02	1.02
Inlet Flow Maldistribution		1.08	
Subassembly Flow Maldistribution Calculational Uncertainties		1.08	
Bundle/Bypass Flow Split		1.10	
STATISTICAL (3σ)(o)			
Inlet Temperature Variation		$1.02^{(\blacklozenge)}$ $1.0^{(+)}$	
Reactor ΔT Variation		$1.04^{(\blacklozenge)}$ $1.0^{(+)}$	
Absorber Maldistribution		1.02	1.02
Cladding Thickness		1.01	
Wire Wrap Orientation		1.01	
Coolant Properties		1.01	
TOTAL	2σ	$1.354^{(\blacklozenge)}$ $1.332^{(+)}$	1.034
	3σ	$1.376^{(\blacklozenge)}$ $1.356^{(+)}$	1.040

(+) Uncertainties due to physics analysis calculational methods (15% on both plenum temperature and burnup) are applied directly on nuclear peaking factors.
(♦) Applies to Plant Expected Operating Conditions.
(+) Applies to Plant T&H Design Conditions.
(o) In addition, the assembly inlet temperature will be increased by 16°F to account for primary loop temperature control uncertainties.

1630 152

TABLE 6.10

CRBRP PRIMARY CONTROL ASSEMBLIES LIFETIME STRUCTURAL CALCULATIONS UNCERTAINTY FACTORS

		Coolant	Film	Cladding	Gap	Absorber	Heat Generation Absorber	Heat Generation Cladding	Heat Generation Coolant
DIRECT(+)									
Power Level Measurement and Control System Dead Band		1.02					1.02	1.02	1.02
Inlet Flow Maldistribution		0.92							
Assembly Flow Maldistribution			0.95						
Calculational Uncertainties		0.92							
Bundle/Bypass Flow Split		1.0							
STATISTICAL (3σ)(o)									
Inlet Temperature Variation		0.96							
Reactor ΔT Variation		0.96							
Absorber Maldistribution and Conductivity		1.01				0.9	1.02		
Wire Wrap Orientation		0.99							
Subchannel Flow Area		1.0	1.0						1.0
Film Heat Transfer Coefficient			0.79						
Cladding Thickness and Conductivity		1.0		0.9				1.03	
Gap Thickness and Conductivity					0.87				
Coolant Properties		0.99							
TOTAL	2σ	0.830	0.817	0.933			1.034	1.04	1.02
	3σ	0.814	0.751	0.90	0.87	0.9	1.04	1.051	1.02

(+) Uncertainties due to physics analysis calculational methods (1.15 on coolant enthalpy rise and on absorber, cladding and coolant heat generation) are applied directly on nuclear radial peaking factors.

(o) In addition, the assembly inlet temperature will be decreased by 16°F, to account for primary loop temperature control uncertainties.

TABLE 6.11

FUTURE CORE ASSEMBLIES T&H TESTS

Component	DRS No.	Test	Description	Performer	Schedule for Completion	Utilization of Results
Fuel Assembly	31.02.16 31.14.16	F/A Inlet Nozzle Test in Water; F/A Cavitation Tests in Water	F/A Orifices ΔP Calibrations	HEDL	6/79	F/A Orifice Calibration and Inlet Flow Maldistribution Uncertainty
	31.02.03	F/A Flow and Vibration Test in Water	Component and Overall ΔP Calibration	HEDL	12/78	F/A ΔP Calibration and Inlet Flow Maldistribution Uncertainty
	02.01	Fuel Failure Potential and Heat Transfer in Large Rod Bundles	Heat Transfer Tests with a 61 Fuel Rod Bundle in Sodium	ORNL	6/81	F/A Flow and Temperature Distribution Calibration and Uncertainty
Radial Blanket Assembly	31.03.02	61 Rod Bundle Radial Blanket Heat Transfer Test in Sodium	Heat Transfer Tests with a Prototypic Blanket Rod Bundle in Sodium	WARD	9/80	Blanket Assembly Flow and Temperature Distribution Calibration and Uncertainty
	31.03.08	Flow and Vibration Test of Radial Blanket Assembly in Water	Component and Overall ΔP Calibration	HEDL	12/79	RB/A ΔP Calibration and Inlet Flow Maldistribution Uncertainty
	31.03.25	Radial Blanket Flow Orificing Test	Orifice ΔP Calibration and Flow Maldistribution Among Assemblies Within LIM	WARD	7/79	RB/A Orifice ΔP Calibration and Inlet Flow Maldistribution Uncertainty
	31.14.41	Air Flow Test of CRBRP Blanket Assembly	ΔP's Axial and Transverse Velocity Distributions in In-Board, Side, and Corner Channels on a 5/1 Scale Model	W R&D	3/79	Blanket Assembly Flow Distribution Calibration and Uncertainty

TABLE 6.11

(Continued)

Component	DRS No.	Test	Description	Performer	Schedule for Completion	Utilization of Results
Primary Control Assembly	31.08.07	Primary Control Assembly Hydraulic Test	Component and Overall ΔP Calibration and Flow Split	WARD	6/79	PCA ΔP and Flow Split Calibration and Uncertainty

7.0 REFERENCES

1. M. C. Chuang, et. al., "Three-Dimensional Thermal-Hydraulic Analysis of Wire-Wrapped Rods in Liquid-Metal Fast Breeder Reactor Core Assemblies", Nucl. Sci. Eng. 64, pp. 244-257 (1977).

2. R. E. Collingham, et. al., "Development and Results of an Electrically Heated Seven-Pin Bundle Assembly for Thermal Hydraulic Testing in Liquid Metals," Liquid Metal Heat Transfer and Fluid Dynamics, pp. 41-49, American Society of Mechanical Engineers, New York, 1970.

3. M. H. Fontana, et. al., "Temperature Distribution in a 19-Rod Simulated LMFBR Fuel Assembly in a Hexagonal Duct (Fuel Failure Mockup Bundle 2A): Record of Experimental Data," ORNL-TM-4113, September 1973 (Availability: USDOE Technical Information Center).

4. P. M. McConnell, F. R. Fisher and R. G. White, "Inlet Plenum Feature Model Flow Tests of the Clinch River Breeder Reactor: Addendum V Results," HEDL-TME 76-33, March 1976 (Availability: USDOE Technical Information Center).

5. P. M. McConnell, "Clinch River Breeder Reactor Fuel Assembly Inlet/Outlet Nozzle Flow Tests," HEDL-TME 77-8, February 1977 (Availability: USDOE Technical Information Center).

6. M. H. Fontana, et. al., "Temperature Distribution in a 19-Rod Simulated LMFBR Fuel Assembly in a Hexagonal Duct - (Fuel Failure Mockup Bundle 2A) - Record of Experimental Data," ORNL-TM-4113, September 1973 (Availability: USDOE Technical Information Center).

7. J. J. Lorenz, T. Ginsberg, and R. A. Morris, "Experimental Mixing Studies and Velocity Measurements with a Simulated 91-Element LMFBR Fuel Assembly," ANL-CT-74-09, March 1974 (Availability: USDOE Technical Information Center).

8. D. R. Pedersen, et. al., "Experimental Investigation of the Hydrodynamic Entrance Length and Subchannel Velocity Profiles in a 91-Element Wire Wrapped Subassembly," ANL/RAS 74-5, April 1974 (Availability: USDOE Technical Information Center).

9. R. E. Collingham, et. al., "217-Pin Wire-Wrapped Bundle Coolant Mixing Test," HEDL-TME 71-146, November 1971. R. E. Collingham, W. L. Thorne, and J. D. McCormack, "Coolant Mixing in a Fuel Pin Assembly Utilizing Helical Wire Wrap Spacers," Nucl. Eng. Des. 24, pp. 393-409 (1973).

10. R. M. Roidt, T. G. Bartholet, and L. J. Harper, "Experimental Determination of Interior Subchannel Crossflow and Axial Flow in a Model of the Clinch River Breeder Reactor Fuel Assembly Rod Bundle with Wire-Wrap Spacers," ASME Paper 76/WA/HT-83. T. G. Bartholet, R. M. Roidt, and L. J. Harper, "Clinch River Breeder Reactor Plant; 11:1 Scale Wire Wrapped Rod Bundle Air Flow Tests. Interior Subchannels," CRBRP-ARD-0108, January 1977 (Availability: USDOE Technical Information Center).

11. K. Takanashi, K. Miyaguchi, and E. Ishibashi, "Experimental Study on Coolant Sodium Mixing Effect in "Joyo" Fuel Assembly with Spiral Wire Spacer II, Result of Test of Blanket Fuel Assembly," JAPFNR-182, October 1974 (Availability: USDOE Technical Information Center).

12. E. Parzen, Modern Probability Theory and Its Applications, J. Wiley and Sons, New York, pp. 374-376, 1960.

13. Y. B. Chen, K. Ip and N. E. Todreas, "Velocity Measurements in Edge Channels of Wire-Wrapped LMFBR Fuel Assemblies," Trans.Amer. Nucl. Soc. 19, pp. 323-324 (1974).

14. D. R. Pedersen, et. al., "Cross Flow Mixing in a 91-Element Bundle", ANL/RAS 74-2, February 1974 (Availability: USDOE Technical Information Center).

15. A. W. Graves and I. Catton, "An Explicit Method for Predicting the Thermal Performance of FBR Wire-Wrapped Fuel Rod Assemblies," Trans. Amer. Nucl. Soc. 15, p. 404 (1972).

16. T. Ginsberg and J. J. Lorenz, "Experimental Mixing Studies in Simulated Wire-Wrap Fuel Assemblies," Reactor Heat Transfer, pp. 13-38, Gesellschaft fur Kernforschung, mbH, Karlsruhe, West Germany, 1973.

17. J. J. Lorenz, et. al., "Experimental Mixing Studies and Velocity Measurements with a Simulated 91-Element LMFBR Fuel Assembly," ANL-CT-74-09, March 1974 (Availability: USDOE Technical Information Center).

18. T. G. Bartholet, R. M. Roidt and J. E. Romano, "Clinch River Breeder Reactor Plant, 11:1 Scale Wire Wrapped Rod Bundle Air Flow Test, Side Subchannels," CRBRP-ARD-0129, January 1977 (Availability: USDOE Technical Information Center).

19. M. S. Kazimi, "Heat Transfer Correlation for Analysis of CRBRP Assemblies," CRBRP-ARD-0034, November 1976 (Availability: USDOE Technical Information Center).

20. O. E. Dwyer and H. C. Berry, "Turbulent-Flow Heat Transfer for In-Line Flow Through Unbaffled Rod Bundles: Molecular Conduction Only," Nucl. Sci. Eng. 46, pp. 284-303 (1971).

21. "Nuclear Systems Materials Handbook," Hanford Engineering Development Lab., Richland, Washington, TID-26666.

22. M. Jakob, Heat Transfer, Vol. 1, p. 85, John Wiley and Sons, New York, 1949.

23. C. A. Bruch and W. E. McHugh, "Radiation Damage Studies of Seven Non-Fissionable Metals," Preprint 37, Session 26, presented at the Nuclear Engineering and Science Conference, March 17-21, 1958, Chicago, Illinois.

24. G. H. Golden and J. V. Tokar, "Thermophysical Properties of Sodium" ANL-7323, August 1967.

25. D. C. Ginnings, T. B. Douglas and A. F. Ball, "Heat Capacity of Sodium between 0° and 900°C, the Triple Point and Heat of Fusion," J. Res. Nat. Bur. Stand. 45 pp. 23-33 (July 1950).

26. D. R. Fredrickson and M. G. Chasanov, "The Enthalpy of Liquid Sodium to 1505K by Drop Calorimetry," J. Chem. Thermodyn. 6, pp. 629-633 (1974).

27. J. P. Stone, et al., "High-Temperature Properties of Sodium, NRL-6241, December 1964.

28. E. G. Hagen, "Ueber Die Wurmeausdehnung des Natriums, des Kaliums und Deren Leigirung im Festen und im Geschmolzenen Zustande," Ann. Phys. Chem. 19, pp. 436-474 (1883).

29. C. T. Ewing, et. al., "Measurements of the Physical and Chemical Properties of the Sodium-Potassium Alloys, Quarterly Progress Report, No. 7," NRL C-3287, May 1948.

30. C. T. Ewing, et al., "Density of the System K-Na," Appendix C in "Measurement of the Physical and Chemical Properties of the Sodium-Potassium Alloy, Quarterly Progress Report, No. 1," NRL P-3010, September 1946

31. I. I. Novikov, et al., "The Heat Transfer and High Temperature Properties of Liquid Alkali Metals," Atomnaya En. 1, (4), 92 (1957).

32. M. E. Rinch and others, "Chimie Physique - Den Sites du Potassium du Sodiume," Compt. Rend. H. 189, pp. 39-41 (1929).

33. M. Nishibayashi, "Density and Viscosity of Molten Materials, Part 1, Density of Sodium and Sodium Hydroxide," WADC 53-308, Part 1, November 1953.

34. E. I. Gol'tsova, "Density of Lithium, Sodium and Potassium up to 1500-1600°C," Teplofiz. Vys. Temper. 4, No. 3, pp. 360-363 (1966).

35. R. B. Baker, R. D. Leggett and D. S. Dutt, "Interim Report: Effect of Burnup on Heat-Rating-to Incipient Fuel Melting - HEDL P-20," HEDL-TME 75-63, 1975 (Availability: USDOE Technical Information Center).

36. R. D. Leggett, E. O. Ballard, R. B. Baker, G. R. Horn, and D. S. Dutt, "Linear Heat Rating for Incipient Fuel Melting in UO_2-PuO_2 Fuel," Trans. Amer. Nucl. Soc. 15, pp. 752-753 (1972).

37. G. H. Golden and others, "Correlation and Interpretation of Data Relative to EBR-II Power Level," in Irradiation Experimentation in Fast Reactors, pp. 314-342, American Nuclear Society, Hinsdale, Ill., 1973.

38. L. B. Miller, et al., "Characterization of the Power in an Experimental Irradiation Subassembly of Mixed-Oxide Fuel in EBR-II", ANL/EBR-047, September 1971.

39. C. Chiu and N. E. Todreas, "Flow Split Measurements in an LMFBR Radial Blanket Assembly," Trans. Am. Nucl. Soc. 26, pp. 455-456 (1977).

40. C. L. Wheeler and others, "COBRA-IV-1: An Interim Version of COBRA for Thermal-Hydraulic Analysis of Rod Bundle Nuclear Fuel Elements and Cores," BNWL-1962, March 1976.

41. A. B. G. Washington, "Preferred Values for the Thermal Conductivity of Sintered Ceramic Fuel for Fast Reactor Use," TRG - Report - 2236, September 1973.

42. J. A. Christensen, R. J. Allio and A. Biancheria, "Melting Point of Irradiated Uranium Dioxide," Trans. Amer. Nucl. Soc. 7, pp. 390-391 (1964).

43. J. L. Krankota and C. N. Craig, "The Melting Point of Plutonia-Urania Mixed Oxide Irradiated to High Burnup," GEAP-13515 , July 1969.

44. H. von Ubish, S. Hall, and R. Srivastav, "Thermal Conductivities of Mixtures of Fission Product Gases with Helium and with Argon," in Proceedings of the Second United Nations International Conference on the Peaceful Uses of Atomic Energy, Geneva, 1958, Vol. 7, pp. 697-700, United Nations, Geneva, 1958.

45. D. J. Clough and J. B. Sayers, "The Measurement of the Thermal Conductivity of UO_2 under Irradiation in the Temperature Range 150°-1600°C, AERE-R-4690, December 1964.

46. A. Biancheria, "The Effect of Porosity on Thermal Conductivity of Ceramic Bodies," Trans. Amer. Nucl. Soc. 9, p. 15 (1966).

47. W. T. Sha and R. C. Schmitt, "THI-3D: A Computer Program for Steady State Thermal-Hydraulic Multi-Channel Analysis," ANL-8112, December 1975, (Availability: USDOE Technical Information Center).

48. M. D. Carelli, C. W. Bach and R. A. Markley, "Hydraulic and Scram Dynamics Analysis on LMFBR Control Rod Assemblies," Trans. Amer. Nucl. Soc. 16, pp. 218-219 (1973).

49. "A Compilation of Boron Carbide Design Support Data for LMFBR Control Elements," HEDL TC-40, December 1973 (Availability: USDOE Technical Information Center).

1630 159

ATTACHMENT

STATISTICAL TOLERANCE LIMITS AND PROPAGATION OF ERROR

J. A. Marshall

SUMMARY

In preparing a safety analysis of the Clinch River Breeder Reactor Plant, the Advanced Reactors Division must take explicit account of various uncertainties. This work leads repeatedly to the need for making a statistical inference in the framework of a propagation of error problem. Unfortunately the problem has no satisfactory general solution. This report deals with a simplified version of the problem for which a reasonable solution can be (and is) produced. Specifically we derive approximate upper (statistical) tolerance limits for a variable given as a linear combination of other variables which have independently and normally distributed uncertainties and for which data are available. These results will serve to produce answers for problems which satisfy the simplified assumptions and as a base from which to consider more difficult problems. The latter will probably have to be approached via computer simulation.

1. INTRODUCTION

This report deals with the propagation of error problem in a statistical context. In the general problem a (dependent) variable is given as a function of other (independent) variables which have uncertain values. This uncertainty propagates through the function to induce a corresponding uncertainty in the dependent variable. In the simplest statistical version of the problem the uncertainties are visualized in terms of probability distributions and one wants to characterize the induced (output) distribution given the (input) distributions of the independent variables. Our problem has the added feature that we want to take explicit account of the effect of incomplete specification of the input distributions on knowledge of the output distribution. This last feature makes the problem one of statistical inference.

The treatment of the above problem that will be given here is meant to provide an approach for certain calculations that arise in the safety analysis of the Clinch River Breeder Reactor Plant (CRBRP). The inference problem is a very difficult one for which no satisfactory general solution exists. We will deal with a simplified version of the problem for which we can produce a reasonable solution. This will serve both to produce answers to those problems for which the simplified assumptions are adequate and as a base from which to consider more difficult problems. The latter will probably have to be approached via computer simulation.

Statistical tolerance limits are a natural and often advocated concept for use in dealing with inference problems of the type which underlie this report. Consequently our development is in terms of tolerance limits of which two kinds are presented; one is the more common, but the other is offered as the more relevant for present purposes.

The more technical treatment of the basic material is given in Appendix A. Appendix B contains some remarks on the application of the basic material to somewhat more complicated problems.

2. PRELIMINARIES

Consider the relationship

$$Y = f(X_1, X_2, \ldots, X_m) \quad (1)$$

If any X is a random variable then Y necessarily becomes one also. The distribution of Y is induced via f by the distribution of the X's, i.e., the "error" in the X's propagates through f to become "error" in Y. If we assign probability distributions to the X's we can ask for the corresponding Y distribution. In general this is not an easy problem. If f is linear and the X's are independently, normally, distributed the problem is easy; Y is then normally distributed with mean and variance given by simple functions of the means and variances (respectively) of the X's. If f is non-linear the distribution of Y will not in general be a "known" distribution. In such cases one can resort to various approximate methods to obtain information about the distribution of Y.

The problem to be addressed in this report contains an additional difficulty; the distributions of the X's are not known. This of course is typical of applied work. The usual approach in such problems is to base the choice of a family of distributions for each X (e.g., normal, uniform, etc.) on general knowledge and to use data to select the specific members of the family which are reasonable candidate distributions for the X's. The proper use of the data to select a set of reasonable candidates and the implications of a given selection for the problem at hand are the concerns of statistical inference. The specific results in this report will be directed at the problem of making inferences about Y when f in (1) is linear, the X's are independently normal, and we have data on each X. The material introduced in connection with this effort will provide background for discussion of more general problems.

3. LIMITS

The type of inference about Y that we are concerned with is to give limits on its possible values. For example if we knew that Y had a normal distribution with mean μ and standard deviation σ we could say

(2a) $$\Pr\{Y \leq \mu + 1.96\sigma\} = 0.975$$

and

(2b) $$\Pr\{\mu - 1.96\sigma \leq Y \leq \mu + 1.96\sigma\} = .95 \quad .$$

Of course there is no inference problem here since everything is known. Suppose however that Y is normally distributed and its unknown mean and variance are estimated from data. Then the problem of giving limits on Y similar to those in (2) is an inference problem. The resulting limits are called tolerance limits by analogy with the corresponding limits used in manufacturing. The one-sided type of limit as given in (2a) will be emphasized in this report.

In this section we will give a basic discussion of tolerance limits when Y is normally distributed and has been observed directly. The necessary modifications when the observations are on the X's will be taken up later. The main purpose here is to introduce the two different types of normal theory tolerance limits and give a practical appreciation of what they are in a simple setting.

If the distribution of Y is normal and $Y_1, \ldots, Y_n$ is a random sample of observations on Y then we might be tempted to define the upper limit in (2a) as $\bar{Y} + 1.96S$ where $\bar{Y}$ is the sample average $(\sum Y_i)/n$ and S is the sample standard deviation $\{\sum (Y_i - \bar{Y})^2\}/(n-1)$. The problem however is that while the limit in (2a) covers 97.5% of the distribution of Y, the corresponding limit based on the sample need not do the same

since $\bar{Y}$ and S need not satisfy the relation $\bar{Y}+kS = \mu+k\sigma$. For given values of μ and σ the coverage of $\bar{Y}+kS$ could be calculated and for a different sample it would generally be different. In fact for any multiplier, k, the coverage of $\bar{Y}+kS$ is a random variable that varies from sample to sample and has a distribution of its own*. Of course in any application we have just one sample and we want a value of k which will do a given job. Statistical theory provides two classical methods for choosing k. Both refer to the distribution of the coverage in hypothetical repeat samples. One controls the average coverage and the other controls the probability that the coverage is at least a given amount. The remainder of this section will consist of a more detailed description of these two approaches.

The first type of tolerance interval is called the β-expectation type. Suppose $Y_1, \ldots, Y_n$ is a random sample from a normal distribution of unknown mean and standard deviation. To find the required k one must consult a table of the t-distribution for a value, say, $t_\beta(n-1)$. This is a value which an n-1 degree of freedom t-variate will exceed with probability $1-\beta$. The upper tolerance limit is then given by

$$\bar{Y} + t_\beta(n-1)\sqrt{1+1/n}\ S \quad . \tag{3}$$

For example if $\beta = .99$ and $n = 10$ then (3) becomes $\bar{Y} + (2.821)(\sqrt{11/10})\ S$ or $\bar{Y} + 2.959S$ and the intervals so computed will have coverage .99 on

---

* To emphasize this fact (which is fundamental to an understanding of the properties of such limits) we follow statistical convention and use upper-case letters (i.e., $\bar{Y}$,S) to denote random variables. When a formula is presented as a recipe for use with a sample of data then lower case letters are appropriate; they represent values assumed by random variables. Of course these remarks do not apply to those symbols that have nothing to do with randomness (e.g., n and k).

the average. Another interpretation is possible, namely, (3) yields a 99% confidence limit for the next observation on Y. To sum up, imagine that one repeatedly takes samples of size n from the normal distribution, computes (3), measures its true coverage, and takes an additional observation. Our assertions are twofold: (1) the average of the coverages will be .99 and (2) in 99% of the trials the next observation will be covered by the limit.

The other type of tolerance limit is called the β-content type. Here the factor k depends on the non-central t-distribution. This distribution depends not only on a degree of freedom parameter but also on a non-centrality parameter (δ say). Let us write $t_\gamma^\delta(w)$ for the value of a non-central t-variate with w degrees of freedom which is exceeded with probability $1-\gamma$. Also write K_β for the value of a standard normal variate (mean 0, variance 1) which is exceeded with probability $1-\beta$. The β-content tolerance limit is given by

$$\bar{Y} + (t^*/\sqrt{n})\, S \tag{4}$$

where $t^* = t_\gamma^\delta(n-1)$ and $\delta = \sqrt{n}\, K_\beta$. Suppose n = 10, β = .99, and γ = .95. Tables of the non-central t-distribution are difficult to use, but for the present example one can look up $k = t^*/\sqrt{n}$ directly in a special tolerance factor table and find that (4) becomes $\bar{Y}$ + 3.981 S. The interpretation is that in repeated sampling 95% of the trials will produce a limit whose coverage is at least .99. One says that a limit of the form (4) has coverage .99 with confidence .95.

Clearly the two limits are doing something different. By way of comparison if we put

$$3.981 = t_\beta(9)\sqrt{11/10}$$

and solve for $t_\beta(9) = 3.7957$ we can ask what value of β this corresponds to. Interpolation in a good t-table shows that β = .9978. Thus the .99 content limit with confidence .95 has an average coverage of .9978 or

alternatively it may be viewed as a 99.78% confidence limit for the next observation. It seems that in many design situations the appropriate inference is to the next "observation", i.e., to the (essentially only) device that will be built using the design. Of course this is not true for, say, production items where the β-expectation tolerance limit could be criticized for controlling the average and leaving the extremes unattended. In such a case the β-content approach has merit. But for a single large project it makes sense to use β-expectation limits.

4. TOLERANCE LIMITS FOR $Y = X_1+X_2$

The formulas of this section extend easily to the case $Y = \sum a_i X_i$ with m terms but for convenience they will be presented for the simple sum $Y = X_1+X_2$. Recall that the X's are supposed normal and independent. Now however instead of having observations directly on Y we have n_1 observations on X_1 and n_2 observations on X_2. This spoils the applicability of formulas (3) and (4) and it is the purpose of this section to supply replacements based on a good approximation.

By way of additional notation let

$$\bar{X}_i = \left(\sum_{j=1}^{n_i} X_{ij}\right)/n_i$$

and

$$S_i^2 = \left(\sum_{j=1}^{n_i} (X_{ij} - \bar{X}_i)^2\right)/(n_i-1)$$

where X_{ij} is the j^{th} observation on X_i (i=1 or 2). Write $\nu_i = n_i-1$ for the degrees of freedom for S_i. Finally we need a suggestive notation for $\bar{X}_1 + \bar{X}_2$ which will play the role of $\bar{Y}$ in (3) and (4); we will use $\hat{Y}$ for this.

Now the β-expectation tolerance limit is given by

$$\hat{Y} + t_\beta(\nu_e)\, S_e \tag{5}$$

where S_e plays the role of $\sqrt{1+1/n}\, S$ in (3) and ν_e is its effective degrees of freedom. Specifically

$$S_e = \{S_1^2(n_1+1)/n_1 + S_2^2(n_2+1)/n_2\}^{1/2}$$

and

$$\nu_e = (S_e^2)^2/\{[S_1^2(n_1+1)/n_1]^2/\nu_1 + [S_2^2(n_2+1)/n_2]^2/\nu_2\}\ .$$

The notation $t_\beta(\nu_e)$ was explained in connection with (3).

The β-content tolerance limit with confidence γ is based on non-central t as described in connection with (4) in the previous section; we will still be using the notation $t_\gamma^\delta(w)$ and K_β introduced there. For the present application modifications to (4) similar to those used in (5) above are required. The limit is

(6) $$\hat{Y} + (t^*/\sqrt{N})\, S$$

where

$$S = \{S_1^2 + S_2^2\}^{1/2} ,$$

$$N = n_1 n_2 \, S^2/(n_2 S_1^2 + n_1 S_2^2) ,$$

and

$$t^* = t_\gamma^\delta(\nu) ,$$

with

$$\delta = K_\beta \sqrt{N} ,$$

and

$$\nu = (S^2)^2/\{(S_i^2)^2/\nu_1 + (S_2^2)^2/\nu_2\} .$$

We turn now to examples of the use of these formulas in simple situations of the type $Y = X_1 + X_2$. The simple modifications of (5) and (6) that are needed to cover the case $Y = \sum_1^m a_i X_i$ (X_i normal) are given in Appendix A.

1630 169

5. EXAMPLES

To give a feeling for the implications of formulas (5) and (6) we have applied them to a series of 15 examples. The examples are chosen to show the effect of variations in s_1, s_2, n_1, and n_2 on the tolerance limits given by formulas (5) and (6). (As per the footnote in Section 3 we have shifted to lower-case letters to represent actual realizations of random variables, e.g., $S_1 = s_1$.) Table 1 gives the specifications of the 15 examples in terms of the s_i and n_i ($i = 1,2$) and shows the values taken, in each case, by the random variables N, ν, S, ν_e, and S_e introduced in the preceding section. The degrees of

Table 1. Specifications (s_1, s_2, n_1, and n_2) and computation of basic quantities (N, ν, s) for 15 examples chosen to illustrate tolerance limits.

	Specifications				Computation of basic quantities				
	s		n		Content			Expectation	
Case	1	2	1	2	N	ν	s	ν	s
1	1	1	∞	∞	∞	∞	1.41	∞	1.41
2	1	1	40	40	40	78	1.41	78	1.43
3	1	1	20	20	20	38	1.41	38	1.45
4	1	1	10	10	10	18	1.41	18	1.48
5	1	1	10	20	13.33	24.43	1.41	24.02	1.47
6	1	1	10	40	16	29.25	1.41	27.98	1.46
7	1	1	10	∞	20	36	1.41	32.8	1.45
8	1	2	10	10	10	13.24	2.24	13.24	2.35
9	1	2	10	20	16.67	26.23	2.24	26.43	2.3
10	1	2	10	40	25	47.95	2.24	47.82	2.28
11	1	2	10	∞	50	225	2.24	193.46	2.26
12	1	2	20	10	11.11	13.66	2.24	13.45	2.33
13	1	2	40	10	11.76	13.86	2.24	13.51	2.33
14	1	2	∞	10	12.5	14.06	2.24	13.56	2.32
15	1	4	10	10	10	10.12	4.12	10.12	4.32

1630 170

freedom (ν_e) and standard deviation (S_e) for formula (5) are given under the heading "Expectation" in the columns labeled ν and s. The columns listed under "Content" apply in a similar fashion to formula (6). Table 2 gives the multiplier (k) and the allowance (ks) for limits of β-expectation (formula (5)) and β-content (formula (6) with γ=95%) for different values of β. For each value of β the column labeled E(C) is the expected coverage achieved by the β-content limit.

Table 2. Factors and allowances for tolerance limits of β-expectation and β-content for the examples of Table 1 (γ=95% for limits of β-content)

	β=97.5%					β=99.9%				
	Expectation		Content			Expectation		Content		
Case	k	ks	k	ks	E(C)	k	ks	k	ks	E(C)
1	1.96	2.77	1.96	2.77	97.5	3.09	4.37	3.09	4.37	99.9
2	1.99	2.85	2.37	3.35	98.91	3.2	4.58	3.64	5.15	99.97
3	2.02	2.93	2.58	3.65	99.19	3.32	4.81	3.93	5.56	99.98
4	2.1	3.12	2.94	4.15	99.41	3.61	5.35	4.43	6.27	99.97
5	2.06	3.03	2.77	3.91	99.33	3.47	5.08	4.19	5.93	99.98
6	2.05	2.99	2.68	3.79	99.28	3.41	4.97	4.07	5.76	99.98
7	2.03	2.95	2.59	3.67	99.2	3.36	4.87	3.95	5.59	99.98
8	2.16	5.06	3.1	6.93	99.45	3.84	9	4.71	10.53	99.97
9	2.05	4.73	2.71	6.05	99.29	3.43	7.89	4.13	9.23	99.98
10	2.01	4.59	2.5	5.59	99.11	3.27	7.45	3.82	8.54	99.98
11	1.97	4.45	2.25	5.04	98.67	3.13	7.07	3.45	7.71	99.96
12	2.15	5.03	3.06	6.85	99.44	3.82	8.92	4.66	10.43	99.97
13	2.15	5.01	3.05	6.81	99.44	3.82	8.89	4.64	10.38	99.97
14	2.15	5	3.03	6.77	99.43	3.81	8.86	4.62	10.33	99.97
15	2.22	9.62	3.3	13.59	99.48	4.13	17.85	5.03	20.74	99.96

An example will serve to clarify all of this. Consider case (or row) 5 in the panel of Table 2 labeled β=97.5%. The entry 2.06 is the value of $t_\beta(\nu_e)$ for ν_e=24.02 (see Table 1), and the entry 3.03 is the product of 2.06 with s_e=1.47 (see Table 1). The entry 2.77 is the value of $t^*/\sqrt{N}$ for N=13.33 and ν=24.43 (from Table 1), and the entry 3.91 is the product of 2.77 with s=1.41 (from Table 1). Finally the entry 99.33 says that the β-content interval with β=97.5% and γ=95%

Table 2 continued

	β=95%					β=99%				
	Expectation		Content			Expectation		Content		
Case	k	ks	k	ks	E(C)	k	ks	k	ks	E(C)
1	1.64	2.33	1.64	2.33	95	2.33	3.29	2.33	3.29	99
2	1.66	2.38	2.02	2.86	97.53	2.38	3.4	2.78	3.93	99.63
3	1.69	2.44	2.21	3.12	98.13	2.43	3.52	3.01	4.25	99.72
4	1.73	2.57	2.53	3.58	98.66	2.55	3.79	3.42	4.83	99.78
5	1.71	2.51	2.38	3.36	98.46	2.49	3.65	3.22	4.56	99.76
6	1.7	2.48	2.3	3.25	98.32	2.47	3.6	3.13	4.42	99.75
7	1.69	2.45	2.22	3.14	98.15	2.45	3.54	3.03	4.28	99.73
8	1.77	4.15	2.66	5.96	98.78	2.64	6.2	3.62	8.09	99.79
9	1.7	3.92	2.32	5.19	98.36	2.48	5.7	3.16	7.07	99.75
10	1.68	3.82	2.14	4.78	97.94	2.4	5.48	2.93	6.54	99.69
11	1.65	3.73	1.92	4.3	97.09	2.35	5.3	2.64	5.9	99.52
12	1.77	4.12	2.63	5.88	98.75	2.64	6.16	3.58	8	99.79
13	1.77	4.11	2.61	5.84	98.73	2.64	6.14	3.56	7.96	99.79
14	1.77	4.1	2.59	5.8	98.71	2.64	6.12	3.54	7.92	99.79
15	1.81	7.83	2.82	11.64	98.88	2.76	11.93	3.85	15.89	99.79

actually achieves an expected coverage of 99.33%. Note that γ=95% applies to the β-content limits and is fixed for all panels of Table 2.

Perhaps it would be useful to indicate an interpretation for some of the quantities appearing in Table 1. Since $\hat{Y}$ in (5) and (6) is not the average of a set of observations we cannot signify its precision by giving the number of observations on which it is based. The quantity N is the <u>effective</u> number of observations for $\hat{Y}$ in the sense that $\hat{Y}$ has the variance that the mean of N observations on Y would have. Notice when $n_1=n_2$ that N is in fact the number of observations on Y. Now s (col. 8) is the estimate of the standard deviation of $Y=X_1+X_2$ by a very familiar formula. However s is not in general of the form of an estimated standard deviation based on a set of observations (as s_1 and s_2 are). Therefore s^2 does not have the sampling distribution that such estimates have and on which many techniques of statistical inference are based. The distribution of s^2 is therefore approximated with the closest fitting member of the usual family of distributions for sample variances;

1630 172

this fitting leads to the degrees of freedom for s represented by ν (col. 7). Notice that when $n_1=n_2$ and $s_1=s_2$ so that the estimate s can be constructed along conventional lines then $\nu=(n_1-1) + (n_2-1)$ as expected. Finally s and ν (cols. 9 and 10) bear the same relationship to each other that s and ν (cols. 7 and 8) do, but s (col. 10) is the estimate of the variance of $(\hat{Y}-Y')$ where Y' is a new observation (say $Y'=X_{1u} + X_{2v}$ where $u=n_1+1$ and $v=n_2+1$) from the distribution of Y.

The factors k given in Table 2 for β-expectation and β-content limits cover a broader range of cases than might at first be realized. For any case in the table the values of s_1 and s_2 can be multiplied by the same constant without changing the value of k. Thus, e.g., case 5 applies to all situations where $s_1=s_2$, $n_1=10$, and $n_2=20$; and case 10 covers all cases where $s_2=2s_1$, $n_1=10$, and $n_2=40$. The conventional "2σ" and "3σ" limits that are often calculated correspond closely to our case 1, Table 2, panels 97.5% and 99.9% respectively.

1630 173

6. COMPUTATIONAL RECOMMENDATIONS

The application of formulas (5) and (6) requires the evaluation of probability points ($t_\beta(\nu)$ and t^*) of the central and noncentral t-distributions respectively. Tables of the probability points of the central t-distribution are widely available, but interpolation is necessary for fractional degrees of freedom. Noncentral t-tables are relatively less available and are much more difficult to use. Thus approximations based on the readily available tables of the standard normal distribution are attractive. There are some rather good normal approximations available (Peizer and Pratt [5], Wallace [6]) for the central t-distribution. Approximations to the noncentral t-distribution have been reviewed by Owen [4]. He finds no overall winner among the candidates, but a certain well known approximation (designated J by Owen) is the best one for the parameter values of interest to us (γ=.95, β=.95 to .999, ν>10). To emphasize the dependence of the candidates' ranking on the parameters, we mention that Owen found approximation J to be third best (out of four) when γ=.90 with β and ν as before. This approximation is actually written to produce the k-value for the β-content interval directly rather than the noncentral t-value. Specific recommendations are given below.

Central t - To find a value of $t_\beta(\nu)$ for use in formula (5) when β and ν are given, first use a standard normal table to find z such that $\Pr\{Z \leq z\} = \beta$. (For example $\Pr\{Z \leq 1.96\} = .975$.) The desired t-value is given by

$$t_\beta(\nu) = [\nu(\exp\{(z^2/\nu)([8\nu+3]/[8\nu+1])^2\}-1)]^{1/2} \quad . \tag{7}$$

This is taken from Wallace [6]. To gauge the quality of this approximation it was used to approximate the entries in Table 2, panels 95% and 99.9%,

columns "Expectation-k". These entries in Table 2 were obtained via careful interpolation in a t-table. The comparison is presented in Table 3 where an extra digit is carried to reveal smaller differences.

Table 3. Comparison of central t-values obtained from formula (7) with those from Table 2.

	β=95%		β=99.9%	
Case	Formula	Table 2	Formula	Table 2
2	1.665	1.665	3.198	3.198
3	1.686	1.686	3.319	3.319
4	1.734	1.734	3.613	3.61
5	1.711	1.711	3.468	3.467
6	1.701	1.701	3.409	3.408
7	1.693	1.693	3.359	3.358
8	1.769	1.769	3.841	3.836
9	1.705	1.705	3.43	3.429
10	1.677	1.677	3.27	3.269
11	1.653	1.652	3.133	3.132
12	1.766	1.766	3.826	3.822
13	1.766	1.766	3.822	3.817
14	1.765	1.765	3.819	3.815
15	1.81	1.81	4.138	4.128

Noncentral t - To find a value of $k=t^*/\sqrt{N}$ for use in formula (6) when β, γ, N, and ν are given put

$$(8) \qquad k = (K_\beta + \{K_\beta^2 - AB\}^{1/2})/A$$

where

$$A = 1 - K_\gamma^2/2\nu \quad ,$$

$$B = K_\beta^2 - K_\gamma^2/N \quad ,$$

and K_p is the value of a standard normal variable which is exceeded with probability 1-P. This is taken from Owen [4]. Table 4 contains a comparison of formula (8) with certain appropriate entries from Table 2

("Content-k"). These entries were obtained by interpolation in a table of the noncentral t-distribution. Clearly this approximation is not as good as the one for central t, but it can still be quite useful.

To sum up, formula (7) is essentially as good as Table 2 for β=95% while for β=99.9% it loses accuracy in the third decimal place for the smaller degrees of freedom. Formula (8) on the other hand has two decimal place accuracy at best (β=95% and large degrees of freedom) and one decimal place accuracy at worst (β=99.9% and small degrees of freedom). To obtain greater accuracy than formula (8) provides, one evidently must use a noncentral t-table and interpolate for the noncentrality parameter and the degrees of freedom. The resulting value of t^* can then be used in (8). For γ=.95 a suitable table is available in [4].

Table 4. Comparison of k-values (related to noncentral t-values) obtained from formula (8) with those from Table 2.

	β=95%		β=99.9%	
Case	Formula	Table 2	Formula	Table 2
2	2.017	2.021	3.635	3.642
3	2.199	2.209	3.915	3.929
4	2.507	2.529	4.405	4.435
5	2.36	2.376	4.17	4.192
6	2.286	2.299	4.054	4.072
7	2.209	2.22	3.937	3.952
8	2.635	2.663	4.672	4.709
9	2.306	2.32	4.106	4.126
10	2.131	2.139	3.81	3.821
11	1.921	1.923	3.444	3.447
12	2.601	2.627	4.628	4.664
13	2.584	2.61	4.607	4.642
14	2.567	2.592	4.587	4.621
15	2.79	2.824	4.986	5.031

1630 176

7. REFERENCES

[1] G.E.P. Box, "Some Theorems on Quadratic Forms Applied in the Study of Analysis of Variance Problems: I. Effect of Inequality of Variance in the One-Way Classification", Annals Math. Stat. 25, pp. 290-302, (1954).

[2] K. A. Brownlee, Statistical Theory and Methodology in Science and Engineering, 2nd Edition, John Wiley, New York, 1965.

[3] Irwin Guttman, Statistical Tolerance Regions: Classical and Bayesian, Hafner Press, New York, 1970.

[4] D. B. Owen, "Survey of Properties and Applications of Noncentral T-Distribution", Technometrics 10, pp. 445-478, (1968).

[5] David B. Peizer and John W. Pratt, "Approximating the Binomial, F, and Commonly Used Related Distributions, I", TR-12 (AD-643954), August 1966.

[6] David L. Wallace, "Bounds on Normal Approximations to Student's and the Chi-Square Distributions", Annals Math. Stat. 30, pp. 1121-1130, (1959).

1630 177

8. APPENDIX A

Derivations for the case $Y=\sum a_i X_i$

Suppose $Y = \sum_1^m a_i X_i$ with the X_i independently $N(\mu_i,\sigma_i^2)$, and $X_{i1}, \ldots, X_{in_i}$ is a random sample of size n_i on X_i $(i=1,\ldots,m)$. We want an upper tolerance limit on Y. Both the β-content type with confidence γ and the β-expectation type will be treated. The basic reference for tolerance concepts will be Guttman[3]. Our basic approach is to modify the usual formulas for the case where $Y_1, \ldots, Y_n$ is a random sample from a $N(\mu,\sigma^2)$. The modification comes from using Satterthwaite's formula for the approximate degrees of freedom to be associated with a linear combination of variance estimates. This will be presented first.

Notice that with the above setup we have

$$\text{Var } Y = \sum a_i^2 \text{Var } X_i$$

and for an estimate of Var Y one would use $\sum a_i^2 S_i^2$. Here Var is the variance operator and S_i^2 stands for the usual sample estimator of Var X_i (with n_i-1 in the denominator). Now each S_i^2 has a mean square distribution with n_i-1 degrees of freedom, but the distribution of

$$S^2 = \sum_1^m a_i^2 S_i^2 \tag{9}$$

in general is not a member of the family of mean square distributions. The idea of using a mean square distribution that approximates the distribution of S^2 is developed in, e.g., Brownlee[2]. The approximation is based on calculating the degrees of freedom for a mean square

1630 178

distribution so that its mean and variance match those of S^2. The result is called Satterthwaite's approximation (original references are given in Brownlee) and in our case it comes to

$$\nu = (S^2)^2 / \sum_1^m a_i^4 (S_i^2)^2 / \nu_i \tag{10}$$

where $\nu_i = n_i - 1$ is the degrees of freedom associated with S_i^2. This approximation has been studied by Box[1] who gives numerical evidence indicating that it is excellent for positive a_i.

To develop an upper β-expectation tolerance limit for Y we use a theorem due to Paulson and given by Guttman[3] which says that a confidence region of confidence β for a future observation from the distribution of Y is a β-expectation tolerance region for the distribution of Y. Thus let Y' be a next observation on Y, i.e., let

$$Y' = a_1 X_{1u} + a_2 X_{2v} + \ldots$$

where $u = n_1+1$, $v = n_2+1$, etc. Write $\hat{Y} = \sum a_i \bar{X}_i$ and observe that

$$Y' - \hat{Y} \sim N(0, \sigma_y^2 + \sigma_{\hat{y}}^2)$$

where

$$\sigma_y^2 = \sum a_i^2 \sigma_{x_i}^2$$

$$\sigma_{\hat{y}}^2 = \sum a_i^2 \sigma_{\bar{x}_i}^2$$

1630 179

and

$$\sigma_{\bar{x}_i}^2 = \sigma_{x_i}^2 / n_i$$

in an obvious notation. Now

$$\mathrm{Var}(Y'-\hat{Y}) = \sigma_y^2 + \sigma_{\hat{y}}^2$$

$$= \sum_1^n a_i^2 \sigma_{x_i}^2 (n_i+1)/n_i$$

and we will estimate this by

$$S_e^2 = \sum a_i^2 S_i^2 (n_i+1)/n_i$$

where of course S_i^2 is the usual estimator of $\mathrm{Var}(X_i)$ with $\nu_i = n_i-1$ degrees of freedom. Thus from Satterthwaite's approximation (10) we have

$$\nu_e = (S_e^2)^2 / \sum_1^n (a_i^2 (n_i+1)/n_i)^2 (S_i^2)^2/\nu_i$$

and so approximately

$$\frac{S_e^2}{\mathrm{Var}(Y'-\hat{Y})} \sim \frac{X^2(\nu_e)}{\nu_e} \quad .$$

Clearly

$$\frac{Y'-\hat{Y}}{\sqrt{\mathrm{Var}(Y'-\hat{Y})}} \sim N(0,1)$$

and therefore

$$\frac{Y'-\hat{Y}}{S_e} \sim t(\nu_e)$$

where $t(\nu_e)$ stands for a "t" distribution with ν_e degrees of freedom (the required independence between S_e and $\hat{Y}$ derives from the classical independence between S_i and $\bar{X}_i$ and the assumed independence among the X_i).

If we write $t_\beta(\nu)$ for a t-variate with ν degrees of freedom which is exceeded with probability $1-\beta$ then

$$\Pr\{(Y'-\hat{Y})/S_e \leq t_\beta(\nu_e)\} = \beta$$

1630 180

and by the usual inversion this becomes

$$\Pr\{Y' < \hat{Y} + t_\beta(\nu_e)S_e\} = \beta \quad . \tag{11}$$

Therefore $\hat{Y} + t_\beta(\nu_e)S_e$ is an upper confidence limit for Y' with confidence β; hence it is also an upper tolerance limit of β-expectation. To recapitulate briefly: Y' is a random variable with the distribution of Y, i.e., $N(\sum a_i\mu_i, \sum a_i^2\sigma_i^2)$; $\hat{Y}$ is an estimator of $\sum a_i\mu_i$ which is independent of Y'; and S_e^2 is an estimator of $\mathrm{Var}(Y'-\hat{Y})$ which is independent of $\hat{Y}$.

Turning now to the β-content tolerance limit let us write (with some redundancy)

$$Y = \sum a_i X_i$$

$$\hat{Y} = \sum a_i \bar{X}_i$$

$$S^2 = \sum a_i^2 S_i^2$$

$$\mathrm{Var}\ Y = \sigma_y^2$$

and

$$EY = \mu_y$$

where E is the expected value operator. In the present case the degrees of freedom for S^2 as taken from Satterthwaite's approximation is given directly by (10). In this development it is convenient to be able to write $\mathrm{Var}(\hat{Y})$ as $\mathrm{Var}(Y)/N$ just as though $\hat{Y}$ were the average of N observations on Y. The N so defined is called the effective number of observations. It is given by $\mathrm{Var}(Y)/\mathrm{Var}(\hat{Y})$ or

$$N = (\sum a_i^2\sigma_{x_i}^2)/(\sum a_i^2\sigma_{x_i}^2/n_i) \quad .$$

1630 181

If the n_i had a common value n then N would equal n and not depend on the unknown variances. Of course if the unknown variances had a common value then N would only depend on the a_i and n_i. In general we must approximate N by replacing the unknown variances by their estimates S_i^2. That is

$$N \tilde{=} (\sum a_i^2 S_i^2)/(\sum a_i^2 S_i^2/n_i) \ .$$

Let K_β be the value of a N(0,1) variate which is exceeded with probability $1-\beta$. We want a value of k so that $\hat{Y}+kS$ will be a β-content tolerance limit with confidence γ . In other words k must be such that

$$\Pr\{\mu_y + K_\beta \sigma_y \leq \hat{Y} + kS\} = \gamma \tag{12}$$

since $\mu_y + K_\beta \sigma_y$ has coverage exactly β and (12) says that $\hat{Y}+kS$ has at least coverage β with probability γ. Rewriting (12) we find

$$\Pr\left[\frac{\sqrt{N}\,\frac{\mu_y - \hat{Y}}{\sigma_y} + \sqrt{N}K_\beta}{\sqrt{\frac{S^2}{\sigma_y^2}}} < \sqrt{N}k\right] = \gamma \ . \tag{13}$$

Since

$$\sqrt{N}(\mu_y - \hat{Y})/\sigma_y \sim N(0,1) \ ,$$

$$S^2/\sigma_y^2 \sim \chi^2(\nu)/\nu \ ,$$

and S is independent of $\hat{Y}$, the expression on the left of the inequality in (13) has a noncentral t-distribution with noncentrality parameter $\sqrt{N}K_\beta$ and degrees of freedom ν. If t^* is the value of such a variate which is exceeded with probability $1-\gamma$ then (13) holds with $t^* = \sqrt{N}k$ or $k = t^*/\sqrt{N}$. The more complete notation used in the report in place of t^*

is $t_{\gamma}^{\delta}(\nu)$ where $\delta=\sqrt{N}K_{\beta}$. The β-content tolerance limit is

(14) $$\hat{Y} + (t^{*}/\sqrt{N})S \ .$$

9. APPENDIX B

More general situations

Appendix A treats the problem of tolerance limits on a Y given by $Y=f(X_1, \ldots, X_m)$ where the X's are independent and normal, f is linear, and observations are available on the individual X's. The approach taken to this problem is somewhat more general than it might appear to be. In this appendix the additional generality will be brought out.

Basically what is needed for a normal theory tolerance limit on Y is a normally distributed estimate of the mean of Y, say $\hat{Y}$, whose variance is given by S^2/N (for some N) and for which S^2 is an estimate (independent of $\hat{Y}$) of the variance of Y having a mean square distribution with ν degrees of freedom. The classical situation in which these conditions are met is where a random sample $Y_1, \ldots, Y_m$ is available on Y and we put $\hat{Y}=\bar{Y}$ and $S^2 = \{\sum(Y_i-\bar{Y})^2\}/(m-1)$. Then $N=m$ and $\nu=m-1$. (Strictly speaking N is required only for the content type limits and not for the expectation type.) In the situation treated in Appendix A the tolerance limits had to be approximated. Approximation was needed for two reasons: (1) the natural estimate of the variance of Y (or of $\{Y'-\hat{Y}\}$ in the expectation type) did not have a mean square distribution and so an approximate one was provided and (2) the effective number of observations (N) involved variances that had to be estimated.

1630 183

The generalities that may be treated with little change in approach include:

i) one or more X_i's determined from a regression on other variables rather than from direct observation,

ii) f is nonlinear,

iii) X_i's not independent.

Consider first the case where an X in $f(X_1, \ldots, X_m)$ is determined from a previously established regression on some variables Z_k. If the regression was linear (in the parameters) then for some matrix of constants (Z) and some vector of estimated coefficients (B) we estimate the X_i contribution to $\hat{Y}$ as $\hat{X}_i = \underline{z}B$. (We are here treating f as linear.) In this notation $\underline{z}$ is a row vector expressing the values of the z-variables at which the value of X_i is desired and B is a column vector. For example if the regression were quadratic in a single z then $\hat{X}_i = a+bz+cz^2$, $B' = \{a,b,c\}$, and $z = \{1,z,z^2\}$. The Z-matrix in this case consists of a column of 1's, a column of z-values, and a column of z-values squared. Now the estimate of the variance of $\hat{X}_i (= \underline{z}B)$ is given by

$$S_i^2 = \underline{z}(Z'Z)^{-1}\underline{z}'S^2$$

where

$$S^2 = \{\sum_i (X_{ij} - \hat{X}_{ij})^2 / (m-p)$$

and X_{ij} represents the values of X_i on which the regression is based. These equations are for any linear regression based on m observations and p parameters. The degrees of freedom for S_i^2 is (m-p). This information is sufficient to alter the formulas in Appendix A so that they would apply to a case where one or more X_i's are based on a linear regression. If the regression is not linear in the parameters the fit will be carried out by a series of linear approximations. The S_i^2 and its degrees of freedom from the final iteration can be used as above.

Consider next the case of a nonlinear f. An approach here would be to linearize f. That is put

$$Y \tilde{=} f(\hat{X}_1, \ldots, \hat{X}_m) + \sum_{i=1}^{m} \{f_i(\hat{X}_1, \ldots, \hat{X}_m)\}\{(X_i - \hat{X}_i)\}$$

where f_i is the partial of f with respect to coordinate i evaluated at $(\hat{X}_1, \ldots, \hat{X}_m)$. This presents Y as a linear combination of variables, which case has been dealt with. The accuracy of this approximation depends on the variances of the distributions of the X_i and the severity of the nonlinearity of f. In practice one often finds the variances to be sufficiently small that the approximation is a good one. It should be noted that there are really two approximations here; one is the linearization about a point and the other is the estimation of that point by $(\hat{X}_1, \ldots, \hat{X}_m)$.

Finally go back to a linear f and suppose the uncertainties in the normal X_i's are not statistically independent. For simplicity consider $Y=X_1+X_2$. In the absence of independence we have Var Y = Var X_1+Var X_2+2 Cov (X_1,X_2) where the last term is twice the covariance of X_1 with X_2. To find Var Y we must obtain Cov (X_1,X_2), and there are two cases to be considered. In one case the dependence arises from known physical relations and based on these an analysis will show the covariance to be (perhaps approximately) a linear combination of Var X_1 and Var X_2. This makes Var Y a linear combination of variances and Satterthwaite's approximation can be used as before. In the other case Cov (X_1,X_2) will be known only through estimation based on data. To be able to make such an estimate we must have pairs of observations (X_{1j},X_{2j}). But this is the same as having direct observations on Y (i.e., $Y_j=X_{1j}+X_{2j}$) which avoids any problem about covariances.

1630 185